

ASSESSMENT OF THE EFFECT OF ADDITION OF NANO PARTICLES ON THERMAL ENERGY STORAGE PARAMETERS OF PHASE CHANGE MATERIALS

Thesis
Submitted in partial fulfillment of the requirements for the
degree of

DOCTOR OF PHILOSOPHY

by
SUDHEER R



DEPARTMENT OF METALLURGICAL & MATERIALS
ENGINEERING

NATIONAL INSTITUTE OF TECHNOLOGY
KARNATAKA,
SURATHKAL, MANGALORE -575025

SEPTEMBER, 2018

DECLARATION

By the PhD Research Scholar

I hereby *declare* that the research thesis entitled “**ASSESSMENT OF THE EFFECT OF ADDITION OF NANO PARTICLES ON THERMAL ENERGY STORAGE PARAMETERS OF PHASE CHANGE MATERIALS**” which is being submitted to the National Institute of Technology Karnataka, Surathkal for the award of the degree of Doctor of Philosophy in METALLURGICAL AND MATERIALS ENGINEERING is a *bonafide report of the research work carried out by me*. The material contained in this Research Thesis has not been submitted to any University or Institution for the award of any degree.

SUDHEER R

(135055)

Department of Metallurgical and Materials Engineering

Place : National Institute of Technology Karnataka, SURATHKAL

Date : 20-September-2018

CERTIFICATE

This is to certify that the thesis entitled “**ASSESSMENT OF THE EFFECT OF ADDITION OF NANO PARTICLES ON THERMAL ENERGY STORAGE PARAMETERS OF PHASE CHANGE MATERIALS**” submitted by **Mr. Sudheer R.** (135055) as the record of the research work carried out by him, is *accepted as the Research Thesis submission* in partial fulfillment of the requirements for the award of degree of Doctor of Philosophy

Dr. K. Narayan Prabhu
Professor and Research Guide
Department of Metallurgical and Materials Engineering
National Institute of Technology Karnataka

Dr. Anandhan Srinivasan
Chairman, DRPC
Department of Metallurgical and Materials Engineering
National Institute of Technology Karnataka

ACKNOWLEDGEMENTS

With immense sense of gratitude I thank my guide Dr. K. Narayan Prabhu, Professor, Department of Metallurgical & Materials Engineering, NITK for encouraging, guiding and leading me through this research work as a thoughtful supervisor and as a sincere friend. His sincere and wholehearted efforts in overcoming various challenges have been the prime inspiration for me along the progress of this work. My association with him in last 7 years had boosted by confidence and motivated me in pursuing a profession with dignity and vision.

I am indebted to my colleagues Mr. Vignesh Nayak U. and Mr. Pranesh Rao K. M. for their invaluable suggestions and support during various stages of my work. I would also like to express my gratitude to Mr. Amarnadh S. for encouraging me in this regard.

I express my gratitude to Dr. Anandhan Srinivasan, HOD, Dept. of Metallurgical & Materials Engineering, NITK and all former HOD's of the department for supporting me in this work.

I am thankful to Dr. M R Rahman and Dr. Amba Shetty for evaluating my work at annual RPAC meetings.

I thank our support staffs, Mr. Dinesha Shettigar, Lab Assistant and Mr. Satish Poojary, Mechanic for sharing their technical expertise.

I thank Mrs. Sharmila Dinesh, Literate Assistant for helping me with all necessary documentations and other activities related to my work in the department.

I extend my gratitude to Ms. Rashmi B. for helping me with micrographs of PCMs, and to Mr. Mohd. Khalifa in preparing ball milled PCM samples.

I am thankful to The Director, and Authorities of NITK for providing all necessary facilities and funds to carry out my work.

Finally, I express my gratitude to all my colleagues in the Department of Metallurgical & Materials Engineering at NITK, my friends, my family and all well-wishers for their encouragement and support.

-Sudheer R.

ABSTRACT

Molten salts have high prospects of being used in solar power plants as phase change materials (PCMs) for thermal energy storage (TES) on virtue of their superior TES functionalities. The suitability of a simple computer aided cooling curve analysis (CACCA) for characterizing thermal energy storage phase change materials (PCM) was proposed in the present work.

In the present work, the effects of addition of various carbon based nanostructures on TES parameters of KNO_3 were investigated. The solidification time of the PCM significantly decreased on nano particle addition indicating an enhancement in the heat removal rate. Graphite nanoparticles and MWCNT additions decreased the thermal diffusivity property of the base PCM while the addition of graphene resulted in higher thermal diffusivity. However, the benefits of addition of nanoparticles to the salt-PCM reduced on thermal cycling. The use of dispersants such as carbon black and TiO_2 significantly reduced the degradation of the nanosalt-PCM on thermal cycling.

Further, solidification of potassium nitrate and zinc-8% aluminium alloy (ZA8) were studied to compare their suitability for TES applications in the concerned temperature range. Metallic PCMs offered higher thermal diffusivity and heat transfer rates while salt PCMs offered higher energy density. These PCMs were chosen to demonstrate the ability of the proposed technique to characterize PCMs freezing at a single temperature as well as over a range of temperatures.

Further, suitability of a novel Hot-Cold Probe Technique for assessment of the heat transfer characteristics of nanosalt-PCMs was determined. The probe-PCM control experiment is a stand-in for a container-PCM unit in a TES system. This perspective is different from the conventional PCM characterization studies. The heat flux curves justify the benefits of decrease in solidification time as the nanoparticle added PCMs ensured higher heat flux into the probes.

Keywords : Thermal energy storage; CACCA; Phase change materials; Nanosalt-PCMs.

CONTENTS

LIST OF FIGURE	III
LIST OF TABLES	VII
NOMENCLATURE	IX
CHAPTER 1 INTRODUCTION	1
1.1 STATE OF THE ART IN THE FIELD	3
1.1.1 Energy storage technology: World scenario	3
1.1.2 Energy storage technology: Indian scenario	4
1.2 THERMAL ENERGY STORAGE	5
1.2.1 Phase change materials (PCM)	6
CHAPTER 2 LITERATURE SURVEY	8
2.1 ORGANIC PCM	8
2.1.1 Organic Nano-PCMs	12
2.2 INORGANIC PCM	14
2.2.1 Salt Hydrate PCMs	14
2.2.2 Salt PCMs	15
2.2.3 Metallic PCMs	18
2.3 NANOSALT-PCMs	19
2.4 CHARACTERIZATION OF ENERGY STORAGE MATERIALS	24
2.4.1 Calorimetric methods	25
2.4.2 T-history method	26
2.4.3 Cycling stability testing	27
2.4.4 Container material compatibility/corrosion testing	27
2.5 SCOPE OF THE INVESTIGATION	27
2.6 OBJECTIVES	30
CHAPTER 3 THEORETICAL BACKGROUND	31
3.1 COMPUTER AIDED COOLING CURVE ANALYSIS	31
3.1.1 Newtonian Technique	32
3.1.2 Fourier Technique	34
3.2 INVERSE ANALYSIS	35
CHAPTER 4 EXPERIMENTAL	37
4.1 NANOPARTICLES FOR NANOSALT-PCM PREPARATION	37
4.2 NANOSALT-PCM PREPARATION METHOD	37
4.3 ADDITION OF DISPERSANTS INTO NANOSALTS	37
4.4 THERMAL CYCLING TESTS	38
4.5 DESIGN OF EXPERIMENTAL SETUP FOR FOURIER	38

	ANALYSIS	
	4.6 NEWTONIAN TECHNIQUE	38
	4.7 FOURIER TECHNIQUE	39
	4.8 MICROGRAPHIC STUDIES	40
	4.9 HOT-COLD PROBE TECHNIQUE	40
CHAPTER 5	RESULTS & DISCUSSION	42
	5.1 DESIGN AND OPTIMIZATION OF EXPERIMENTAL SETUP FOR FOURIER TECHNIQUE	42
	5.2 EFFECT OF ADDITION OF MICRO AND NANO GRAPHITE PARTICLES ON TES FUNCTIONS OF SALT-PCMs	47
	5.3 EFFECT OF SAMPLE PREPARATION METHOD ON TES FUNCTIONS OF NANOSALT-PCM	55
	5.4 EFFECT OF ADDITION OF VARIOUS CARBON NANOSTRUCTURES ON TES FUNCTIONS OF SALT-PCM	58
	5.5 EFFECT OF DISPERSANTS ON THE SOLIDIFICATION OF NANOSALT-PCM	66
	5.5.1 MWCNT+TiO ₂ (1:9) dispersed in KNO ₃	68
	5.5.2 MWCNT+Carbon Black (4:6) dispersed in KNO ₃	69
	5.6 ASSESSMENT OF PCM-CONTAINER HEAT TRANSFER USING A HOT-COLD PROBE TECHNIQUE	69
	5.7 COMPARATIVE STUDY OF METAL (ZA8) AND SALT (KNO ₃) PCMs	79
CHAPTER 6	CONCLUSION	86
	REFERENCES	89

LIST OF FIGURES

Fig. No.	Caption	Page No.
2.1	A schematic sketch of T-History technique set up	26
3.1	Schematic sketch of (a) Newtonian technique, (b) Fourier technique set up	34
4.1	A schematic sketch of Fourier technique set up	39
4.2	A schematic sketch of probe used in Hot-Cold Probe technique	40
5.1	Assignment of Mold material properties and discretization of model	42
5.2	Assignment of PCM material properties in SolidCast	43
5.3	Cylindrical PCM samples with varying L/D ratios drafted in SolidCast.	44
5.4	Simulation parameter for solidification of PCM.	44
5.5	Liquidus time distribution in PCM sample with L/D ratio of 1	45
5.6	Liquidus time distribution in PCM sample with L/D ratio of 5	46
5.7	Cooling curve and cooling rate curve of KNO ₃	49
5.8	Cooling curves of various PCMs with graphite particle addition	49
5.9	Effect of thermal cycling on cooling curve of Graphite particle added PCM	50
5.10	Effect of thermal cycling on heat removal rates in various PCMs	51
5.11	Agglomeration of nanoparticles after (A) 1 st thermal cycle, (B) 10 th thermal cycle	52
5.12	Thermal diffusivity curves of graphite particle added salt-PCM (KNO ₃).	54
5.13	Cooling curves of ball milled and manually mixed nanosalt-PCMs	56
5.14	Effect of thermal cycling on heat removal rates of Nanosalt-PCM	57
5.15	Thermal diffusivity curves of ball milled and manually mixed nanosalt-PCM	57
5.16	Cooling curves of various nanosalt-PCMs	59
5.17	Effect of thermal cycling on the heat removal rates of various nanosalt-PCMs	60
5.18	SEM images showing agglomeration of nanoparticles in salt-PCM on thermal Cycling. (a) 0.1% Graphite + KNO ₃ PCM, (b) 0.1% MWCNT + KNO ₃ PCM, (c) 0.1% Graphene + KNO ₃ PCM	61
5.19	Thermal diffusivity curves of nanoparticle added (0.1% by wt.) KNO ₃ PCM	63

Fig. No.	Caption	Page No.
5.20	Thermal diffusivity curves of PCMs with varying concentration of MWCNT	64
5.21	Cooling curves of nanosalt-PCM with dispersants	66
5.22	Effect of thermal cycling on heat removal rates of nanosalt-PCM with dispersant	67
5.23	Effect of dispersants on thermal diffusivity curve of nanosalt-PCM	67
5.24	Cooling Curve of Cu Hot Probe when immersed in various PCM composites	71
5.25	Cooling Curve of SS Hot Probe when immersed in various PCM composites	71
5.26	Heating Curve of Cu Cold Probe when immersed in various PCM composites	72
5.27	Heating Curve of SS Cold Probe when immersed in various PCM composites	72
5.28	Cooling Rate Curve of Cu Hot Probe when immersed in various PCM composites	73
5.29	Cooling Rate Curve of SS Hot Probe when immersed in various PCM composites	73
5.30	Heating Rate Curve of Cu Cold Probe when immersed in various PCM composites	74
5.31	Heating Rate Curve of SS Cold Probe when immersed in various PCM composites	74
5.32	Integral heat flux curve of Cu Hot Probe when immersed in various PCM composites	75
5.33	Integral heat flux curve of SS Hot Probe when immersed in various PCM composites	75
5.34	Integral heat flux curve of SS Cold Probe when immersed in various PCM composites	76
5.35	Integral heat flux curve of Cu Cold Probe when immersed in various PCM composites	76
5.36	Cooling curve and Cooling rate curve of KNO ₃ , Newtonian method	80
5.37	Cooling curve and Cooling rate curve of ZA8, Newtonian method	80
5.38	Thermal diffusivity curve of ZA8, Fourier method	81
5.39	Thermal diffusivity curve of KNO ₃ , Fourier method	81
5.40	FDC and Baseline of ZA8, Fourier method	82

Fig. No.	Caption	Page No.
5.41	FDC and Baseline of KNO_3 , Fourier method	82
5.42	Cooling rate versus temperature curves, Newtonian method	83
5.43	Enthalpy curve of KNO_3	83
5.44	Enthalpy curve of ZA8	83

LIST OF TABLES

Fig. No.	Caption	Page No.
2.1	List of a few organic PCMs.	9
2.2	List of salts with melting temperature and heat of fusion.	17
2.3	List of a few metal alloys with melting temperature and heat of fusion	18
5.1	Relevant properties of select materials used to optimize Fourier set up	43
5.2	Effect of graphite particle addition on TES fuctions of KNO ₃	53
5.3	Effect of nanoparticle addition on TES parameters of KNO ₃ salt-PCM	64
5.4	Effect of dispersants on TES parameters of KNO ₃ salt-PCM.	68
5.5	Melting point and Latent heat of fusion of PCMs predicted by CACCA method	84

NOMENCLATURE

A	Surface area of the sample/Probe, m ²
BL _F	Fourier Baseline
C _p	Specific heat capacity at constant pressure, kJ/kg.K
CR _p	Cooling rate reversal point
C _v	Specific heat capacity at constant volume, kJ/kg.K
f _s	Solid Fraction
H	Heat release rate, W
k	Thermal conductivity, W/mK
L	Latent Heat , kJ/kg
M	Mass of the sample, kg
m	ratio of time steps for heat flux and temperatures
n	number future time temperatures
nf	nanofluid
np	nanoparticle
ns	nanolayer region
q	Heat flux, W/m ²
Q	Heat Transferred per unit mass, J/kg
r	Radius of cylindrical sample, m
R ₁	Distance of thermocouple 1 position from mould wall, m
R ₂	Distance of thermocouple 2 position from mould wall, m
s	Base salt

T	Temperature, °C
t	Time, s
t _e	Time at solidus point, s
T _n	Calculated Temperature, °C
t _s	Time at liquidus point, s
U	heat transfer coefficient, W/m ² .K
W	Mass fraction
Y _n	Measured Temperature, °C
Z _c	Newtonian Baseline
α	Thermal diffusivity, m ² /s
ρ	Density of material, kg/m ³

1. INTRODUCTION

Energy crisis being an inevitable scenario in coming years, renewable energy sources are hope for the future. Increasing societal and industrial energy demands, shortage of fossil fuels, and concern over environmental impact are providing impetus to the development of renewable energy sources such as solar, biomass, and wind energy. There is an urge among the developed and developing economies to develop and deploy sustainable energy systems. Currently the renewable energy technologies are highly expensive and unpredictable. Development of many solar power plants in various locations in India is an indication that dependence over the conventional sources of energy will not help the economy meet its energy demands in coming years. So, the indigenous development of all necessary infrastructure and technical know-how is of prime importance.

Considering the unpredictability of renewable energy sources such as solar and wind power, the technologies to buffer the mismatch between the energy demands and the supply are extensively studied, and has attracted huge investments. Energy storage technologies have emerged to be the most convincing in our pursuit of stable, reliable, robust and un-interrupted energy supply.

Thermal energy storage (TES) systems cannot be considered as a non-conventional source of energy but, as a method to reduce the loss of generated energy in the form of heat. It contributes in designing more efficient energy systems. They function as source of energy in solar power plants where, during night, the primary heat is received from TES systems.

Due to the unpredictable energy output of renewable energy-based systems, reliable, robust and efficient energy storage units need to be an integral part of these systems. Development and production of commercial heat storage units are rather labor-consuming and long-term processes, demanding attention of scientists and experts of various specialties. TES systems have found importance in several engineering applications other than solar power plants such as in off-peak electricity storage, solar

water/air heating systems, solar green house, solar cookers, spacecraft thermal control applications, building applications, space cooling, ice storage, conservation & transport of sensitive materials etc.

Solar technologies are broadly characterized as either passive solar or active solar depending on the way they capture, convert and distribute solar energy. Active solar techniques include the use of photovoltaic panels and solar thermal collectors to harness the energy. Passive solar techniques include orienting a building to the Sun, selecting materials with favourable thermal mass or light dispersing properties, and designing spaces that naturally circulate air.

Solar power is the conversion of sunlight into electricity, either directly using photovoltaic cells (PV), or indirectly using concentrated solar power (CSP). Photovoltaic cells convert light into electric current using the photoelectric effect. Concentrated-solar technology systems use mirrors or lenses with tracking systems to focus a large area of sunlight onto a small area. The concentrated light is then used as heat or as a heat source for a conventional power plant (solar thermoelectricity).

CSP is unique among renewable energy generators because even though it is variable, like solar photovoltaics and wind, it can easily be coupled with thermal energy storage (TES) systems as well as conventional fuels engines, making it highly dispatchable. By coupling TES with a CSP plant, the thermal energy can be stored for later use to drive a heat engine.

The absence of accurate and reliable data on the cost and performance of renewable power generation and storage technologies is a significant barrier to the uptake of these technologies. Providing this information will help governments, policy-makers, investors and utilities make informed decisions.

1.1 STATE OF THE ART IN THE FIELD

1.1.1 Energy storage technology : World Scenario

Energy storage technologies have been widely appreciated as they offer an increase in the efficiency and decrease in levelised cost of energy (LCOE) in sustainable energy systems. Their impact on concentrated solar power technology has been extensively analyzed. There are several CSP plants under construction in USA and North Africa with Spain being the largest producer of electricity using CSP technologies. [Irena (2012)]

Direct solar radiation is necessary to generate electricity in CSP plants. Only direct solar radiation can be concentrated to generate electricity in CSP plants. This restricts CSP units to hot and dry regions. To be economically feasible a CSP plant needs direct normal irradiance levels (DNI) of 2 000 kWh/m²/year or more. Lower LCOE is expected from the CSP plants located in regions with high DNI compared to that from plants located at regions with low DNI, provide all other parameters are equal. Higher levels of DNI have a good influence on the LCOE, although not one-to-one.

Parabolic Trough plants have very low capacity factors of 0.2 to 0.25. Even without provisions for thermal energy storage the parabolic trough plants have a low capital cost of US \$ 4600/kW. With inclusion of thermal energy storage units for a duration of 6 hours the capital cost would increase from US \$ 7100/kW to 9800/kW, but allows capacity factors to be doubled. CSP plants can offer power cost between US \$ 6300 and US \$ 10500/kW when TES is between 6 and 15 hours. These plants can have capacity factors as high as 0.80. [irena (2012)]

Many CSP plants are under construction worldwide accounting for more than 20 GW. Spain and the United States are the major markets for CSP power. Spain has a total installed capacity of around 2330 MW. The United States has an installed capacity of 1760 MW operational by 2017. [MENA (2018)]

Today, virtually parabolic trough systems account for the 94% of the installed CSP technology, with a capacity of 1.8 GW (approx). Solar tower plants account for around 70 MW. Spain has about 31 MW of Fresnel reflector capacity and while

Australia has about 4 MW of it. The IEA's CSP technology roadmap estimates a global CSP capacity of 147 GW by 2020, with 50 GW in USA and 23 GW each in Africa and the Middle East. By 2030 the total installed CSP capacity is expected to rise to 337 GW and then triple to 1089 GW by 2050. [Irena (2012)]

1.1.2 Energy storage technology : Indian Scenario

India receives abundant solar radiation as it is located in the equatorial belt of earth. The annual global radiation varies from 1600 to 2200 kWh/m², which is comparable with radiation received in the tropical and sub-tropical regions. The equivalent energy potential is about 6,000 million GWh of energy per year. It is observed that the highest annual radiation is received in northern Gujarat, Rajasthan and Ladakh. Andhra Pradesh, Maharashtra, Madhya Pradesh also receive fair amount of solar radiation as compared to many parts of the world such as Europe, Japan and USA where deployment of solar technologies is maximum. [<http://mnre.gov.in>]

Ministry of New and Renewable Energy (MNRE) has brought out various schemes for promoting solar power projects in different capacity ranges. Government of India launched Jawaharlal Nehru National Solar Mission (JNNSM) in January 2010 with a view to accelerate development and promotion of solar energy technologies in the country.

The first Solar Thermal Power Plant in India with a 50kW capacity was installed by MNES. It followed parabolic trough collector technology. It was installed at Gwalpahari, Gurgaon, commissioned in 1989 and operated till 1990. The plant was shut down due to lack of spares, and is now being revived. The Government of Rajasthan has sanctioned a CSP thermal plant in Mathania with a capacity of 140MW. The project involves a 35MW solar power generating system and a 105MW conventional power system with an approved grant of US\$ 40 million.

Many regions in Rajasthan, Gujarat, and Karnataka receive solar radiation of more than 2000 kWh/m²/year DNI. CSP plants would be economical at these regions as per current statistics. Improvement in TES systems and decrease in technology cost offers inclusion of a large part of Indian mainland into this as they receive 1500 to 2000

kWh/m²/year. Research on efficient TES techniques would be beneficial in India's quest for energy sufficiency.

1.2 THERMAL ENERGY STORAGE

Energy storage technology is one way to lower the levelised cost of energy (LCOE) in almost all major applications. In order to achieve this, energy storage technologies require efficient materials and high energy densities. So, prime attention should be given to improve a materials ability to receive and dispatch energy with easiness. For this, heat transfer paths should be altered by modifying thermal conductivity, thermal diffusivity, heat capacity, contact resistance etc. in the concerned energy storage technique.

Thermal energy storage can be categorized in to three types, namely,

- Sensible heat energy storage (SHS),
- Latent heat energy storage (LHS),
- Thermochemical energy storage (TCS).

SHS systems store energy by raising the temperature of a medium without causing a phase change (usually a solid or a liquid). The highest operating temperature should be below any phase change temperature. Here, the energy density of the medium is strictly by virtue of its temperature. Heat capacity and thermal diffusivity being the lone factors that determine the energy density, the rate of energy release and extraction in the TES system.

LHS systems have latent heat of fusion and coefficient of thermal expansion along with other thermo physical parameters as design parameters. Latent heat storage is almost an isothermal process that can significantly enhance the storage quantities when compared to an SHS system of same temperature range. Density of energy stored in LHS systems is 5-14 times higher to that stored in a SHS system. For example, specific heat capacity of NaNO₃ is 1.2 kJ/kg.K (approx.), while its latent heat of fusion is approximately, 177kJ/kg. Being that the storage capacity of LHS

systems is governed by heat of fusion and not just by specific heat capacity, this can offer a compact, more efficient and a lower cost alternative to SHS systems.

Thermochemical storage systems are the least investigated storage technology though it can potentially store more energy due to heat of reactions involved. These systems rely on heat to drive reversible chemical reactions. Exothermic and endothermic heat interactions are the additional features in TCS systems which are absent in LHS and SHS systems. Challenges in controlling reaction kinetics make design of TCS systems a very complex affair.

1.2.1 Phase change materials (PCM)

Every application is specific to a temperature range of concern. As per the temperature range of interest many materials have been found to be ideal candidates for TES systems. PCMs can be classified as follows. 1) Organic (Paraffin, Non Paraffin), 2) Inorganic (Salt, Salt Hydrate, Metallic), 3) Eutectic (Organic-Organic, Inorganic-Inorganic, Inorganic-Organic).

The PCM to be used in the design of thermal energy storage systems should possess the desirable thermo physical, kinetics and chemical properties which are as follows,[Sharma et al. 2009]:

- Suitable phase transition temperature
- High heat of fusion
- High heat transfer rates i.e. High thermal conductivity.
- Congruent melting
- High energy density i.e. High heat capacity
- Small change in volume during phase transition
- Low vapour pressure
- No supercooling on solidification
- Sufficient crystallization rate
- Thermal cycling stability
- Long term chemical stability
- Compatibility with materials of construction

- No toxicity
- No fire hazard
- Cost effective
- Abundant in availability

All major research carried over TES materials are focussed on technologies for attaining the above mentioned ideal properties.

1.3 ORGANIZATION OF THE THESIS

This thesis is divided into six parts. Chapter 1 gives an introduction to the research work carried out, and describes the state of the art in the concerned field. Chapter 2 gives a detailed survey of the literature, describing various types of PCMs, their merits, demerits, applications. It is followed by scope of the present investigation and the objectives of this work. Chapter 3 discusses the theory of computer aided cooling curve analysis and the inverse analysis used to study heat transfer by conduction. Chapter 4 describes the various experiments and methods used in the present investigation. Chapter 5 gives an elaborate discussion on the results attained. Chapter 6 lists the major conclusions drawn based on the results obtained.

2. LITERATURE SURVEY

A detailed survey on various aspects of latent heat storage using PCMs was carried out. Storage of thermal energy as latent heat of fusion in materials, also termed as phase change materials (PCMs) have higher prospects compared to various sensible heat storage alternatives. PCMs are classified into organic PCMs, Inorganic PCMs and their Eutectics. Their respective merits, demerits and suitability for TES applications are discussed as follows.

2.1 ORGANIC PCM

Paraffins, fatty acids, glycols, esters and their eutectics were reported to be suitable for thermal energy storage. Organic PCMs show good nucleating properties, reproducible melting and freezing cycles, and congruent melting with no supercooling. All organic PCMs have low thermal conductivity causing long freeze-melt cycles.

Organic energy storage materials are suitable for low temperature applications. This makes them unfit for energy storage in CSP plants. Low temperature energy storage technology using organic PCMs have been commercialized successfully.

A list of few organic PCMs suitable of thermal energy storage applications are shown in Table 2.1, with their melting point and heat of fusion values. These PCMs have been extensively studied for their TES prospects as described by Salunkhe and Shembekar (2012), Sharma et al (2009) and Zalba et al. (2003). Their applications varied from cold storage, packaging materials, construction materials to heat transfer systems using heat exchangers.

A Tube in Shell heat exchanger system with paraffin (melting point of 44.23°C) as the PCM was developed by Akgun et al.(2007). Here, the PCMs were filled in between the shell and outer surface of the inner tube. A heat transfer fluid was lead through the inner tube to investigate the effect of inlet temperature and flow rate of HTF. An

enhancement in heat transfer rate was achieved by changing the geometry of the storage unit. Similar investigations were carried out by Medrano et al. (2009) where a comparative study of 5 small heat exchanger systems with paraffin RT35 (35C, 157kJ/kg) was performed.

Table 2.1 : List of select organic PCMs. Sharma et al (2009), Zalba et al. (2003)

PCMs	Melting Temperature (°C)	Heat of fusion (kJ/kg)
Paraffin C14	4.5	165
Paraffin C15-C16	8	153
Polyglycol E400	8	99.6
Dimethyl Sulfoxide	16.5	85.7
Paraffin C16-C18	20-22	152
Polyglycol E600	22-24	189
1-Dodecanol	26	200
Paraffin C18	28	244
1-Tetradecanol	38	205
Paraffin C16-C28	42-44	189
Paraffin C22-C45	58-60	189
Paraffin Wax	64	173.6
Polyglycol E6000	66	190
Biphenyl	71	119.2
Propionamide	79	168.2
Naphthalene	80	147.7
Erythritol	118	339.8

Palmitic acid was studied by Sari and Kaygusuz (2002) as a PCM in a tube-in tube heat exchanger system. Flow rate and inlet temperature of heat transfer fluid (HTF) were varied in this study. Results were not attractive as the system efficiency was just 53.3%. They came up with thermal cycling studies of stearic, palmitic, myristic and lauric acids (2003). Corrosion resistance of these fatty acids with container materials like Stainless steel, carbon steel, aluminium and Copper too was investigated.

Eutectic mixtures of the above mentioned fatty acids were studied for their thermal properties and cycling reliability by Sari et al. (2004). These eutectics were reported to have good stability with respect to thermal cycling for a utility period of one year..

Paraffin binary mixtures of tetradecane and hexadecane were synthesised and used as phase change material for cool storage in district cooling systems by Bo et al.(1999).

PCMs such as the organic PCMs and Salt PCMs have low thermal conductivity. This results in decreased heat transfer rates. Modifications such as sulfonation (Alkan 2006), addition of expanded graphite (Zhang et al. 2011) successfully improved thermophysical properties of paraffins.

Techniques to enhance heat transfer rates in PCMs have been investigated in the past. Salunkhe et al. (2012) listed few techniques to enhance heat transfer rates, and they are:

1. Use of fins
2. Inserting high conductivity metal-matrix into PCMs
3. Dispersing high conductivity particles into PCMs.
4. Microencapsulation of PCMs

Encapsulation of PCMs can be classified based on its size.

- (i) Macro (above 1 mm)
- (ii) Micro (1-1000 μ m)
- (iii) Nano (1-1000nm)

Micro encapsulation is primarily done to hold the liquid or the solid phase of the PCM, and to isolate it from the surrounding. This prohibits its reaction with the surrounding. Phase segregation on melting is reduced to a great extent. Other advantages of encapsulation involve the enhancement in heat transfer rates, thermal reliability for large number of cycles, improved mechanical stability, avoid the spillage of PCM when in liquid state etc. Most of the organic PCMs are flammable.

The flammability can be reduced by encapsulating the PCM with inorganic material. (Salunkhe et al. 2012)

There are physical and chemical methods to microencapsulate the PCMs. Spray drying, Centrifugal method and Fluidized bed method are the major physical methods of microencapsulation. In situ polymerisation was reported to be the most accepted chemical method for microencapsulation due to its excellent shell structure and smaller capsule size. Interfacial polycondensation and complex coacervation being the other chemical methods for microencapsulation of PCMs. Encapsulation shell material, core to coating ratio and the encapsulation geometry are the major factors that influence efficiency in TES applications. A critical review of these parameters was reported by Salunkhe et al. (2012).

Brown et al. (2003) microencapsulated dicyclopentadiene with urea formaldehyde via, in situ polymerisation technique. Microcapsules of 10-1000 μ m in diameter were prepared by appropriate selection of agitation rate from 200-2000rpm. Surface morphology and shell wall thickness were analyzed. Bey et al. (2014) investigated the effect of varying the PCM weight fractions.

In building applications, these microencapsulated PCMs are incorporated with the construction materials. They reduce the load on space cooling systems. The capsule shells remain stable and ensure leak tightness (Zhang et al.2012, Xue et al.2009). So, these materials are referred as form stable or shape stabilized PCMs.

Dispersion of the encapsulated PCMs in HTF can increase the heat transfer rate. PCMs can then be pumped back to store or release the thermal energy. Such a mixture is called a Phase Change Slurry (PCS). Microencapsulated PCS with paraffin as the PCM (Gschwander et al.2005, Yang et al. 2003) were investigated for their thermal reliability and material compatibility with a heat exchanger and piping system.

Utilization of granulated phase change composite materials of 1-3mm diameter (GR27, GR41) was carried out by Rady (2009) for packed bed thermal energy storage.

Xuan et al. (2009) developed a novel type of suspension of magnetic microencapsulated phase change material (MMPCM) which possesses the advantages of a microencapsulated phase change material (MPCM) and a magnetic fluid (MF) for controllable and efficient energy transport processes. They investigated the effects of mass fraction of components in MMPCM and external magnetic field on the thermal properties of the fluid.

2.1.1 Organic Nano-PCMs

Nano materials have attracted many researchers throughout the world for their superior properties and compatibility to many applications. Nano PCMs are the latest in the league of potential candidates for thermal energy applications. The introduction of nano structures (Nano particles, Nano tubes, Nanofibers) into PCMs offer significant enhancement of material functionalities, which being the focus of thermal energy storage material research in recent times. Many researchers have reported significant enhancement of material properties, especially the thermal conductivity in PCMs. Encapsulating the PCMs into structures of nano size is another method to enhance heat transfer rates. Most of the publications do not consider PCMs encapsulated to nano dimensions as nano PCMs, as no nano structures have been introduced. Here, we shall discuss them as Nano PCMs because the enhancement in material functionalities concerned to TES applications is significant on nano encapsulation of PCMs.

Fang et al. (2009) prepared Nano capsules (100nm) of n-tetradecane with urea-formaldehyde shell by insitu polymerisation method, with Sodium dodecyl sulphate as the emulsifier and resorcin as the system modifier. Decrease in subcooling was reported with good heat of fusion for the novel PCM. Thermal stability studies showed that 2-5% of NaCl by wt. of PCM sample improved the efficiency of nanocapsules.

Harikrishnan et al.(2012) added CuO nanoparticles of varying sizes (1-80nm) into Oleic acid from 0.5 to 2.0 % by wt. of PCM sample. The solid-liquid composite phase

change material was tested for its suitability in TES applications. An enhancement in heat transfer rates were reported. A decrease of 28.57% and 27.67% in melting and freezing time respectively were the most significant result obtained, on addition of 2% of CuO particles by wt. of PCM sample. Similar to this, Wu et al. (2009) prepared nano fluid with Al₂O₃ particles dispersed in water. Thermal response tests showed a drop in subcooling and freezing time of the PCM. 0.2% of nano particles by weight in water caused a reduction in freezing time by 20.5%. They reported that this PCM was suitable for TES in cooling systems. Kodadadi et al. (2007) carried out simulation studies of melting-freezing of nano fluid composed of Cu nanoparticles dispersed in water. They reported that simultaneous increase in thermal conductivity and reduction in heat of fusion offered higher heat transfer rates.

Investigations by Cui et al.(2011), Ho and Gao (2009), and Kim and Drzal (2009) prove the increase in thermal conductivity of PCM on addition of nano structures in paraffins. In addition to this Cui et al. (2011) reported that CNFs were more effective compared CNTs due its better dispersion in the PCM matrix. Addition of Al₂O₃ particles had no effect on melting-freezing parameters of paraffin (Ho and Gao 2009). Qingwen et al. (2008) reported higher thermal stability for Nano PCMs. They added Ag nano particles in to Aminoplast, the shell material, used to encapsulate the bromohexadecane paraffin. The PCM was prepared by in situ polymerisation method. Wu et al. (2012) investigated numerically and experimentally the effect of Cu nano particle additions on the solidification parameters of paraffin PCMs. Increase in thermal conductivity and heat transfer rates with decrease in freezing time was reported.

Salaun et al. (2008) reported a decrease in thermal conductivity of PCMs on addition of polymer nano particles. Paraffin encapsulated with melamin-formaldehyde resin were introduced with poly (vinyl) alcohol/hydrated salts cross linked by diisocyanate. The novel PCM showed improvement in mechanical properties with no considerable change in its heat of fusion.

Recently, Babaei et al. (2013) utilized molecular dynamic simulations to investigate the relationship between the structure of paraffins in solid and liquid states and its thermal conductivity. They observed that upon crystallization a nano crystalline

paraffin structure develops and the thermal conductivity doubles. CNT and Graphene additions enhanced the thermal conductivity of the paraffin. This enhancement was not only due to conductive fillers, but also due to the filler-induced alignment of paraffin molecules.

From the above discussion it is observed that the nano encapsulation and additions enhance thermal conductivity of PCMs significantly. This would offer better heat transfer characteristics at TES set ups. So far, the influence of these nano additions on various TES aspects have been extensively studied for low temperature applications. The findings promise tremendous improvement in energy storage technology for high temperature applications as well.

2.2 INORGANIC PCM

Major phase change materials with thermal energy storage potential in this category are salt hydrates, salts, metals, their eutectics and their binary mixtures. Inorganic PCMs have higher heat of fusion and thermal conductivity in comparison with their organic counterparts. This makes them more attractive for thermal energy storage applications. They offer materials over wider range of temperatures. Salt hydrates and their eutectics, with melting temperatures up to 150°C, are suitable for lower temperature applications. Salts and metals can be used for temperature ranges up to 900°C.

2.2.1 Salt Hydrate PCMs

Salt hydrates are crystalline solids composed of inorganic salts and water of crystallization with a general formula $AB \cdot nH_2O$. The phase change associated with salt hydrates is the liquid-solid transition of the water of crystallization. It must not be confused with the actual melting/freezing of the inorganic salts present in them. This is the reason for lower heat of fusion in salt hydrates compared to that of corresponding salts.

The major challenge is the incongruent melting of salt hydrates. The inorganic salt separates out on melting of crystallized water, and settles down. The released water of crystallization is not sufficient to dissolve all the produced salt. Another problem common to salt hydrates is that of supercooling. An undercooling of 5-10°C can reduce the enthalpy stored to very large extent. Thickening gels and nucleating agents are commonly added to minimize or eliminate the above discussed problems.

Inorganic salts are suitable for high temperature TES applications such as in solar power plants by virtue of their higher melting temperatures. Binary mixtures of these salts can be designed to meet the specific temperature requirements. Most of the inorganic salts are corrosive in nature. Fluorides and chlorides are the major corrosive halides. Ceramic coatings to the container walls can decrease the corroding effect, but they decrease the effective heat transfer rates.

Incongruent melting of Sodium Acetate Trihydrate was eliminated by using thickening agents and gellants such as bentonite, starch and cellulose (Cabeza et al. 2003). They found that cellulose was not effective above 65°C. Addition of $\text{Na}_2\text{HPO}_4 \cdot 7\text{H}_2\text{O}$ eliminated supercooling but, the heat of fusion was lowered. Similar studies were carried on Glauber's salt with polyacrylamide and gelatin gel (Gok et al. 2006), and borax (1-2%) as the nucleator. Thermal analysis showed improvement in thermal properties.

Phase diagrams of $\text{NH}_4\text{NO}_3\text{-LiNO}_3\text{-H}_2\text{O}$ and $\text{NaNO}_3\text{-LiNO}_3\text{-Mg(NO}_3)_2$ were predicted (Li et al. 2010) with eutectics at 15°C and 25°C respectively.

2.2.2 Salt PCMs

Glatzmeir et al. (2011) carried out an intensive study over mixtures of inorganic salts suitable for cascaded PCM arrangements in solar power plants for a temperature range of 300-400°C. Homogenous samples of $\text{KNO}_3\text{-KCl-KBr}$, NaCl-KCl-LiCl and $\text{MgCl}_2\text{-KCl-NaCl}$ were prepared and their thermal properties and thermal stability were investigated. Chemical stability of the container material with molten salt was evaluated in controlled atmosphere furnace under N_2 gas.

Michel and Pitz-Paal (2007) experimentally analyzed the suitability of PCMs like NaNO_3 , KNO_3 and eutectic of KNO_3 - KCl in cascaded latent heat storage systems. He reported that NaNO_3 had superior characteristics in terms of heat of fusion and corrosiveness. Simulation of cascaded PCM systems was done to compare its effectiveness over non cascaded PCM systems.

The charging and discharging of various salt-PCMs suitable for CFLR, MTSA and parabolic trough collector systems were modeled and analyzed for a range of 500-1300°C by Hoshi et al. (2005). Cost effectiveness of these systems was also analyzed.

Morisson et al. (2008) investigated the heat transfer and fluid flow parameters in the latent heat storage units adapted to direct steam generation technology with numerical simulations. Potential of new PCM composites were analyzed along with it.

Herrmann et al. (2004) carried out a study to evaluate a concept, where another liquid medium (less expensive) such as molten salts was used as a storage medium rather than the HTF itself in a solar thermal power plant with 2 tank storage system (where HTF also serves as storage medium). The salts used were as follows. Hitec, a ternary mixture of NaNO_2 , NaNO_3 and KNO_3 solidifying at 120 °C; Hitec XL, a ternary mixture of $\text{Ca}(\text{NO}_3)_2$, NaNO_3 , and KNO_3 , solidifying 130 °C; and a binary salt mixture of NaNO_3 and KNO_3 , solidifying at 220 °C. Detailed performance and cost analysis found no major barriers to realize this concept.

Liu et al. (2014) compared six gaseous and liquid HTFs to assess their suitability for its application in a high temperature thermal storage system with flat slabs of PCMs. Based on the capacity rates the liquid sodium (99.4%) was identified as the best HTF. It delivered the highest electrical energy to the grid. Solar salt achieved a value of 93.6%. The gaseous fluids of atmospheric air, air at 10 bar and steam at 10 bar achieved between 87.9% and 91.3% of the ideal delivered electricity. This study showed that gaseous fluids are comparable to liquid HTFs in PCM storage facilities.

Table 2.2: List of salts with melting temperature and heat of fusion.[Kenisarin (2010)]

Metal	Flouride	Chloride	Sulphate	Nitrate	Carbonate
Melting Temperature (°C)					
Lithium	849	610	858	253	732
Sodium	996	801	884	307	858
Potassium	858	771	1069	335	900
Magnesium	1263	714	1137	426	990
Calcium	1418	772	1460	560	1330
Heat of Fusion (J/g)					
Lithium	1041	416	84	373	509
Sodium	714	482	165	177	165
Potassium	507	353	212	88	202
Magnesium	938	454	122	-	698
Calcium	381	253	203	145	-

The most critical problem for the molten salt solar power plant is the freezing of HTFs in the flow pipes and equipment. A candidate way to solve these problems is cold filling. Liao et al. (2014) simulated the cold filling of molten salt into a receiver tube by integrating the volume of fluid method and the enthalpy method. The detailed mechanism of melting-solidification was demonstrated. Further, the evolution of pressure drop along the tube was demonstrated as well. The influence of cold filling on the temperature across the tube wall was analyzed as well. This study gives practical reference to the application of cold filling in molten salt receiver.

Laing et al.(2011) proposed a three-part storage system where a phase change material (NaNO_3) storage will be deployed for the two-phase evaporation, while concrete storage will be used for storing sensible heat, i.e. for preheating of water and superheating of steam. After 172 cycles no degradation was detected with a melting temperature of 306°C .

Expanded graphite additions had influence over the TES prospects of NaNO_3 , KNO_3 , their binary mixtures (Xiao et al. 2013), and on their eutectic mixture (Bauer and Tamme 2006). The enhancement of thermal conductivity was reported in both cases.

2.2.3 Metallic PCMs

Low heat conductivity, corrosivity, the significant change in volume on melting, considerable overcooling and high cost are the major limitations of a salt-PCM when used for high temperature applications. Metals, as a rule, are devoid of these limitations. Although they have lower density of heat storage by mass, in comparison with the salt-PCMs, metals are potential candidates for TES applications. One of the pioneering works on metallic-PCMs was performed by Birchenall and Reichmann (1980). The suitability of binary and ternary alloys of Al, Cu, Mg, Si, and Zn over a wide temperature range from 616K to 1219K was investigated. It was reported that the alloys rich in Si or Al offered the highest heat storage densities on a mass or volume basis. Their reported outstanding storage density of 774kJ/kg at 1219K for Mg₂Si-Si eutectics.

Later, similar studies with eutectics of Al, Ca, Cu, Si, Mg, and Zn were carried out by Farkas and Birchenall (1985). Eutectic temperatures of all the alloys were reported and the heat of fusion of the new eutectics and intermetallics were measured.

Wang et al. (2006) used the Al-20%Si and eutectic Al-12%Si as PCM for units set to shift peak electrical loads. A novel high temperature phase change heater was developed. The results showed Al-12%Si was suitable for such applications.

Table 2.3: List of few metal alloys with melting temperature and heat of fusion.

Allos (wt%)	Melting Temperature (°C)	Heat of Fusion (J/g)
46.3 Mg - 53.7 Zn	340	185
96 Zn -4.0 Al	381	138
34.6 Mg – 65.35 Al	497	285
60.8 Al – 33.2 Cu – 6.0 Mg	506	365
64.1 Al -5.2 Si – 28 Cu - 2.2 Mg	507	374
68.5 Al – 5.0 Si – 26.5 Cu	525	364
66.92 Al – 33.08 Cu	488	372

Thermal reliability and corrosion studies were carried by Sun et al. (2007) with Al-34%Mg-6%Zn alloy as the metallic PCM. SS304L and SteelC20 were selected as the PCM container materials. After 1000 cycles an undercooling of 3-5.3°C was observed

with a drop in enthalpy up to 10.98%. SS304L was reported to be more suitable for this PCM in long term TES applications.

A novel reflux heat transfer system (RHTS) was developed and tested by Adinberg et al. (2010) for producing superheated steam (350-400°C). Zn-Sn alloy was used as the PCM which gradually melted between 200-370°C. TES properties were measured using lab scale apparatus.

Recently, Kotze et al. (2013) came up with a concept that integrated TES unit and steam generation into a single unit. Eutectic mixture of Na-K was found to be a suitable HTF for this purpose. Eutectic Al-12%Si alloy was used as the PCM. Thermodynamic and heat transfer analysis showed that the concept was viable.

2.3 NANOSALT-PCMs

Salt PCMs have poor thermal conductivity and low viscosity which decreases their potential as an ideal TES material. The development of salt PCMs with dispersed nano-sized particles, also termed as Nano-salts, has offered promising enhancements in certain energy storage functions. Solid particles are added as they conduct heat much better than the base liquid. The settlement of particles is the major limitation of such fluids. In comparison to micro particles, the nano sized particles are expected to stay suspended for a much longer duration of time due to their high surface area/volume ratio which is 1000 times larger than that of micro sized particles. On account of its large surface area, the nanoparticles offer higher heat transfer rates.

Nano suspensions can be prepared through two methods: a single step method which simultaneously makes and disperses the nano particles into the base fluid and a two-step method where the nano powders are manufactured prior to its physical addition into the base fluid. In either case, a well-mixed and uniformly dispersed nanofluid is required to enhance the relevant properties, Das et al. (2008).

A significant account of various effects of nano particle additions on thermo-physical properties of the base fluid, its effect on properties such as thermal conductivity and

specific heat capacity has been discussed in the literature. Many researchers have reported a considerable increase in the thermal conductivity of base fluids on addition of nanoparticles. The effects of concentration of nano additives, their size, their stability, etc. on thermo physical properties of base fluid have been reported. Nanofluids of water and other organic liquids have shown an increase in the thermal conductivity, and a simultaneous decrease in the specific heat capacity, Das et al. (2008), Hentschke (2016). However, nanofluids with molten salts as the base fluid have not been reported of any increase in thermal conductivity. Instead they have shown a decisive increase in the specific heat capacity property, Lasfargues et al. (2015). It is evident that the specific heat capacity of salt mixtures is enhanced by every type of nanoparticle used, Hentschke (2016).

Cheiruzzi et al. (2013) prepared eutectic nanosalts of NaNO_3 and KNO_3 with various nano particles such as SiO_2 , Al_2O_3 , TiO_2 and $\text{SiO}_2\text{-Al}_2\text{O}_3$ mixture. An increase in specific heat capacity was reported for all concentrations of nanoparticles. In addition, a drop in melting point of the PCM was reported as well. For an optimum concentration of $\text{SiO}_2\text{-Al}_2\text{O}_3$ nanoparticles an increase in specific heat capacity was reported. Specific heat capacity increased by 57% in solid phase and by 22% in liquid phase. The effect of SiO_2 nanoparticles alone was analysed by Cabedo et al. (2014). They reported a 25% increase in the specific heat capacity of the PCM when loaded with nano particles constituting 1% by weight of the sample. It is observed that many researchers suggest an optimum concentration of nanoparticle to attain an increase in heat capacity, above which the property value is observed to drop. Cabedo et al. (2014) investigated the thermal stability of nanosalts. 8 successive thermal cycles of PCMs were performed. A theoretical model based on formation of nano layers was assumed to explain the observed increase in the specific heat capacity of nanosalt-PCMs. According to the model, the salt ions order themselves around the nanoparticles due to electro statical interactions forming fractal like structures, Lasfargues et al. (2015), Cabedo et al. (2014).

Lasfargues et al. (2015) studied the effect of CuO and TiO_2 nano particle addition to the Solar Salt, the eutectic mixture of potassium nitrate and sodium nitrate. Both type of nano particles caused an increase in specific heat capacity (SHC) separately.

However, their effect with the variation in particle concentration level differed. The increase in SHC on addition of CuO particles decreased with the increase in concentration of CuO in the base fluid. This dependence on concentration level of nano additives was not observed in the PCM with TiO₂ additives. The enhanced SHC values were retained even on increasing the TiO₂ concentration level. This result was different from the general understanding of a requirement of an optimum concentration of nano additives for enhancing the SHC value of salt-PCMs. TiO₂ particles were observed to form networks in the base fluid while the CuO particles formed agglomerates.

Carbon nanostructures were dispersed in salt-PCMs to study their effect on thermal characteristics of the base salt. Addition of MWCNT increased the SHC values of both the liquid and solid phase of eutectic mixture of lithium carbonate and potassium carbonate as reported by Jo and Banerjee (2015). The enhanced SHC values were observed to be in proportion to the increase in concentration of MWCNT. The MWCNT concentration was varied from 0.1% to 5% of the sample weight, and observed the SHC value was observed to increase with the additive concentration which is another example of deviations from the general notion of optimum concentration level of nano additives for SHC enhancement. In the reports discussed earlier the SHC values increased by 20-50% on nano particle addition. However, in this case the increase in SHC was marginal, with an increase of SHC by 5% in liquid phase and by 12% in solid phase of the salt-PCM. Xe et al. (2016) dispersed graphite nanoplatelets in the solar salt and observed an increase in SHC value by 16.7% in liquid phase. They reported a considerable decrease in the solidification temperature on nano addition.

Nanosalt PCMs can also be modified by preparing its composite with a ceramic support material. A ceramic support material is used to enhance the shape and structural stability of PCMs, while the nano particles enhance the thermophysical properties. A composite of Li-Na carbonate eutectic salt with MgO as the support material, and nano additives of graphite flakes and CNT were prepared by Ge et al. (2014). Uniaxially compressed green pellets of these composites were prepared. They were sintered at 550°C. The samples were experimented over 28 thermal cycles

which did not show any significant change in transition temperatures, mass or heat of fusion promising a good chemical and thermal stability. They observed that the support material would rearrange itself in the PCM composite and increase the bulk density, as it wets significantly with the liquid salt. However, due to poor wettability of liquid salt on the graphite flakes and CNT nanoparticles, they tend to form networks like chain structures which would increase the bulk density. These effects counter each other and ensure minimal changes in bulk density of the PCM composite. The PCM composite showed an increase in thermal conductivity to 5W/mK and 4.3 W/mK for a carbon loading of 20% and 10% by weight respectively. On the same lines Ye et al. (2014) studied the effect of MWCNT additions to Na_2CO_3 salt with MgO as the support material. Thermal conductivity of the nano composite was observed to increase from 0.75 to 0.901, 0.976, 1.048, and 1.127W/mK for MWCNT composition of 0.1%, 0.2%, 0.3% and 0.5% by weight of the sample respectively. They observed that the thermal conductivity of the composite increased with the temperature. The convective and radiative heat transfer in the porous support material and in the associated pores were attributed for the increase in thermal conductivity. These are the very few studies that report a thermal conductivity enhancement in salt-PCMs on addition of nano structures.

Wang et al. (2006) investigated the effect of particle size and temperature on the SHC values of the nanosalt-PCMs. They reported that the SHC values increased with the temperature, and was inversely proportional to the size of the particles dispersed. i.e. lower the nano particle size higher is the SHC value enhancement.

It is hypothesised that ions in the molten salt form nano layers, a network like ordered layers near the surface of nano particles, is attributed to the anomalous rise in the SHC values. This interfacial layer is semi-solid in nature. The nanolayers alone cannot cause the rise in SHC values as they have a lower SHC value compared to that of the base fluid. Higher SHC values of the Nano-salt PCMs are due to the heat of fusion of the salt entrapped in the semi-solid region. The ordering of liquid atoms adjacent to an interface with a crystal has been a topic of discussion for a long time. Oh et al. (2005) observed this in system of liquid aluminium with dispersed alumina particles. The ordering of liquid Al atoms at the solid-liquid interface was recorded using a HR-

TEM. With that evidence, the theory of nano layer formation and its role in enhancing the SHC values became more authentic and reliable. The increase in SHC in solid phase can be attributed to the effect of higher temperature of the PCM.

Shin and Banerjee (2014) observed the peculiar chain-line structures (nano layers) in the SEM images of nano salt after a melting-solidification cycle. The same structures were not found in the base salt sample and had proposed a modified model for SHC as shown in the Eq. (1).

$$C_{P_{nf}} = W_{np} \cdot C_{P_{np}} + W_{ns} \cdot C_{P_{ns}} + (W_s - W_{ns}) \cdot C_{P_s} \quad (1)$$

where, nf= nanofluid, np= nano particle, ns = nano layer region, s = base salt, W= mass fraction.

A meso layer theory was proposed by Henstchke (2016) which assumes the influence of the nano particles in the surrounding liquid over a long range. A marginal increase in the SHC in these layers of ordered atoms in the surrounding liquid can increase the overall SHC considerably provided the nano particles had a long range influence. These layers can overlap as the concentration of the nano particles rise. It could explain the peak in the SHC v/s Concentration of nano particles observed in many publications.

Another possibility of higher SHC of the PCMs are the nano particles themselves, Lasfargues (2015). The nano particles have higher SHC values compared to that of the coarse grained crystals of the same material. The SHC of a material is related to its structure. The vibrational and configurational entropy which is limited by the surroundings or neighbour configurations contribute into the SHC of the particle. The nano grained structures in nano particles expose more atoms to the surface as they possess higher surface area to volume ratio. The surface atoms are less constrained when compared to the atoms at the centre. Therefore, the nano particles have higher energy structures compared to the coarse grained crystals. Atoms at the surface of nano particles have excess volume to expand. Their thermal expansion too has been recorded to be twice as that of the latter. Wang et al (2001) proved this by comparing the infrared spectrum of nano sized Al_2O_3 with that of a coarse grained Al_2O_3 . A blue

shift in the wave number of the nano grained Al_2O_3 was recorded which emphasises that the nano particles possess higher energy compared to the perfect crystals.

Tan et al (2009) studied the heat capacity enhancements in certain metal oxide, metal and zeolite nano materials, and compared it with their coarser crystals. The nano grained materials offered higher SHC compared to the latter which can be attributed to the excess volume in the nano particles. Many other factors such as density, thermal expansion, sample purity, surface absorption, size effect etc had considerable effect on the property enhancement.

Interfacial thermal resistance could also contribute into the enhancement of heat capacity. Nano particles with high surface area would possess more energy at the surface. Well dispersed nano particles would offer higher energy densities compared to the agglomerated ones.

From the above discussion, it is clear that although formation of nano layers or the nano grains in the particle are the dominant cause for the anomalous rise in the specific heat capacity of the nanosalt-PCMs, there are many other factors that can pose considerable influence on it as discussed above. More studies are necessary to quantify and predict the contribution of every factor on the rise in SHC. The reliability of the results solely depends on the suitability of the measurement technique.

2.4 CHARACTERIZATION OF ENERGY STORAGE MATERIALS

Four characteristics of a PCM are:

- Temperature of phase change
- Enthalpy of phase change
- Heat capacity in solid phase
- Heat capacity in liquid phase

Most PCMs are not pure materials and melt over a range of temperature instead of melting at a temperature. It is recommended to report the stored thermal energy as a function of temperature, discussed by Mehling and Cabeza (2008). This is similar with the definition of the heat capacity as the heat stored per temperature interval of 1°C. Various methods have been used to characterize energy storage materials. They are discussed here.

2.4.1 Calorimetric methods

There are many calorimetric methods with definite advantages and disadvantages. The most commonly used are Differential Scanning Calorimetry (DSC) in dynamic mode, in step mode and the T-history method.

DSC can be based on two working principles namely as Power compensating and Heat exchanging calorimeters. Power compensating calorimeters use electrical heaters to compensate the temperature difference between reference material and sample. Heat exchanging calorimeters which are also known as the heat flux DSC (hf-DSC) are very common. They determine the difference in the heat exchanged between the ambient and the sample, and between the ambient and the reference material.

hf-DSC can be operated in 2 different modes namely, dynamic mode and step mode. In dynamic mode the temperature of the sample is varied between an initial and final value at a constant rate. Besides the hf-DSC there is another kind called the temperature modulated DSC (m-DSC). The measurement is done by modulating the sample temperature, to get a signal to determine the heat flux. The signal is not large enough to affect the investigated thermal parameter.

A major limitation of DSC is the small size of the sample, weighed in milligrams. Such small sample sizes are unsuitable for studying inhomogeneous materials. Such small sample are not representative anymore. Subcooling observed in DSC is also do not represent the subcooling reported for larger samples. A method with large sample size is mandatory to study inhomogeneous materials. Such a method is the T history method.

2.4.2 T-history method

The T-history method was first proposed by Yinping et al. (1998). It is a simple and economic way to calculate of the stored thermal energy in a PCM as a function of temperature. Here, the samples, and a reference material of known properties, are raised above the melting point of the PCM and then subjected to ambient air for cooling. Their temperature history is recorded. A comparative analysis of the curves, assuming identical heat transfer coefficients between sample and ambient, as well as reference and ambient, allows the estimation of the thermal energy stored in the sample. This method uses constant values for heat capacities, melting temperature and melting enthalpy. Marin et al. (2003) improved this method by calculating heat capacities as a function of temperature. They took the samples in temperature controlled environment, which enhanced the accuracy of the data and additionally allowed measurement upon heating, and not only on cooling. Sole et al. (2013) reviewed the evolution of T-history method and discussed in detail the various modifications in the experimental arrangement designed so far.

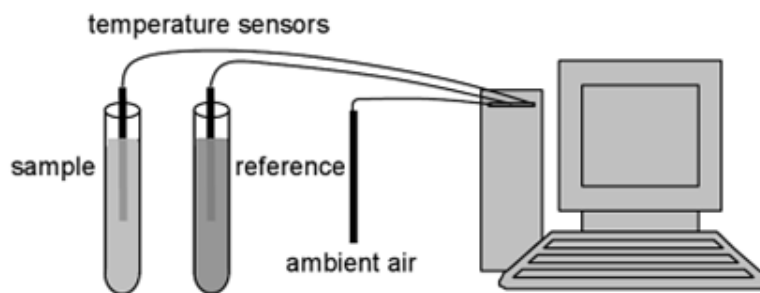


Figure 2.1: T-history set up (Yinping et al. 1998)

This technique has serious limitations that diminish its utility for high temperature studies. T-history method requires a reference material of known properties (specific heat capacity, thermal conductivity, thermal coefficient of expansion etc.) in the concerned operating temperature range.

2.4.3 Cycling stability testing

Cycling tests are performed to assess the reproducibility of phase change, also termed as Cycling Stability of PCMs. A PCM which separates on phase change will show a reduction of enthalpy of fusion after repeated cycling. If the change is significant, the PCM is declared unstable during cycling. For encapsulated PCMs, the encapsulation can be tested for leakage after repeated melting and solidification. The sample can be cycled in a thermostat or a climate chamber and be taken out after a set of cycles to measure study its response to cycling. An alternative method is to perform cycling and sample analysis in the same apparatus, similar to the cycling and testing for enthalpy in the DSC.

2.4.4 Container material compatibility/ corrosion testing

There are two aspects that should be considered while investigating the compatibility of materials with PCMs. First aspect being the leak tightness of the encapsulation and, the other being its chemical stability. These aspects should be considered for long term applications. Failure and corrosion of encapsulation material can be analyzed by measuring the change in mass using TGA.

2.5 SCOPE OF THE PRESENT INVESTIGATION

Characterization of TES materials to obtain information on its specific heat capacity and latent heat of fusion have been solely carried out using DSC by most of the researchers. This technique uses small quantity of sample (in milligrams) to determine relevant properties. The information from this test does not represent a large sample (more than 20grams). In CSP plants, TES units contain PCMs in bulk (in tonnes), which emphasis on a need to develop a novel technique to determine specific heat capacity and latent heat.

T-history method was developed in recent years [Yinping et al. (1998)], which determines heat capacities from large samples. This technique has been successfully

used to characterize low temperature energy storage materials (like organic PCMs). This technique has serious limitations that diminish its utility at high temperature studies.

T-history method requires a reference material of known properties (specific heat capacity, thermal conductivity, thermal coeff. of expansion etc.) in the concerned operating temperature range. For high temperature studies, use of water and low carbon organic compounds is not possible as they vaporize easily (at temperatures above 150°C). Low temperature melting metals, alloys (alloys of Ga, In) and, heat transfer fluids (like Liquid Na, NaK) are very expensive. High carbon organic compounds are suitable candidates but they are highly inflammable and show a rise in melting point with increase in carbon number. In addition to this, container material needs to be selected judiciously. Chemical interactions such as corrosion, needs to be studied for every pair of PCM-Container material over wide temperature range. A detailed database for this purpose is not available at present. The use of borosilicate and quartz eliminates such chemical interactions but they are brittle and are prone to failure at higher temperatures. Ceramics containers are ideal for these conditions. Unfortunately, this technique requires a cylindrical container with $L/D > 16$. Manufacturing ceramic cylinders of such dimensions with thin wall thickness to ensure higher heat transfer rates does not appear to be feasible. A survey of the literature suggests that all reference materials are suitable only over a certain temperature ranges. Developing a standard reference material suitable for a wide temperature range say, 200-1000°C appears to be impossible. These factors discussed above convincingly advocate for a novel technique to determine heat capacity and heat of fusion of energy storage materials over a wide range of temperatures.

Thermal Analysis, extensively used to analyse phase changes in a sample (large samples) from its thermal history in foundries, can be an alternative for the determination of latent heat of fusion. Newtonian and Fourier cooling curve analysis are the 2 primary methods in this technique. Along with thermal analysis, Laser Flash Technique and DSC would aid in measuring thermal diffusivity and specific heat capacity of the material respectively.

Energy Storage materials with higher thermal conductivity and thermal diffusivity would offer higher heat transfer rates during charging and discharging process. It is observed that salts (suitable for high temperature applications) have very low thermal conductivity in solid phase. This decreases heat extraction during discharging process. The addition of Nano structures into the TES material have been successfully performed and analysed in low temperature PCMs. Their compatibility and effectiveness in high temperature applications have not been studied extensively. Enhancement of heat transfer rates being very relevant, National Renewable Energy Laboratories, USA has launched a project to study the effect of nano additions on heat transfer characteristics of TES materials. High temperature ultrasonication of nanoparticle embedded molten salts is a serious challenge faced in developing such materials. Homogenization and prevention of nanomaterial agglomeration in the matrix is a complicated process at high temperatures.

Characterization of TES materials was primarily focussed on determining the enthalpy vs. Temperature curves. This approach does not throw light on various solidification parameters during heating and cooling of PCMs. These limitations have restricted energy storage research to develop single temperature transforming PCMs. Alloys and binary (or more) mixtures of salts that solidify over a temperature range have not been studied and are not considered as suitable candidates for energy storage applications. Various methods and approaches used to study directional solidification of castings in foundries would be beneficial in developing and analysing many novel energy storage materials that solidify over a range of temperatures.

Inverse Heat Conduction technique is an efficient tool to analyse heat transfer characteristics at the heat exchanging surfaces. So far, this technique has not been used to study heat transfer in TES units.

A thermal analysis technique based on Computer Aided Cooling Curve Analysis (CACCA) to characterize the solidification path of salt-PCMs can be used for quantitative measurement of thermo-physical characteristics of the investigated material. The method has an edge over other techniques as it is simple, inexpensive and yields consistent results.

2.6 OBJECTIVES OF THE PRESENT WORK

The following are the objectives of the present study.

- To assess the TES parameters of carbon based Nanosalt-PCMs
- To analyze the influence of various dispersants on performance of Nanosalt-PCMs.
- To study the response of Nanosalt-PCMs to thermal cycling.
- To compare the suitability of metallic and salt PCMs for TES applications.
- To propose a simple and novel technique for determination of heat transfer characteristics of nanosalt-PCMs.

3. THEORETICAL BACKGROUND

3.1 COMPUTER AIDED COOLING CURVE ANALYSIS

Computer aided cooling curve analysis (CACCA) is very useful in rapid assessment of various properties. It is based on the attribute that the thermal events as a heating or cooling curve are directly related to phase transformation occurring in a sample. Thermal analysis techniques monitor temperature changes in a sample as it cools through a phase transformation interval.

Thermal analysis can be very effective in creating databases on phase change materials with different chemical compositions. The method is useful for commercial applications for a number of reasons. It is simple, inexpensive and provides consistent results.

Thermal analysis can provide information about the composition of the alloy, the latent heat of solidification, the types of phases that solidify, and even dendritic coherency. There are also many other uses for thermal analysis, such as, determining dendrite arm spacing, degree of modification and grain refinement, the liquidus and solidus temperatures, and characteristic temperatures related to the eutectic regions and intermetallic phase transformations as described by Malekan et al. (2011).

There are two methods, Newtonian and Fourier that have been successfully employed to calculate latent heat and solidification fraction distribution using cooling curve analysis. The Newtonian technique does not consider the local temperature gradients developed within the sample during solidification. On the other hand, the Fourier technique incorporates the effect of thermal gradients developed during solidification. This comparison indicates that the predictions of Fourier and Newtonian methods are appreciably different. The Newtonian method uses a single thermocouple placed at the centre of the test sample while the Fourier technique uses a minimum of two thermocouples with one offset from the centre.

The primary information obtained from cooling curves are the phase transition temperatures. The first derivative curve is the most important tool in CACCA. Transition temperatures appear as a kink along with a significant change in slope in the first derivative curve. The increase in the slope due to nucleation while its drop would indicate cooling or remelting of the sample. Undercooling appears as loops while eutectic transitions appear as straight lines.

3.1.1 Newtonian Technique

The Newtonian technique is a simple method employing one thermocouple at the centre of the sample to generate cooling curve of PCMs. The assumptions used in Newtonian technique are listed below, as described by Djurdjevic et al. (2011):

- The test sample is assumed as “a lumped thermal system” with a Biot number < 0.1 . The lumped thermal system assumes a uniform temperature distribution throughout the thermal analysis test sample.
- The specific heat capacity of the PCM can be assumed as temperature independent, and constant in the melting temperature range.
- The heat transfer coefficient from the test sample to its surrounding can be characterized by the temperature function for the given experimental conditions.

The first derivative (FDC) curve of the obtained cooling curve is of prime importance. Start and end of phase transformations appear as sharp peaks in FDC. Area under FDC can be used to determine the total heat lost to the mould from the sample.

Determination of latent heat requires another curve called the Zero Curve or the Base line (Z_C). The Base line, in principle, is the derivative of a cooling curve, wherein it is understood that the sample undergoes phase transformation without the evolution of latent heat of fusion. This obviously is an imaginary line. Its calculation is a very contentious issue in CACCA. The difference in area between the FDC and Z_C is used to determine the latent heat evolved during solidification.

The heat balance equation for the solidifying sample-mould system can be written as :

$$\frac{dQ}{dt} - MC_p \frac{dT}{dt} = UA(T - T_0) \quad (2)$$

where, M is the mass of the sample, C_p is specific heat of the metal, T is the metal temperature, t is time, U is overall heat transfer coefficient, A is sample surface area, T₀ is ambient temperature, and Q is latent heat of solidification. If no heat of fusion is evolved, $dQ/dt = 0$, then the cooling rate of the test sample (first derivative of the cooling curve, FDC) can be written as:

$$\frac{dT}{dt} = \frac{-UA(T - T_0)}{MC_p} = Z_c \quad (3)$$

The curve corresponding to Eq. (3) represents the “**Newtonian zero curve**” or the **Baseline** (Z_c).

Fitting of FDC to obtain Z_c is usually done in three methods; (i) Polynomial Fitting, (ii) Experimental Fitting, (iii) Curve Fitting. Haq et al. (2004) have discussed that polynomial fitting (2^o order) and exponential fitting modes show inaccuracy and inconsistency in obtained results. On the other hand, the results obtained by fitting the FDC linearly are reproducible.

Baseline traces the same path as that by the cooling rate curve of the original sample for temperatures before the liquidus point and after the solidus point. The difference between integral areas of these two curves represents the latent heat of solidification as shown in Eq. (4). The solid fraction (f_s) can be obtained from Eq. (5).

$$L = C_p \int_{T_{liquidus}}^{T_{solidus}} \left(\frac{dT}{dt} - Z_c \right) dt \quad (4)$$

$$f_s = \frac{C_p \int_{T_{liquidus}}^{T_{solidus}} \left(\frac{dT}{dt} - Z_c \right) dt}{L} \quad (5)$$

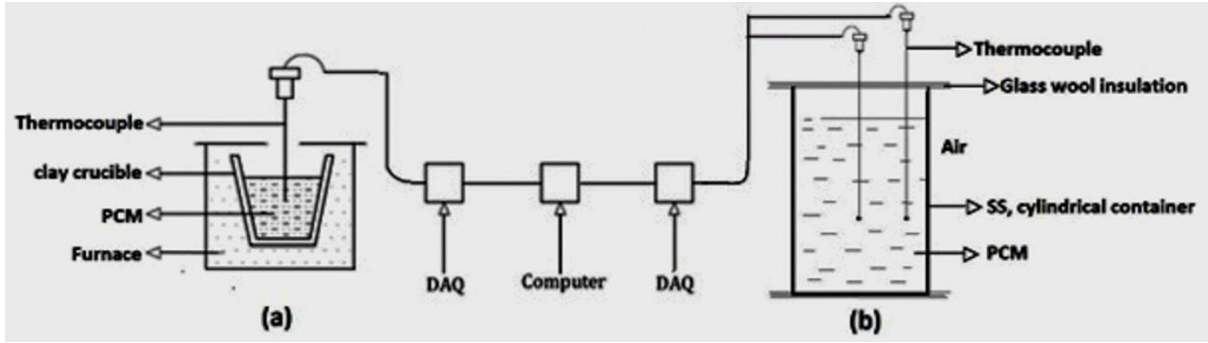


Fig 3.1: Schematic sketch of (a) Newtonian Technique, (b) Fourier Technique setups.

3.1.2 Fourier Technique

Theory of Fourier technique was first suggested by Frasz et al. (1993). The Fourier equation with heat source can be expressed as shown in Eq. (6), which can be rewritten as Eq. (7) where BL_f stands for Fourier baseline.

$$\frac{\partial T}{\partial t} = \alpha \nabla^2 T + \frac{1}{c_v} \frac{\partial Q}{\partial t} \quad (6)$$

$$\frac{\partial Q}{\partial t} = c_v \left(\frac{\partial T}{\partial t} - BL_F \right) \text{ where } BL_F = \alpha \nabla^2 T \quad (7)$$

A baseline represents an imaginary line connecting the liquidus and the solidus points in the cooling curve of the sample with an assumption of no latent heat being released on solidification. The difference in the integral area of the cooling rate curve and that of its corresponding baseline (BL_F) would represent the latent heat of solidification when multiplied with the specific heat capacity of the PCM, as shown in Eq. (11).

During transient heat conduction, the temperature within a cylindrical sample depends on axial coordinates (z , r and θ), and time t . With an L/D ratio of 4 or more the heat transfer takes place only in the radial direction (r axis). This ensures that the process is axially symmetric and temperature is independent of θ coordinate. Radial solidification of PCMs is mandatory in Fourier method.

Heat conduction equation under transient conditions, without any heat source in a cylindrical sample with an L/D ratio of 5 can be expressed as shown in Eq. (8).

Fourier technique assumes the temperature distribution at an instant of time in such sample to be parabolic, which can be expressed as $T = Ar^2 + B$, where r is the radius of the sample. This assumption can be used to compute Eq. (9).

$$\nabla^2 T = \frac{1}{r} \frac{\partial}{\partial r} \left(r \frac{dT}{dr} \right) \quad (8)$$

$$\nabla^2 T = \frac{4(T_2 - T_1)}{R_2^2 - R_1^2} \quad (9)$$

$$\alpha = \frac{\frac{\partial T}{\partial t}}{\nabla^2 T} \quad (10)$$

$$L = \int_{t_s}^{t_e} \frac{\partial Q}{\partial t}(t) dt \text{ where } \frac{\partial Q}{\partial t} = C_v \left(\frac{\partial T}{\partial t} - BL_F \right) \quad (11)$$

With temperature data obtained from thermocouples positioned at radii R_1 and R_2 , the thermal diffusivity can be obtained from Eq. (10). The CACCA technique and its mathematical equations have been discussed by Sudheer and Prabhu (2016), and Djurdjevic et al. (2011) in detail.

3.2 INVERSE ANALYSIS

Inverse analysis is used when the direct measurement of heat flux at a concerned surface cannot be done using the conventional methods.

In the current study, heat flux transients across the probe-PCM interface (probe surface) need to be measured. Inverse method is suitable for this condition. The temperature data measured at locations within the probe can be used to compute the heat flux at the probe surface. Such heat transfer problems are called ill-posed problems while, the conditions where the direct measurement of heat flux is possible are called well-posed problems or Direct problems.

Inverse heat transfer problems can be classified in accordance with the nature of heat transfer process, such as IHTP of conduction, IHTP of convection, IHTP of radiation,

their combinations, and IHTP of phase change. IHTP can be one-, two- or three – dimensional. Also, IHTP can be linear or non-linear.

In the current study, a 1-dimensional IHTP of conduction is solved where the temperature data recorded from locations within the probe is used to analyze heat conduction within the probe and, the subsequent heat flux transients at the probe-PCM interface. A non-linear estimation technique developed by Beck et al. (1985) was employed here, and is as described below.

The one dimensional transient heat conduction equation in cylindrical coordinates given below was solved inversely.

$$\rho C_p \frac{\partial T}{\partial t} = \frac{k}{r} \frac{\partial}{\partial r} \left(r \frac{\partial T}{\partial r} \right) \quad (12)$$

Where,

k is the thermal conductivity of the probe material, W/m.K

ρ is the density of the probe material, kg/m³

C_p is the specific heat capacity of the material, J/kg.K

In this inverse technique, the surface heat flux density is estimated from the knowledge of measured temperatures inside the probe. This is done by minimizing function,

$$F(\mathbf{q}) = \sum_{i=1}^m (\mathbf{T}_{n+1} - \mathbf{Y}_{n+1})^2 \quad (13)$$

Where, \mathbf{r} is the number of future time temperatures $(n) + 1$, and $\mathbf{m} = \frac{\Delta\theta}{\Delta t}$. $\Delta\theta$ and Δt are the time steps for heat flux and temperatures, respectively, Y_{n+i} and T_{n+i} are measured and calculated temperatures, respectively, at locations near to the surface where the boundary condition is unknown.

Applying the condition $\frac{\partial F}{\partial q} = 0$ on Eq. (13) for minimization, the correction for the heat flux (Δq) at each iteration step is estimated. This procedure is continued until the ratio $\left(\frac{\Delta q}{q}\right)$ becomes less than 0.001 (convergence limit). This procedure simultaneously yields the temperature of the specimen surface in contact with the PCM and the interfacial heat flux.

4. EXPERIMENTAL

4.1 NANOPARTICLES FOR NANOSALT-PCM PREPARATION

The salt-PCM (KNO_3) was mixed with the nano particles separately to study their respective effects on the TES parameters. The nanoparticles used were MWCNT (OD >50nm, ID 5-15nm, Length 10-20 μm), Graphite (400nm, 50 μm) and Graphene (Thickness 1-5nm), procured from Chengdu organic chemical Co Ltd, Chinese Academy of Sciences and from Reinste Nanoventures, Delhi. The PCM mass was fixed at 1kg for every trial into which the particle additives weighing 0.1%, 0.3% and 0.5% of the PCM weight were added. Every sample was melted and then solidified for 10 cycles to analyse the thermal-cycling effects on cooling behavior of PCMs.

4.2 NANOSALT-PCM PREPARATION METHOD

The effect of employing a high energy ball milling method for the dispersal of nanoparticles in salt-PCMs was also studied as it improves homogeneity or even dispersal of nanoparticles. Graphite nanoparticles were dispersed into the pulverized salt PCM by, (i) thorough manual mixing, (ii) using planetary ball milling. A high energy planetary ball milling facility (Retch PM100, at 150rpm, for 20min, 87 steel balls of $\phi 10\text{mm}$) was used for this purpose.

4.3 ADDITION OF DISPERSANTS INTO NANOSALT-PCMS.

The effect of dispersants on solidification of nano salt-PCM was studied by dispersing the mixtures of MWCNT particles with TiO_2 and Carbon Black separately in KNO_3 samples. The weight of MWCNT to that of TiO_2 and carbon black in their respective dispersant mixtures were 1:9 and 4:6 respectively. The commercially available dispersant-nanoparticle mixtures were procured from Chengdu organic chemical Co Ltd, Chinese Academy of Sciences.

4.4 THERMAL CYCLING TESTS

A thermal cycle consists of melting and subsequent solidification of a PCM sample. To assess the response of nanoparticle additions to the salt-PCM, thermal cycling tests were performed. Nanosalt-PCM samples were subjected to 10 successive thermal cycles. Thermal history of samples was recorded during solidification in every thermal cycle.

4.5 DESIGN OF EXPERIMENTAL SETUP FOR FOURIER ANALYSIS

In Fourier technique the PCMs must solidify radially in a cylindrical mold as described in the previous section. Length to diameter ratio (L/D) of the cylindrical mold, mold thickness and the thermophysical properties of both the mold and the solidifying material(PCM) are the factors that govern directional solidification in the PCMs. Solidification of the PCM (KNO_3) was simulated by using a simulation software, “SolidCast 8.2.0” Finite Solutions Inc. (USA). Solidification of KNO_3 in molds of graphite, SS304 and mild Steel of thickness varying from 1.5mm to 5mm, with an L/D ratio varying from 1 to 5 were simulated.

4.6 NEWTONIAN ANALYSIS

Unlike Fourier technique, Newtonian technique employed one thermocouple to record thermal history of solidifying samples. PCM samples (KNO_3) of 1kg mass were raised to 360°C and allowed to cool. A thermocouple is inserted to the centre of the solidifying sample, and the temperature values were recorded using DAQ NI9213 device with a scanning frequency of 10Hz. Laboratory prepared, calibrated K-type thermocouples enclosed in ceramic beads were used for studying ZA8 alloy while, calibrated K-type Inconel sheath thermocouples were used for studying KNO_3 . The recorded data were plotted using Origin Pro software. The obtained cooling curves were then used to analyze TES parameters of various PCMs.

4.7 FOURIER ANALYSIS

Salt-PCM sample of 1kg was melted in a resistance furnace. Molten salt sample was poured into a cylindrical mold of stainless steel at a temperature of 360°C (KNO_3). The schematic sketch of the experimental set up is shown in Figure 4.1. The mold was instrumented with two thermocouples. The temperature history of the solidifying sample was recorded using a DAQ NI9213 device with a scanning frequency of 10Hz. Laboratory prepared, calibrated K-type thermocouples enclosed in ceramic beads were used for studying ZA8 alloy while, calibrated K-type Inconel sheath thermocouples were used for studying KNO_3 . The recorded data were plotted using Origin Pro software. The cooling curves obtained were then used to analyze TES parameters of various PCMs.

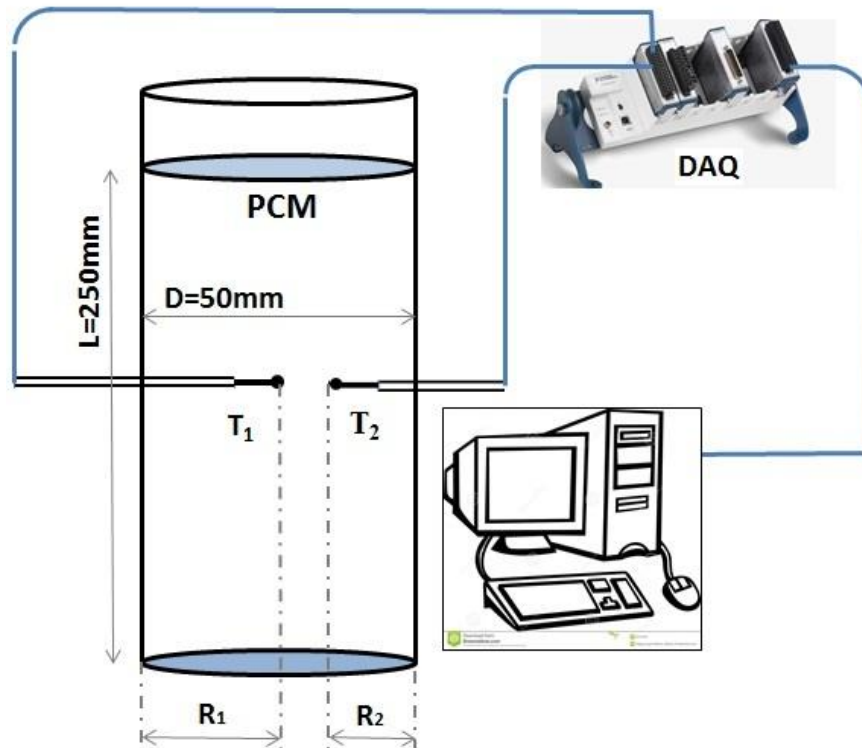


Fig 4.1: A schematic sketch of Fourier technique set up.

4.8 MICROGRAPHIC STUDIES

The specimens for micrographic study were prepared from sections of solidified PCM samples. The microstructures of each specimen at different locations were then examined using JEOL JSM 6380LA analytical Scanning Electron Microscope at different magnifications.

4.9 HOT- COLD PROBE TECHNIQUE

Cylindrical probes of Length 60mm and diameter 12.5mm (L/D of 4) were prepared of Copper and Stainless Steel (type 304). Axial holes of diameter 1mm were drilled to the mid plane of the probe to locate thermocouples during the experiment. Two series of experiments were performed. Firstly, a probe at room temperature (cold probe) is immersed into a pool of molten PCM held at 360°C. 1kg of PCM was used in every experiment. Secondly, a hot probe (at 570°C) was immersed into finely pulverized PCM (at room temperature).

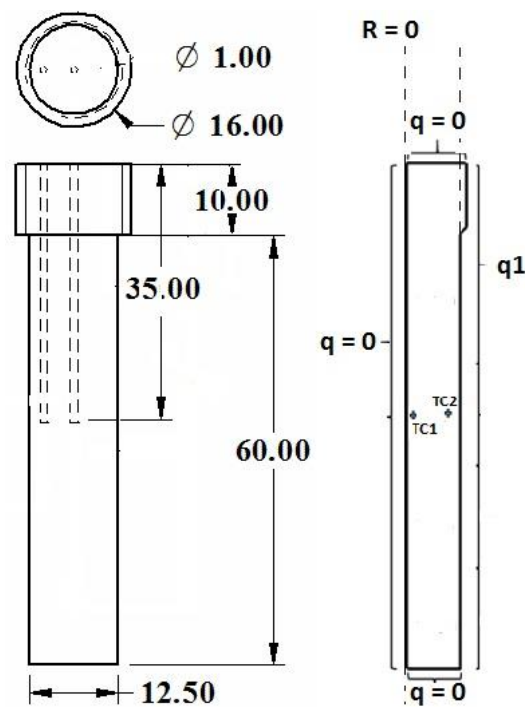


Fig 4.2: Schematic sketch of probe used in Hot-Cold Probe Technique.

The probes were instrumented with 2 thermocouples of 1mm diameter each. The temperature histories of probes were recorded in both the cases using a DAQ NI9213 device, and were processed to compute the heat transfer interactions at the probe-PCM interface. Figure 4.2 shows a 2D model of the probe. This model was used to estimate the unknown heat flux transient (q_1) using TmmFe software (Thermet Solutions Pvt. Ltd., Bangalore, India).

The model was meshed with 1 side graded four node quadrilateral elements, resulting in 448 elements on discretization. Thermophysical properties such as thermal conductivity, specific heat, and density of probe materials (Cu and SS304) were used as input to the model. The boundary surfaces represented by $q = 0$ indicate insulated boundary condition. The temperatures measured by the near surface thermocouples were assigned to locations TC (1), and TC (2), shown in the model. To obtain the inverse solution to the heat conduction problem, the procedure detailed by Prabhu and Ashish (2002), and Kumar (2004) was used.

5. RESULTS & DISCUSSION

5.1 DESIGN AND OPTIMIZATION OF EXPERIMENTAL SET UP FOR FOURIER TECHNIQUE

Radial solidification of the PCM is a mandatory criterion for accurate computation of solidification parameters in Fourier technique. Preliminary simulation studies were performed in SolidCast software to optimize the conditions for radial solidification of PCM samples in a cylindrical mold. A solid cylinder was drafted in the software which represents a solidifying PCM sample as shown in Figure 5.1. The casting material was assigned to potassium nitrate, and SS304, Mild steel and Graphite were chosen for mold material with all the necessary properties as shown in Table 5.1, Figure 5.2 and Figure 5.3. The drafted components were then discretized as shown in Figure 5.3. After simulation, the solidification history of the PCM sample was analysed.

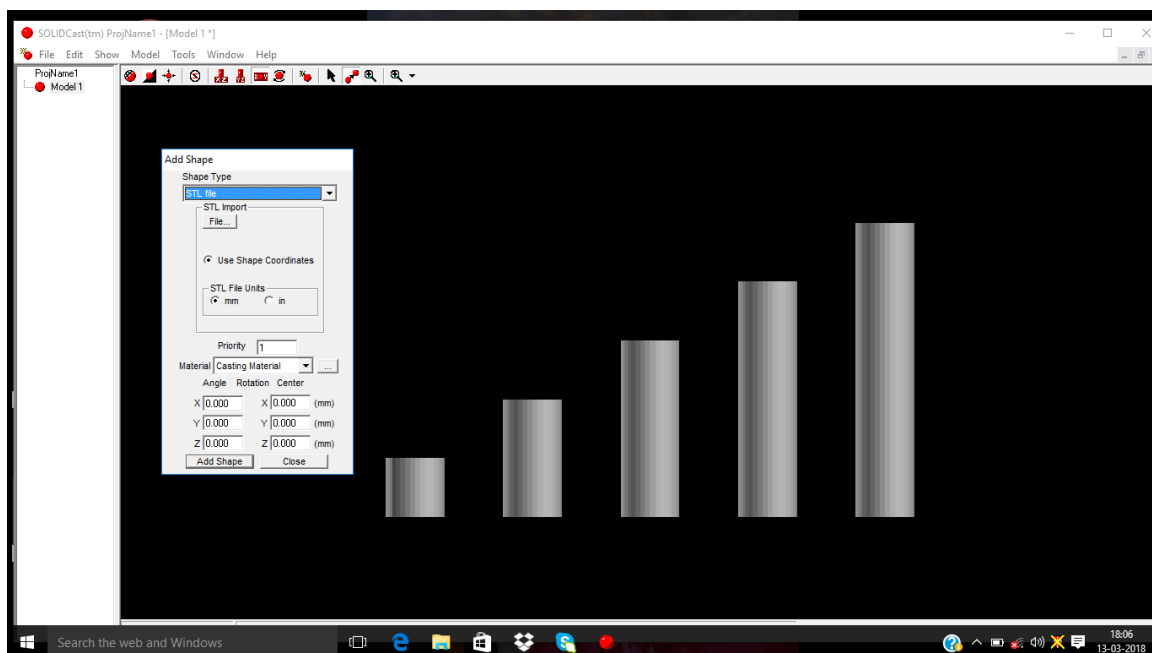


Fig 5.1: Cylindrical PCM samples with varying L/D ratios drafted in SolidCast.

Table 5.1: Relevant properties of select materials used to optimize Fourier set up.

Name	Thermal Conductivity W/mK	Specific Heat Capacity kJ/kg.K	Density Kg/m ³	Initial Temperature °C	Freezing Range °C	Latent Heat kJ/kg
Graphite	200	0.8	1300	25	-	-
SS304	17	0.5	7850	25	-	-
Mild Steel	30	0.49	7700	25	-	-
KNO ₃	0.6	0.9506	0.002	380	335°C	90

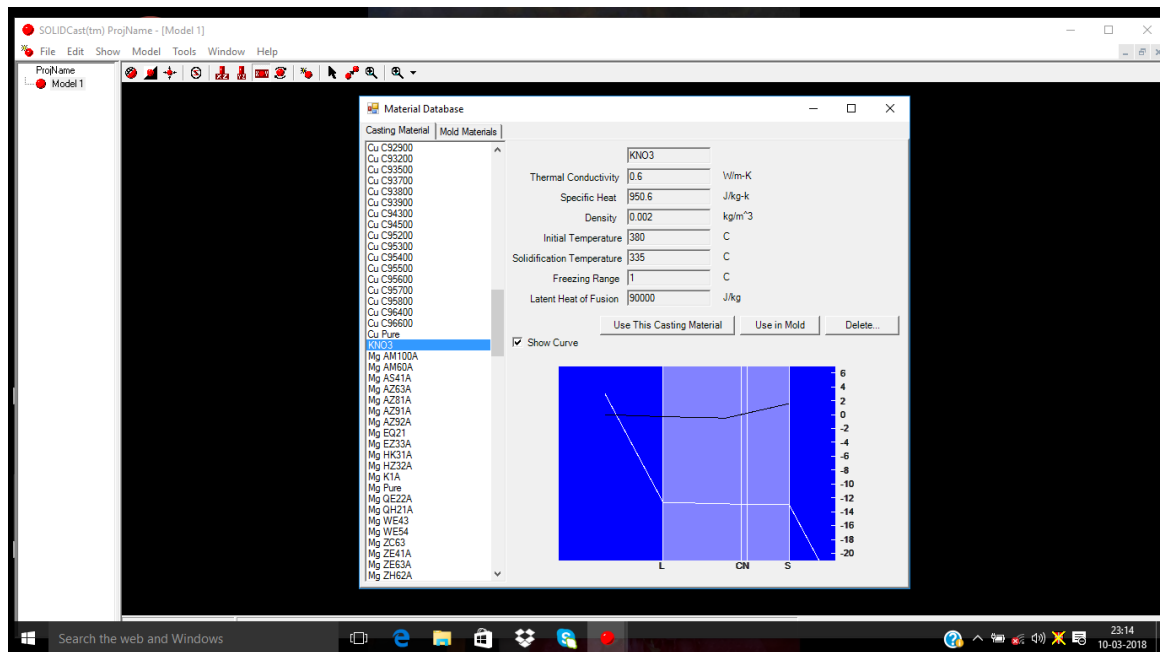


Fig 5.2: Assignment of PCM material properties in SolidCast.

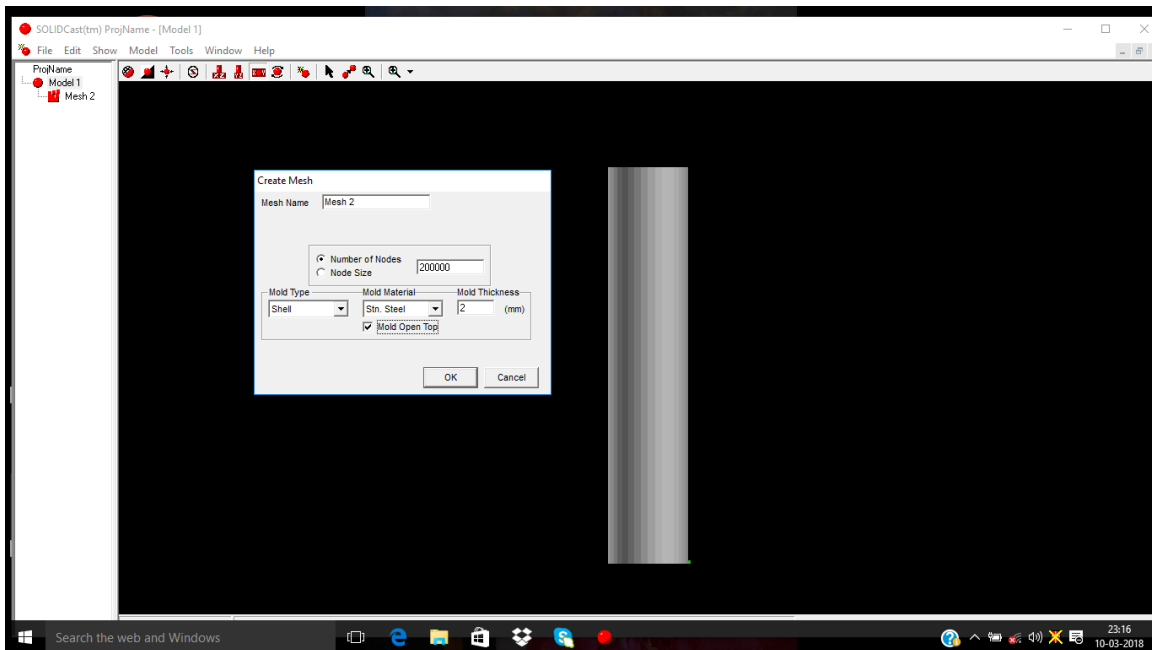


Fig 5.3: Assignment of Mold material properties and discretization of model.

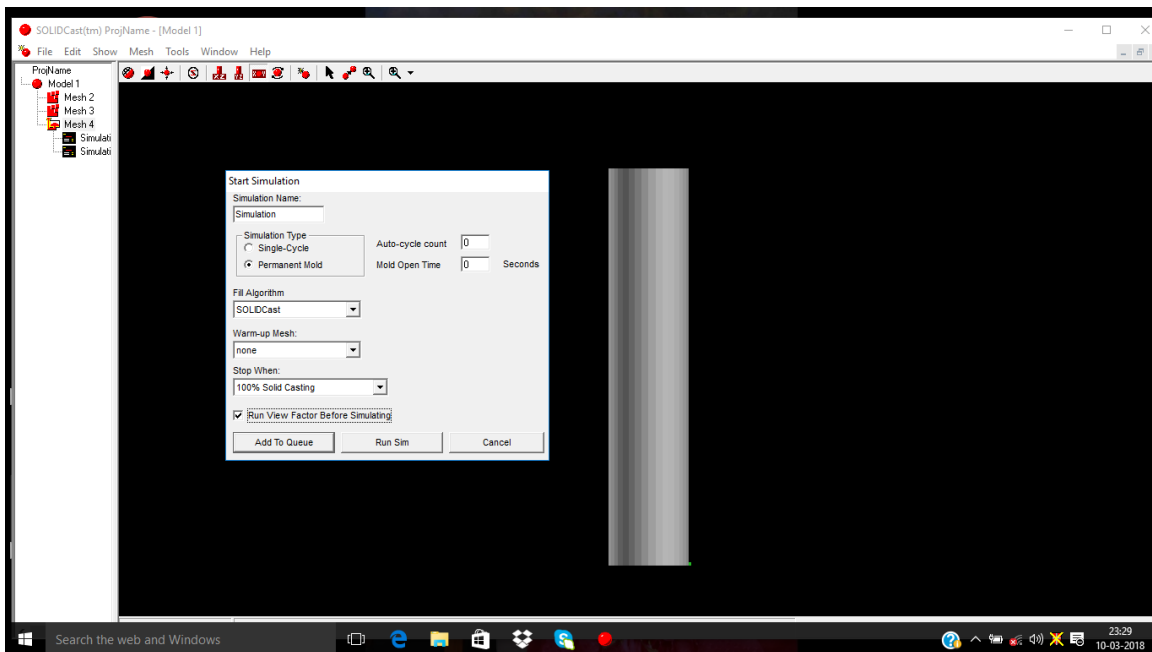


Fig 5.4: Simulation parameter for solidification of PCM.

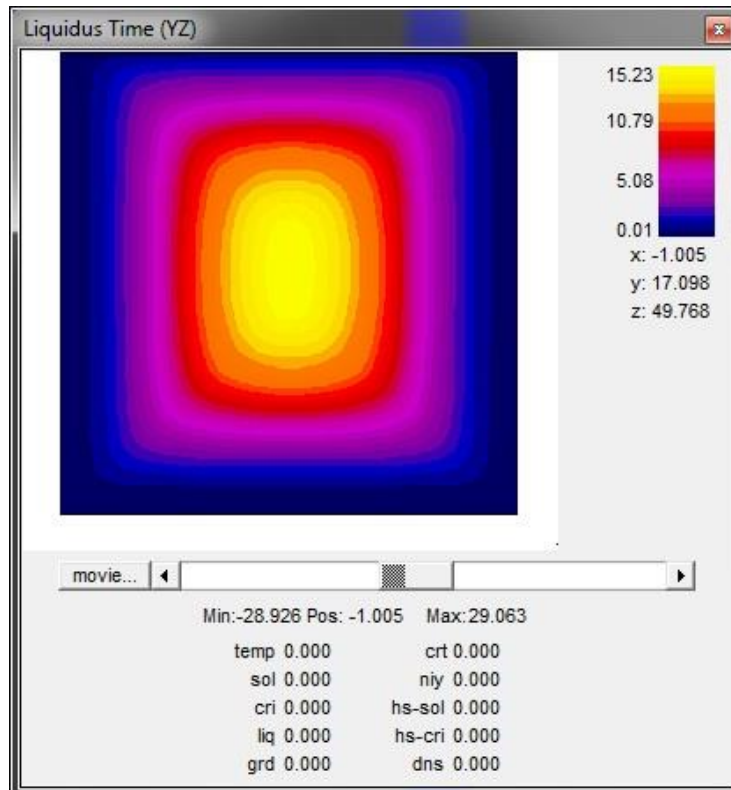


Fig 5.5: Liquidus time distribution in PCM sample with L/D ratio of 1.

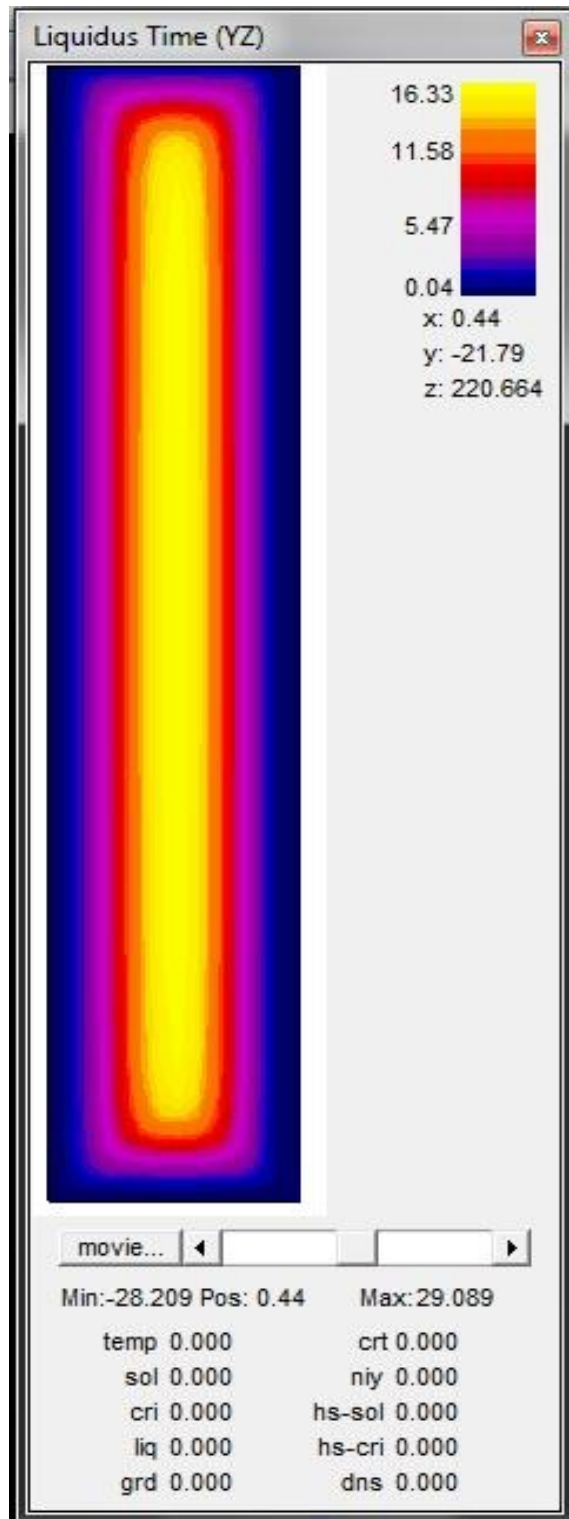


Fig 5.6: Liquidus time distribution in PCM sample with L/D ratio of 5.

Simulation studies were performed for 3 different mold materials, such as SS304, mild steel and graphite. Graphite mold, on virtue of its superior thermo physical properties such as specific heat capacity and thermal conductivity in comparison to that of mild steel and SS304 offered higher heat transfer rates in radial direction.

Another parameter analyzed here was the thickness of the mold. The mold thickness was varied from 1.5mm to 5.0mm. Thermal gradients within the PCM sample decreased with an increase in the thickness of the mold. Thickness of the mold could only influence the solidification in the region near to the mold inner-surface.

Length to diameter ratio of the cylindrical mold was a significant parameter governing the radial solidification in the PCM sample compared to the other parameters analyzed. L/D ratio was varied from 1 to 5 with a diameter value fixed at 50mm. Radial heat transfer was evident in the sample with an increase in L/D ratio from 1 to 5. The liquidus time variation shown in the Figure 5.6 proves that a cylindrical molds with an L/D ratio of 4 or more is necessary to ensure radial heat transfer within the PCM. This study predicted a perfect radial solidification at the mid-cross section of the sample.

A cylindrical mold of SS304 with a thickness of 1.5mm and an L/D ratio of 5 was chosen to perform characterization studies based on Fourier technique. Fourier technique of computer aided cooling curve analysis was employed to study solidification path of PCMs in further studies. It was used to predict cooling curves, solidification time and compute thermal diffusivity of salt-PCM with nano and micro additives as described in the next section.

5.2 EFFECT OF ADDITION OF MICRO AND NANO GRAPHITE PARTICLES ON TES FUNCTIONS OF SALT-PCMS.

The solidification temperature of the PCM (KNO_3) was observed in the cooling curve to be at 335°C (Figure 5.7). The PCM sample of size 1kg was solidified in $850\pm 30\text{s}$. The solidification temperature of the PCM was not influenced by the additive

particles as the composite PCM of KNO₃ and graphite particles (both nano and micro particles) solidified at 335°C. However, the solidification time decreased significantly on graphite particle addition. The addition of 0.1% of graphite micro particles by weight of the PCM sample reduced the solidification time to 760±10s which indicated an increase in the heat removal rate by 11.8%. The addition of 0.5% of graphite micro particles further decreased the time for solidification to 728±10s offering an 18% increase in heat removal rate, which was maintained over next 10 thermal cycles. The decrease in solidification time of the PCM is beneficial as the same amount of thermal energy can now be extracted at a much higher rate, improving the effectiveness of TES systems in power generation units. Eq. 14 is used to calculate the percentage change in the heat removal rate as shown below, where **t** is the solidification time of PCM.

$$\% \Delta H = \frac{t_{\text{pure salt}} - t_{\text{nanosalt}}}{t_{\text{nanosalt}}} \times 100 \quad (14)$$

Nano particles were observed to be more effective in decreasing the solidification time compared to the micro particles. The manually mixed mixture of KNO₃ and graphite nanoparticles (0.1% and 0.5% by weight of PCM) decreased the time for solidification from 850±30s to 600s and 590s respectively in the first thermal cycle (melting-freezing). The corresponding change in the heat release rate showed a significant increase of 41% and 44% respectively. Unlike the previous case, the time for solidification increased to 750s and 720s respectively on successive thermal cycles, and remained consistent thereafter. Nanoparticles agglomerate on every thermal cycle accompanied by a decay the TES functions of the PCM.

The benefits of a decrease in the time for solidification on addition of nanoparticles diminished in 4-5 thermal cycles and the performance was then comparable to the microparticle embedded salt-PCM thereafter. The cooling curves of various PCMs investigated here are as shown in Figure 5.8. Figure 5.9 highlights the changes in the cooling curves obtained from the 1st and the 10th thermal cycle of graphite particle (both micro and nano sized particles) dispersed salt-PCM. Figure 5.10 shows the effect of thermal cycling over the increase in heat removal rate of PCMs .

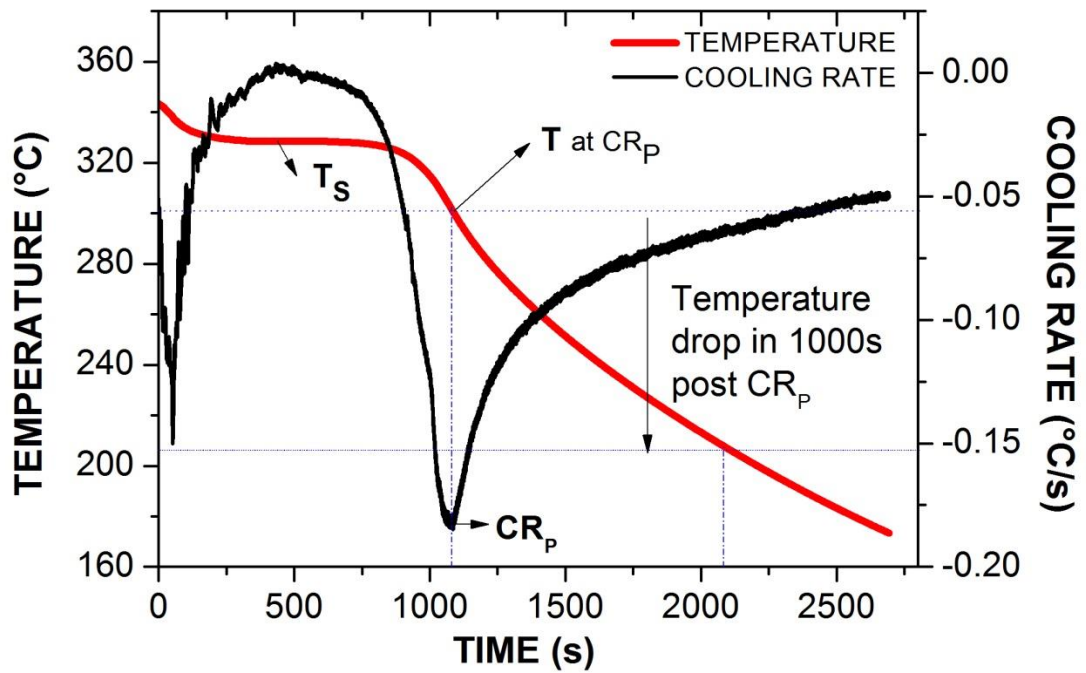


Fig 5.7: Cooling curve and cooling rate curve of KNO_3 .

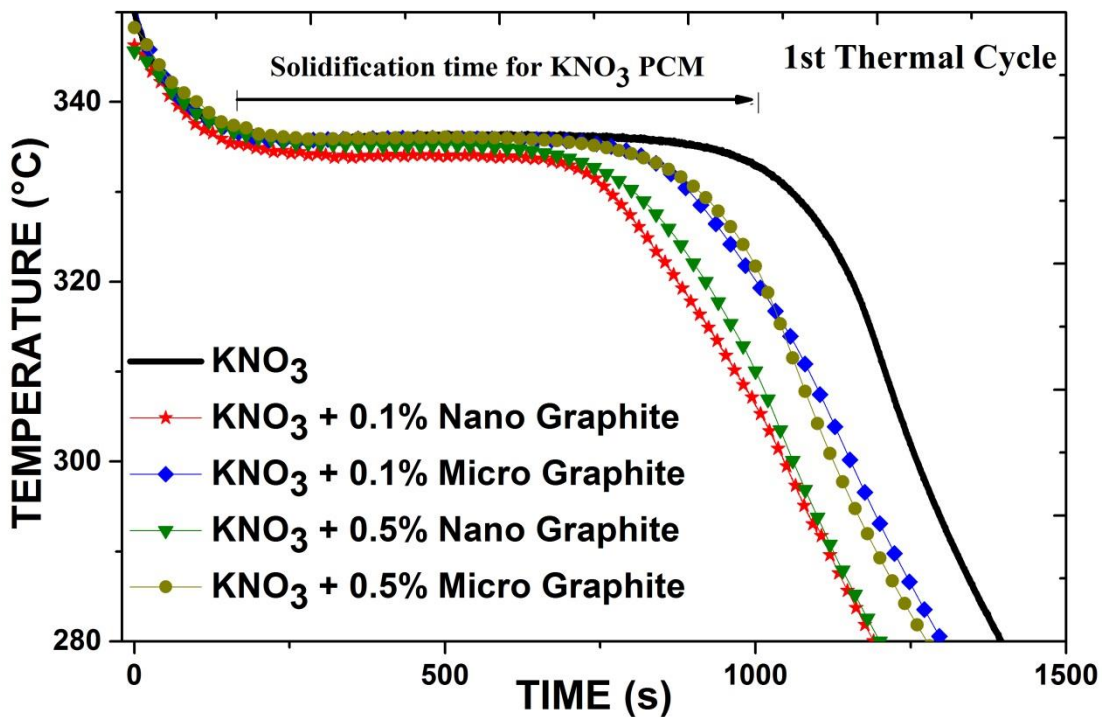


Fig 5.8: Cooling curves of various PCMs with graphite particle addition.

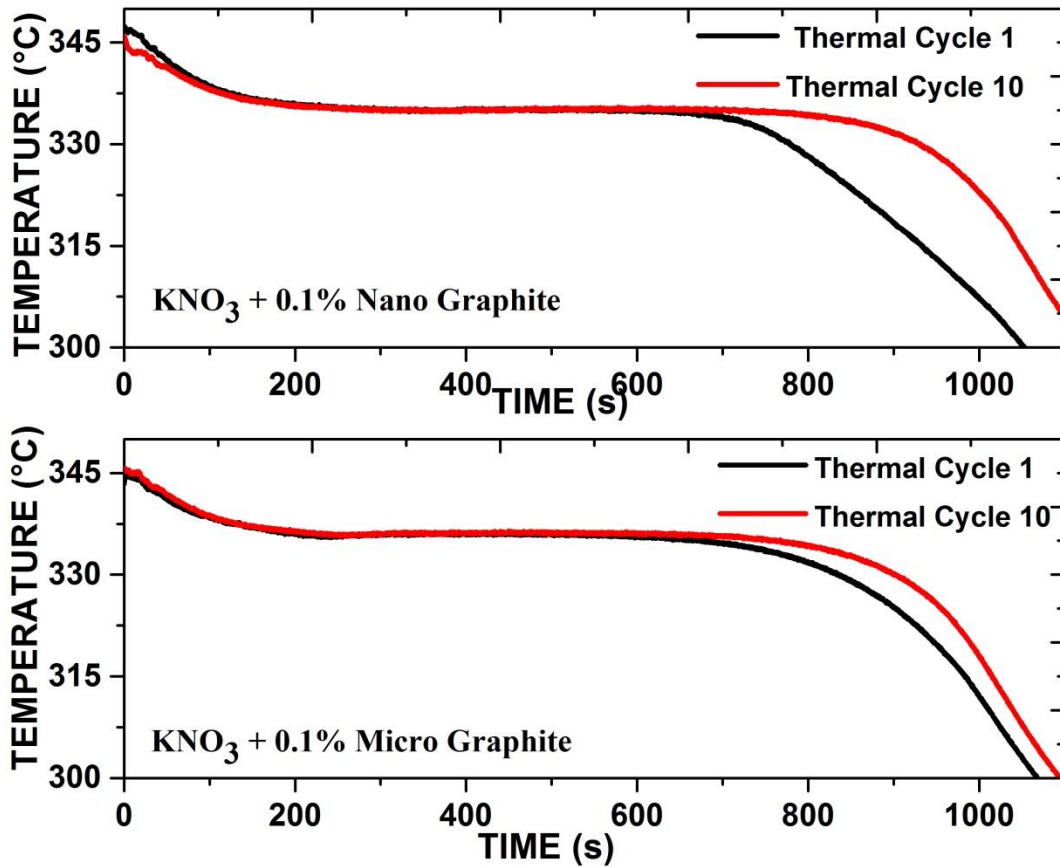


Fig 5.9: Effect of thermal cycling on cooling curve of Graphite particle added PCM.

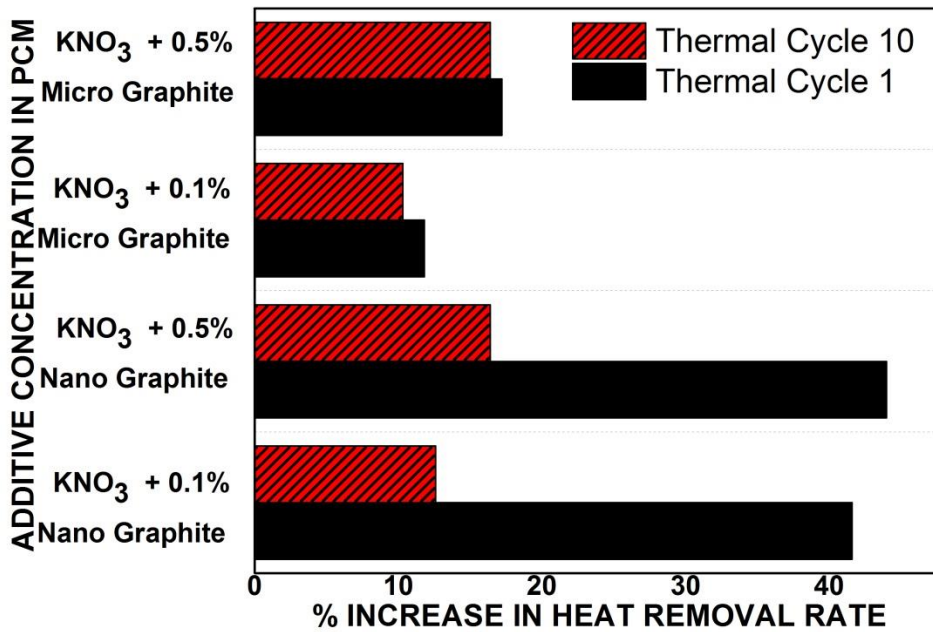


Fig 5.10: Effect of thermal cycling on heat removal rates in various PCMs.

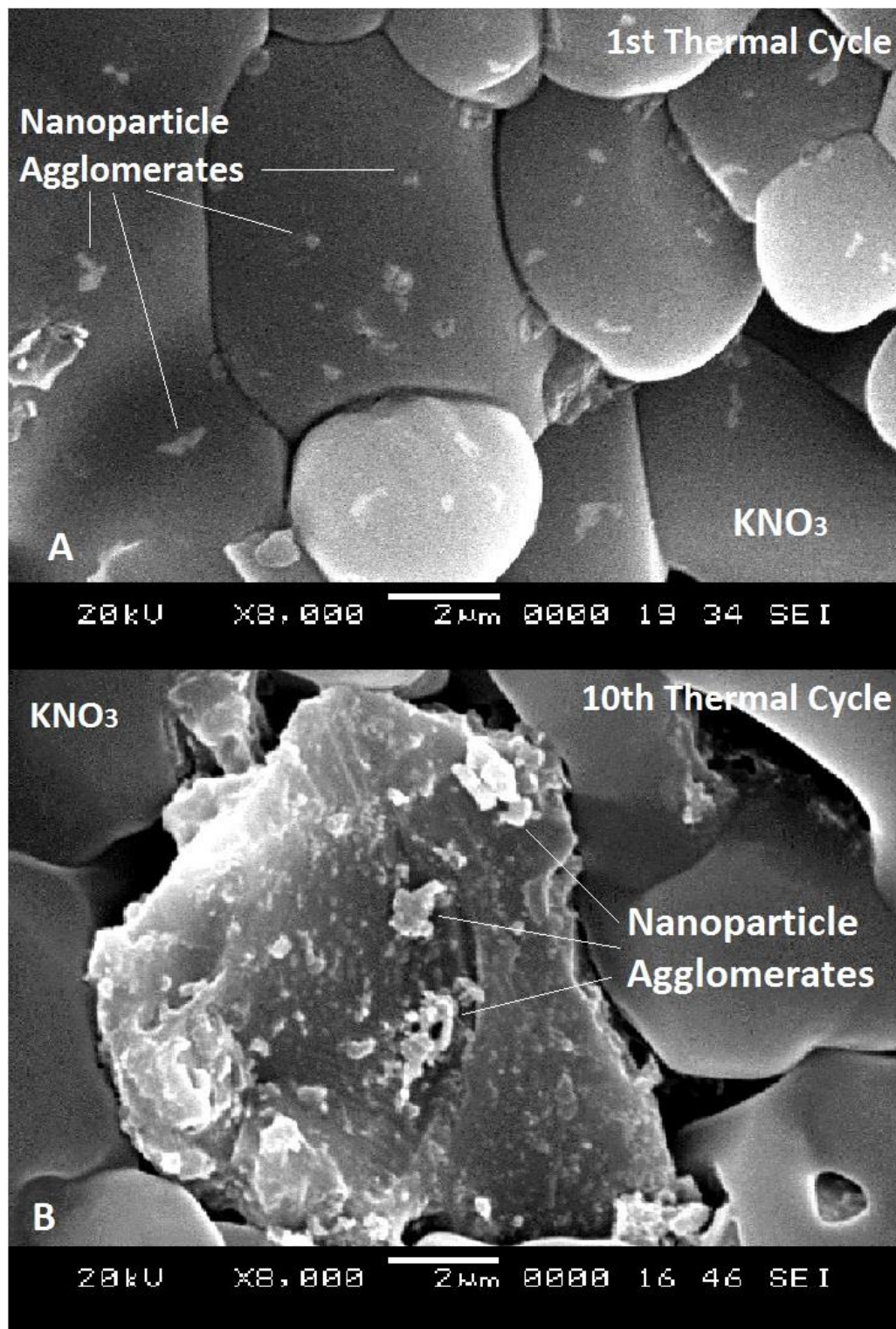


Fig 5.11: Agglomeration of nanoparticles after the (A) 1st thermal cycle, (B) 10th thermal cycle

The SEM images show considerable agglomeration of graphite nano particles on thermal cycling. The increase in the time for solidification over successive thermal cycling is attributed to the agglomeration of nanoparticles in the nanosalt-PCM. SEM images of the PCM with 0.1% of graphite nanoparticles is shown in Figure 5.11.

Another efficient tool in cooling curve analysis is the cooling rate curve. The cooling rate curve of KNO_3 is shown in Figure 5.7. As observed in the curve, the cooling rate decreases to a value close to zero during solidification of the sample and quickly increases post-solidification. The liquidus and the solidus points are not sharply observed in the cooling curve, which is reflected on the cooling rate curve as a slow transition from the solidus point (end of solidification) to the point of cooling rate reversal (**CR_P**). Point of cooling rate reversal is a point where the latent heat released during solidification is withdrawn completely from the vicinity of the thermocouple, and the sample cools thereafter along with the container. This delay is due to low thermal diffusivity of salt-PCMs. In the case of metallic PCMs, by virtue of their high thermal diffusivity the transition will be sharp in the cooling curve, and the time lag between the solidus point (solidification temperature) and the **CR_P** will be minimum.

The effect of particle addition on the cooling curve parameters is as shown in Table 5.2. It is evident that post solidification, the particle additions do not have considerable influence on the cooling rates of the PCM. A drop of 98-102°C over 1000s after **CR_P** in cooling rate curves of all PCM mixtures was observed. The temperature at which **CR_P** occurred was observed to be around 300-304°C in all the PCM mixtures in the first thermal cycle. It increased to 315°C (approximately) by the fourth cycle and remained constant thereafter.

The thermal diffusivity property of PCMs was predicted as shown in Eq. (9) in Chapter 3. The variation of thermal diffusivity values with temperature for various PCMs post-solidification is shown in the Figure 5.12. The thermal diffusivity of KNO_3 decreased to $1.5\text{-}1.6 \times 10^{-7} \text{ m}^2/\text{s}$ from $1.9\text{-}2.1 \times 10^{-7} \text{ m}^2/\text{s}$ on addition of graphite particles. The size of the particle did not considerably influence the thermal diffusivity property.

Table 5.2: Effect of graphite particle addition on TES functions of KNO₃.

TES Parameter	Thermal Cycle No:	Nano particle Concentration by weight of PCM		Microparticle Concentration by wt. of PCM	
		0.1%	0.5%	0.1%	0.5%
Solidification Time (s)	1	600	610	770	725
	2	610	720	750	725
	3	680	725	759	743
	4	750	720	770	720
	10	755	730	760	730
Temperature At CR_p (°C)	1	300	304	303	315
	2	303	311	310	317
	3	307	313	313	299
	4	315	316	315	314
	10	315	315	314	314
Cooling Rate At CR_p (°C/s)	1	0.16	0.17	0.17	0.21
	2	0.16	0.22	0.20	0.20
	3	0.20	0.22	0.22	0.19
	4	0.21	0.21	0.21	0.22
	10	0.22	0.21	0.21	0.23
Temperature Drop in 1000s Post CR_p (°C)	1	95	98	95	101
	2	95	98	98	101
	3	99	102	101	100
	4	99	103	99	100
	10	99	103	100	105
Solidification Temperature (°C)		335			

Thermal diffusivity indicates on how easily heat can propagate in the PCM, and how quick a material responds to a change in temperature. It is the ratio of thermal conductivity of a material to the product of its mass density and specific heat capacity. The absence of changes in cooling rates and a simultaneous decrease in thermal diffusivity property indicates an increase in the specific heat capacity (SHC) of the PCM on addition of graphite particles. An increase in specific heat capacity of PCMs on addition of nanoparticles is attributed to the formation of nanolayers as described earlier in section 2.3 of Chapter 2.

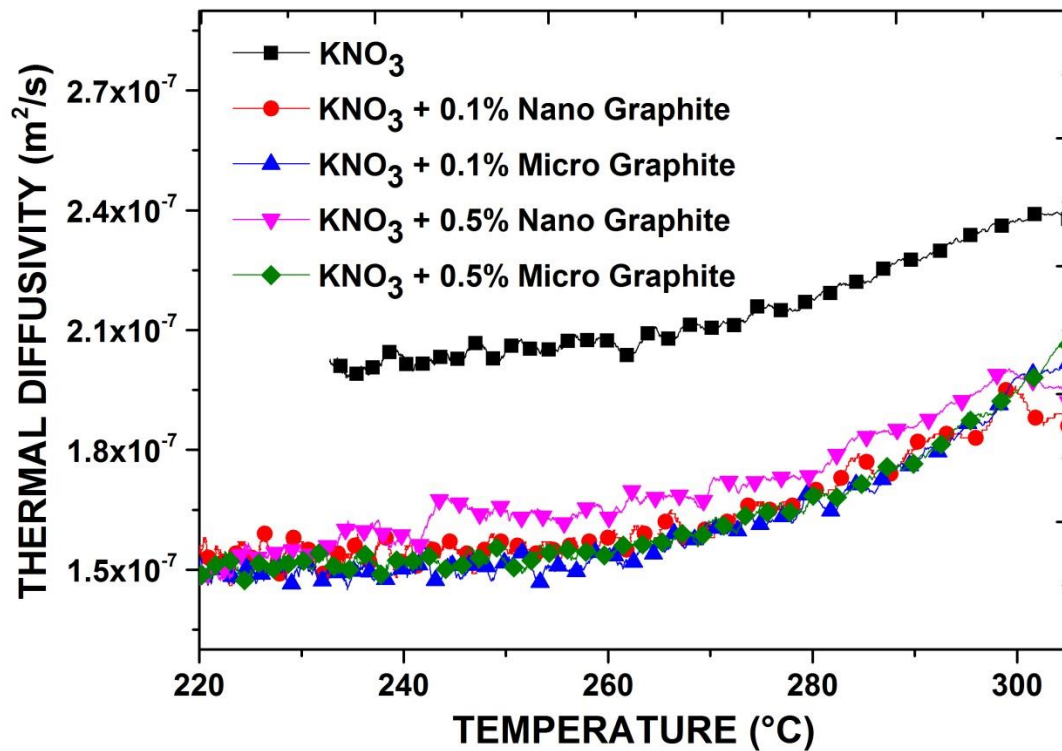


Fig 5.12: Thermal diffusivity curves of graphite particle added salt-PCM (KNO_3).

One of the reasons for high specific heat capacity of nanosalt-PCMs is the nanoparticles themselves. The structure of a material is related to its SHC. Nanoparticles have nano-grained structures and expose more atoms to the surface as they possess high surface area to volume ratio. Compared to the atoms at the centre, the surface atoms are less constrained. Therefore, the nanoparticles possess more energy in comparison to the coarse-grained particles. Wang et al. (2001) recorded a blue shift in the wave number in infrared spectrum of nano grained Al_2O_3 compared to that of coarse grained Al_2O_3 . With this, it is evident that the nanoparticles possess higher energy. Other parameters such as temperature, size effect, density, thermal expansion interfacial thermal resistance etc. too influence the SHC values of nanosalt-PCMs.

An anomalous increase in the specific heat capacity value of molten salt is attributed to the hypothesised network of ordered layers near to the surface of nanoparticles, which are known as Nanolayers. These semi-solid layers offer higher SHC where the latent heat of fusion of the entrapped PCM is taken into consideration.

When the additive concentration was raised from 0.1% to 0.5% by weight (by 5 times) a slight increase of 6% and of 2% in the change in heat removal rate for micro and nano particle embedded salt-PCMs respectively was observed. Further, this increase in concentration did not influence the cooling rate curves and the thermal diffusivity curves. A critical graphite additive concentration of 0.1% by wt. of the PCM sample offered the highest enhancement in TES functions. Agglomeration of nano particles diminishes the significant enhancements observed in TES parameters of nanosalt-PCMs.

5.3 EFFECT OF SAMPLE PREPARATION METHOD ON TES FUNCTIONS OF NANOSALT PCM.

Ball milling method can be employed in dispersing nanoparticles into salt-PCMs. The use of this method can improve the even dispersal or homogeneity of nanoparticles in PCMs. Here the effect of using a high energy ball milling method to disperse nanoparticles in salt-PCMs was also investigated. Graphite nanoparticles were dispersed into the pulverized salt-PCM sample by, (i) using planetary ball milling, (ii) thorough manual-mixing. A high energy planetary ball milling facility (Retch PM100, at 150rpm, for 20min, 87 steel balls of $\phi 10\text{mm}$) was employed here. Every sample was melted and then solidified for 10 cycles to analyze the effects of thermal-cycling on TES parameters of these inhomogeneous PCMs.

In the first thermal cycle, the ball milled PCM mixture (with 0.1% graphite nanoparticle by weight) solidified in 610s. Later, the time for solidification increased to $720\pm 10\text{s}$ in successive cycles. On the other hand, the time for solidification of manually mixed PCM sample was observed to be 600s in first thermal cycle, which later increased to 750s on thermal cycling. This can be observed in the cooling curves as shown in Figure 5.13.

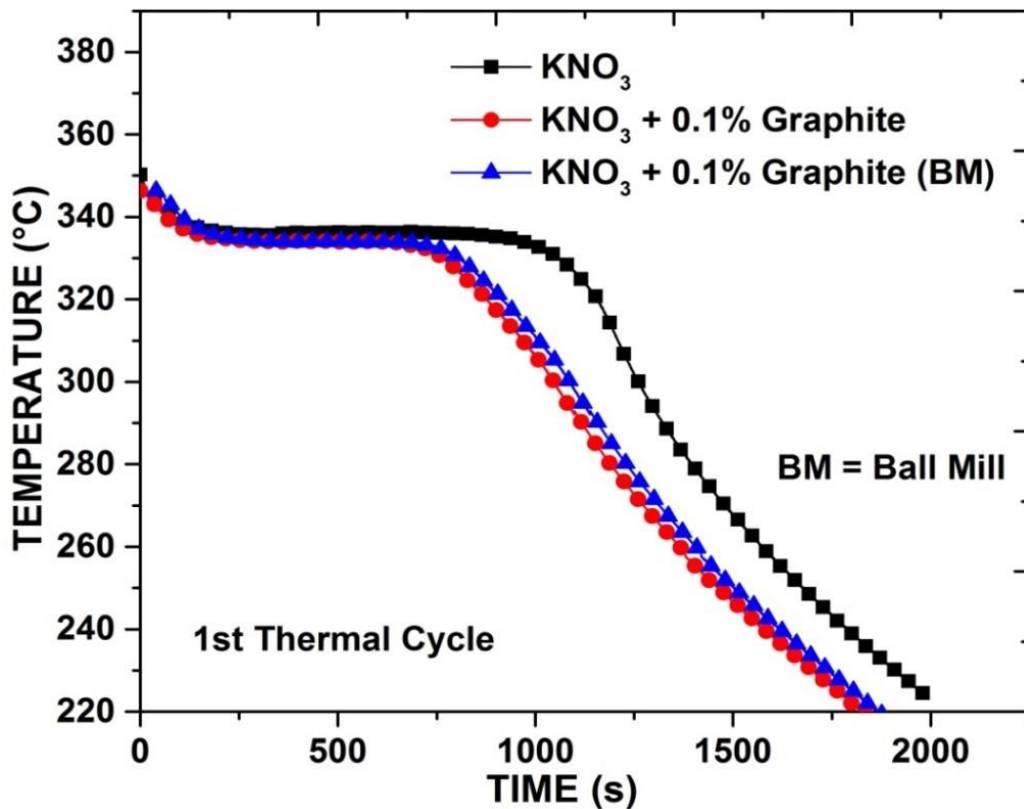


Fig 5.13: Cooling curves of ball milled and manually mixed nanosalt-PCMs.

It is evident that in comparison to the manual mixing method, the ball milling method for dispersal of nanoparticles did not considerably influence the solidification time of the PCM sample. However, it is important to mention the slight improvement in the PCM's response to thermal cycling (Figure 5.14). compared to a hand-mixed PCM sample, the ball milled sample offered less decay in heat release rates on thermal cycling.

The thermal diffusivity curves were plotted as shown in Figure 5.15. The addition of nanostructures lead to a decrease in thermal diffusivity property. The ball milled sample offered higher thermal diffusivity values compared to the manually mixed PCM sample.

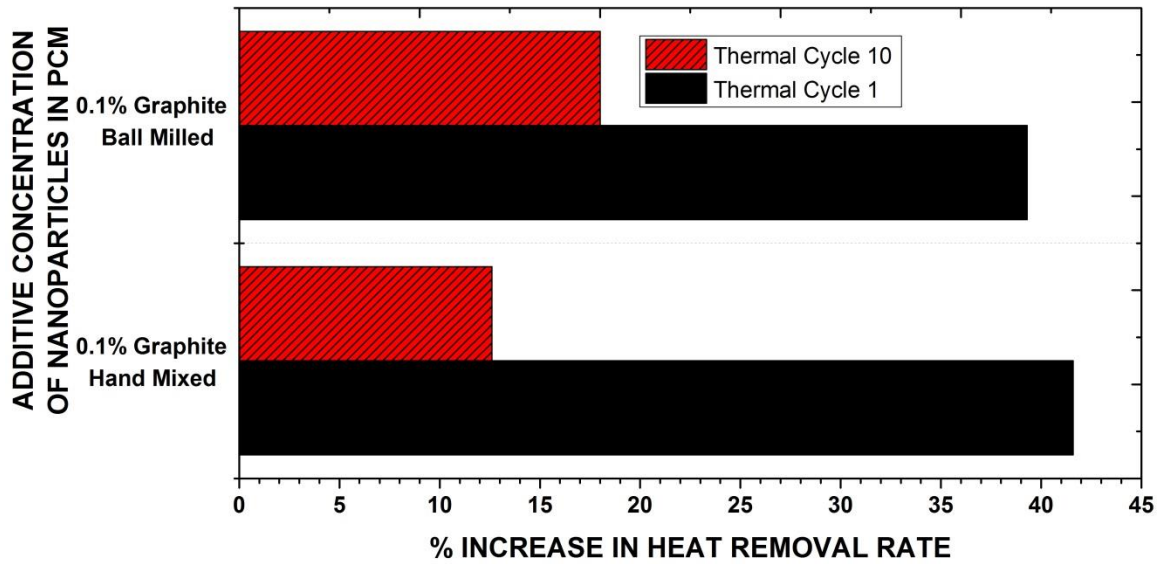


Fig 5.14: Effect of thermal cycling on heat removal rates of Nanosalt-PCM.

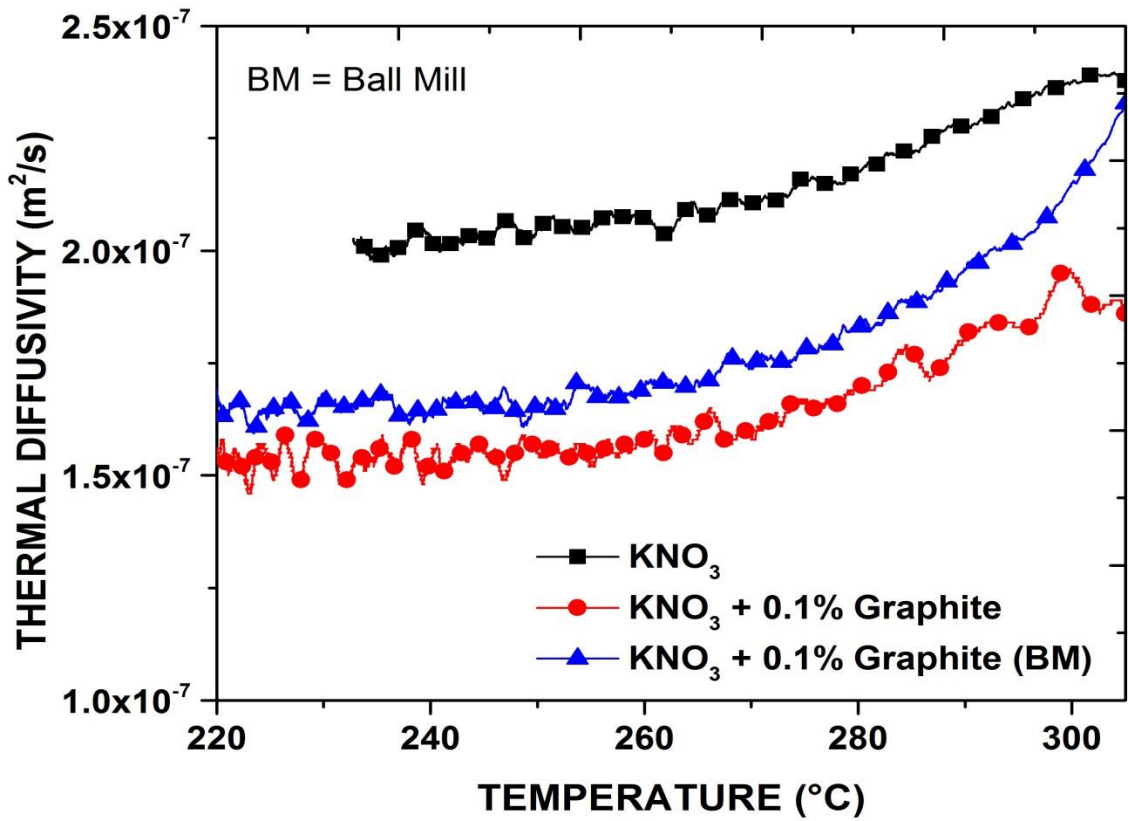


Fig 5.15: Thermal diffusivity curves of ball milled and manually mixed nanosalt-PCM.

All the manually mixed PCM samples showed a drop of 98-102°C over 1000s after the point of cooling rate reversal (CR_p). The ball milled sample showed a drop of 116°C over 1000s after CR_p in the first cycle, which can be attributed to the uniformity in distribution of nanoparticles in the salt-PCM. This effect diminished in successive thermal cycles. The temperature at which CR_p occurred was observed to be around 300-304°C in all the PCM mixtures in the first thermal cycle. It increased to 315°C (approximately) by the fourth cycle and remained constant thereafter. Unlike above, the ball milled PCM mixture had CR_p at 324°C initially which dropped to 315°C in successive cycles. In addition to this, an increase in the cooling rates at CR_p was observed in ball milled PCM samples.

Ball milling of nanosalt-PCM mixture ensured more uniformity in distribution of nanostructures which lead to considerable improvement in TES functions as discussed above. However, the use of ball mills would elevate the cost of nanosalt-PCM preparation. This diminishes the benefits of employing such a method in the preparation of nanosalts.

5.4 EFFECT OF ADDITION OF VARIOUS CARBON NANOSTRUCTURES ON TES FUNCTIONS OF SALT-PCM

The solidification temperature of the PCM (KNO₃) was observed in the cooling curve to be at 335°C. The PCM sample of size 1kg solidified in 850±30s. The addition of carbon nanostructures had negligible effect on the solidification temperature of the PCM. The nanoparticles CNT, Graphene and Graphite were added separately to the KNO₃ samples. The mixtures were mixed manually, and were subjected to 10 consecutive thermal cycles across the melting point.

Solidification time of salt-PCM decreased on addition of nano particles. This effect is beneficial as the stored thermal energy in the sample can now be withdrawn at higher rates.

For an additive concentration level of 0.1%, the MWCNT+KNO₃ sample solidified in 670s while the Graphene+KNO₃ and Graphite+KNO₃ samples solidified in 743s and 600s respectively, as shown in Figure 5.16. The effect of nanoparticle addition on the solidification time of KNO₃ sample is significant and beneficial in increasing the heat removal rate of the PCM sample by 26%, 14% and 41% for MWCNT, graphene and graphite embedded salt-PCM respectively. This parameter was further improved considerably with the increase in concentration of the nanoparticles in the salt-PCM, as shown in Figure 5.17 and Table 5.2. The change in heat removal rate (ΔH) is calculated using the Eq. (14).

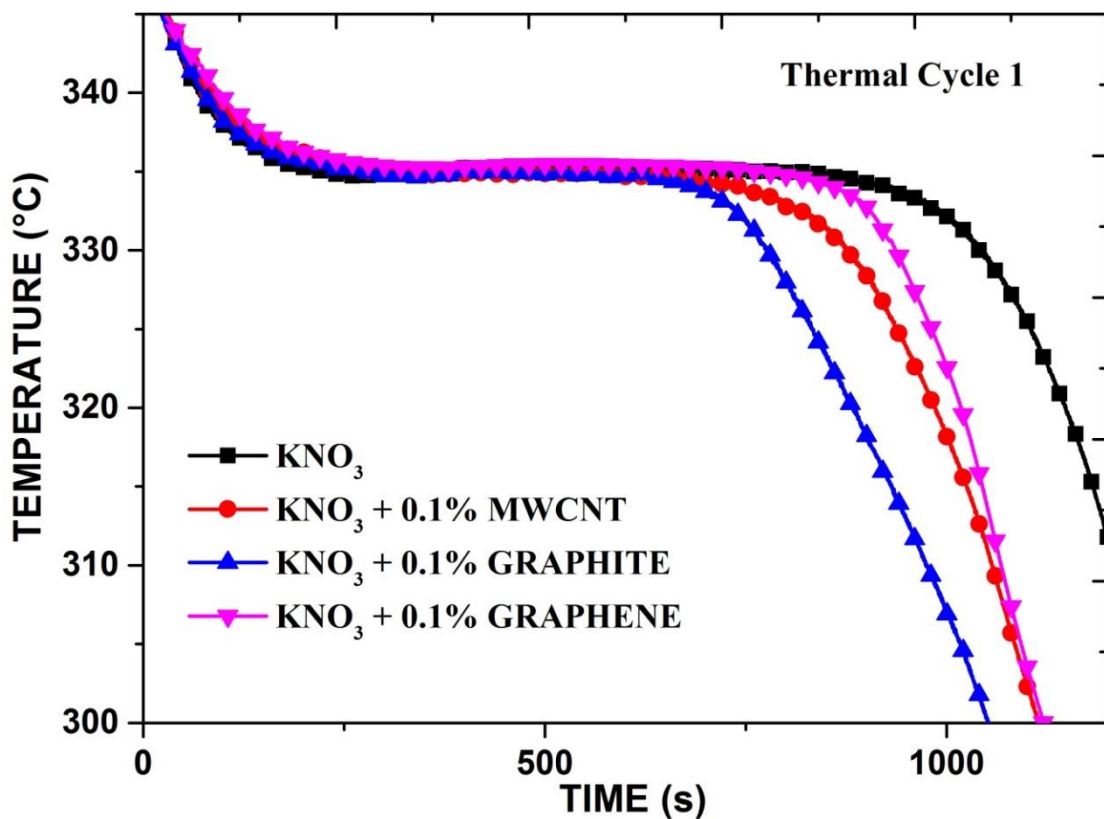


Fig 5.16: Cooling curves of various nanosalt-PCMs.

It is evident from the results that the solidification time of KNO₃ sample showed significant decrease with the increase in the nanoparticle concentration from 0.1% to 0.5% by weight of the salt sample. This was distinctly observed in MWCNT and graphene embedded salt-PCMs. Solidification times of 670s, 650s and 610s were observed in MWCNT embedded salt samples with a concentration level of 0.1%,

0.3% and 0.5% respectively. The increase in concentration level caused an increase in heat removal rates where the $\% \Delta H$ increased from 26% to 39% approximately as shown in Table 5.2. Similarly in the graphene embedded PCM the $\% \Delta H$ increased from 14% to 25% along with the nanoparticle concentration level from 0.1% to 0.5%. However, the graphite embedded PCM did not show considerable response to the changes in the concentration levels of the additive. Here the overall increase in the $\% \Delta H$ was from 41% to 44%. It is recommended to work with low concentrations of graphite in the salt PCM (around 0.1% or less) as the increase in the concentration of the graphite nanoparticles from 0.1% to 0.5% had insignificant effect on the solidification time of the PCM as shown in Figure 5.17 and Table 5.2.

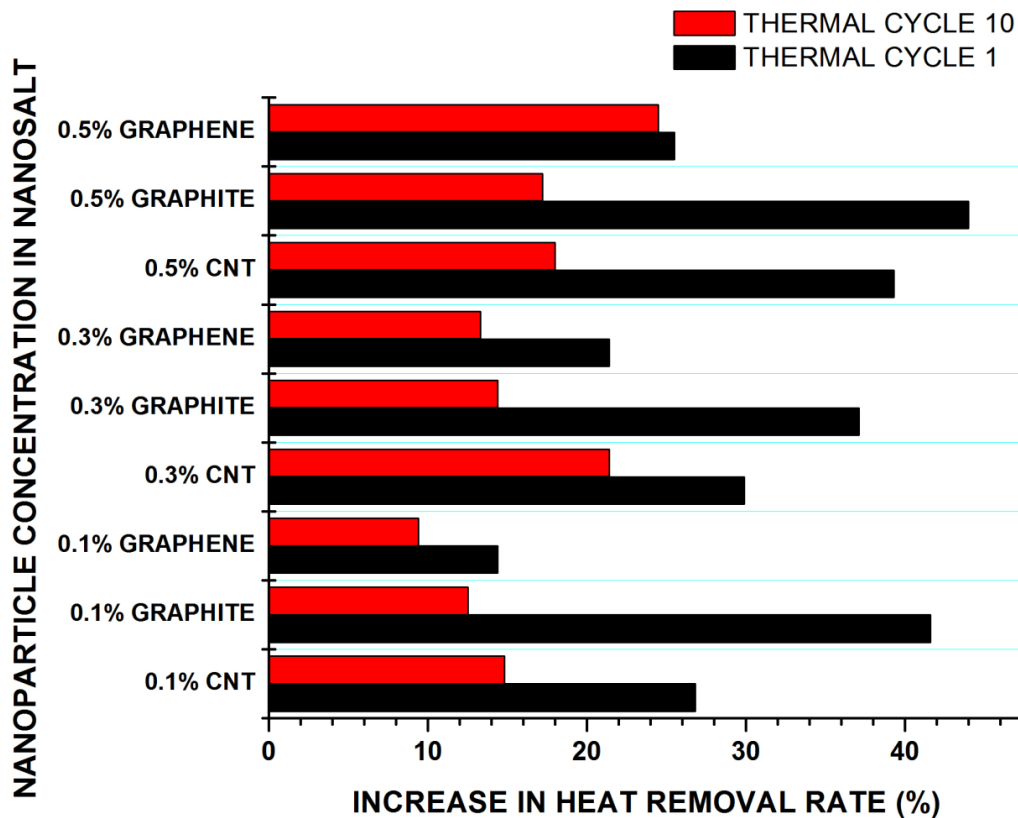


Fig 5.17: Effect of thermal cycling on the heat removal rates of various nanosalt-PCMs.

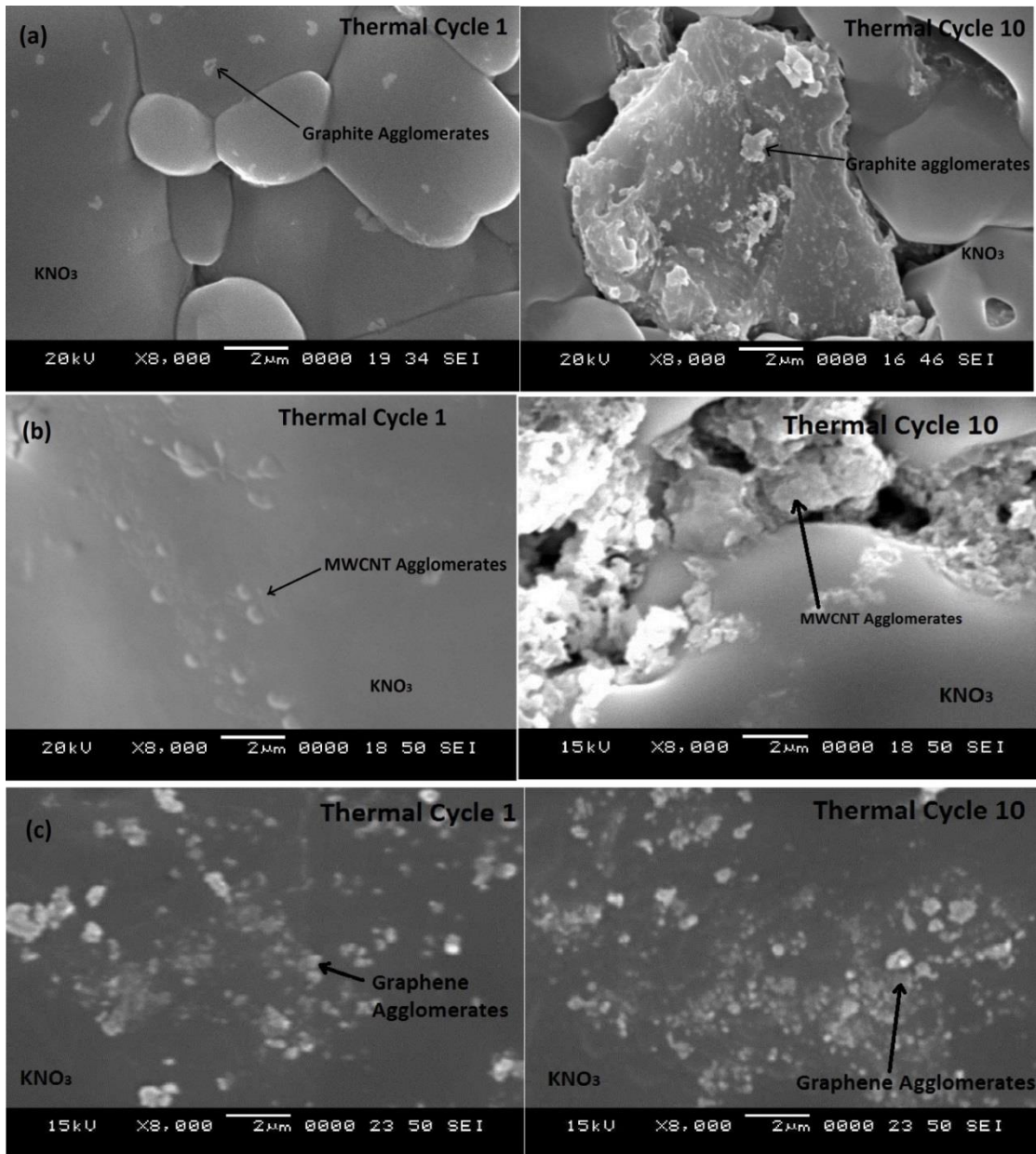


Fig 5.18: SEM images showing agglomeration of nanoparticles in salt-PCM on thermal Cycling. (a) 0.1% Graphite + KNO₃ PCM, (b) 0.1% MWCNT + KNO₃ PCM, (c) 0.1% Graphene + KNO₃ PCM.

Nanoparticles form interconnected clusters in the base fluid which is well discussed in the literature, offering an easy path for thermal transport. They have superior thermal conductivity compared to the base salt causing higher heat transfer rates through conduction. The pools of molten salt which is entrapped within these hypothesised clusters exchange heat to this network and cool down quickly. A well dispersed nano

salt bath will have molten salt pools of nano scale which can be credited for the significantly high heat removal rates as observed here. In addition to this nanoparticles can act as nucleating agents initiating solidification within the sample. In this context, its role as a nucleating agent is minimal as the solidification of the PCM is directional, originating from the mold walls.

These nanoparticle embedded PCM samples were subjected to thermal cycling test. The samples were melted and frozen for 10 consecutive cycles and the solidification parameters were obtained. It is observed that the benefits of nanoparticle additions on the solidification time of KNO_3 samples, and its corresponding effect on the heat removal rates deteriorated on thermal cycling. The solidification time of the nanosalt-PCMs increased on thermal cycling. Figure 5.17 gives a representation of deterioration of the nanosalt PCMs on thermal cycling. The Graphite embedded PCMs displayed a significant decrease in the heat removal rates while the graphene embedded PCMs were more stable in this regard.

For 0.1% MWCNT+ KNO_3 sample the solidification time increased from 670s to 720s on thermal cycling over 10 cycles. This caused a drop in the $\% \Delta H$ from 26% to 15%. Similarly, the 0.1% Graphene+ KNO_3 sample showed an increase in solidification time from 743s to 777s with a corresponding drop in the $\% \Delta H$ from 14% to 9%. The 0.1%Graphite+ KNO_3 showed the highest order of deterioration when the solidification time varied from 600s to 755s in 10 thermal cycles. Here, the $\% \Delta H$ varied from 41% to 12%.

This deterioration is due to the agglomeration of the nanoparticles. SEM images (Figure 5.18) of nanosalt-PCMs show agglomeration of nanoparticles on thermal cycling. From the experimental observations graphene added salt-PCM have deteriorated the least in comparison to the other two nano salts. Graphene particles displayed homogenous mixing in the PCM without considerable separation out or any formation of clumps. Graphene sheets have self-repairing mechanisms of receiving carbon atoms into its vacancies every time it bombards with other carbon rich structures. This phenomenon imparts higher capability in graphene sheets to rebound the advancing cracks, when compared with the other carbon structures considered

here [Atif and Inam (2016)]. MWCNTs, being rolled layers of graphene are more reactive due to the increased curvature. It can be observed from Table 5.3 that on thermal cycling the solidification time varied over 150s in 0.1% Graphite+KNO₃ while it varied over just 50s and 30s in 0.1%MWCNT+KNO₃ and 0.1% Graphene+KNO₃ respectively. Similar trends were obtained for higher concentrations of the nanostructures in the salt-PCM.

Generally the PCM modifications such as nanoparticle additions are expected to influence the thermal conductivity and the specific heat capacity. A simultaneous increase or decrease of both the properties cannot occur on such modifications as these properties counter the effect of the other. Thermal conductivity gives a measure of ease in heat transfer within the sample whereas heat capacity is an indication of the thermal energy stored. Thermal diffusivity is the thermal conductivity of the material divided by the product of its density and specific heat capacity. This makes thermal diffusivity property a much better indicator of TES characteristics of a PCM.

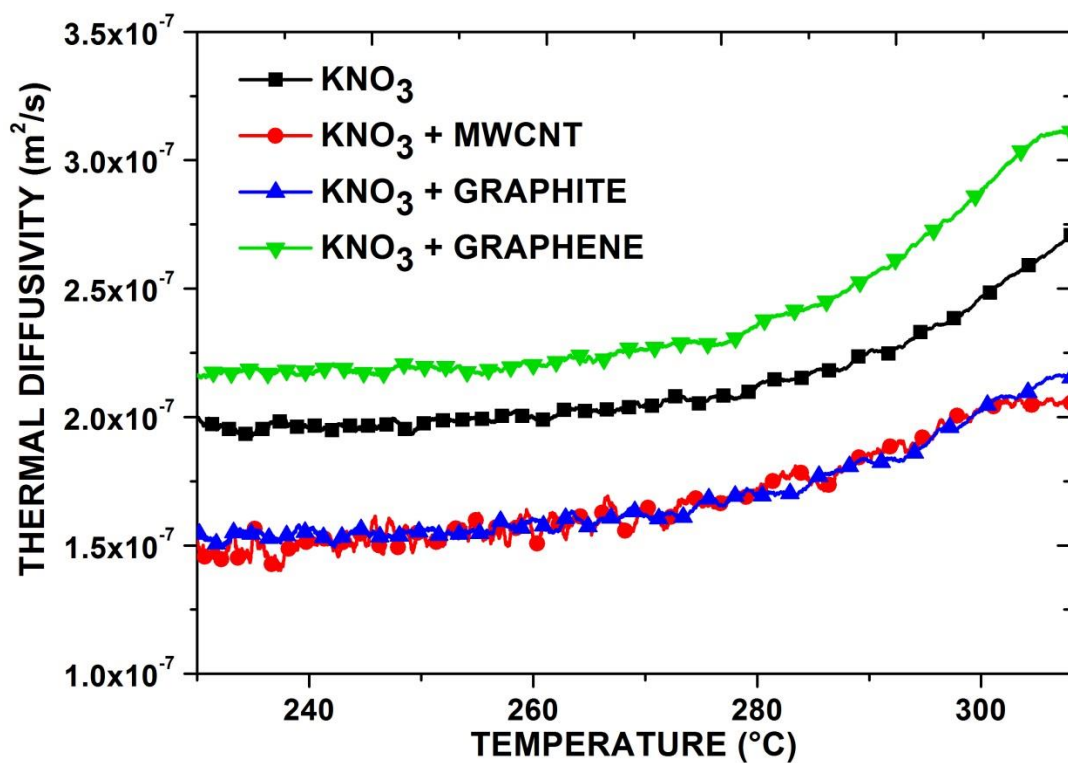


Fig 5.19: Thermal diffusivity curves of nanoparticle added (0.1% by wt.) KNO₃ PCM.

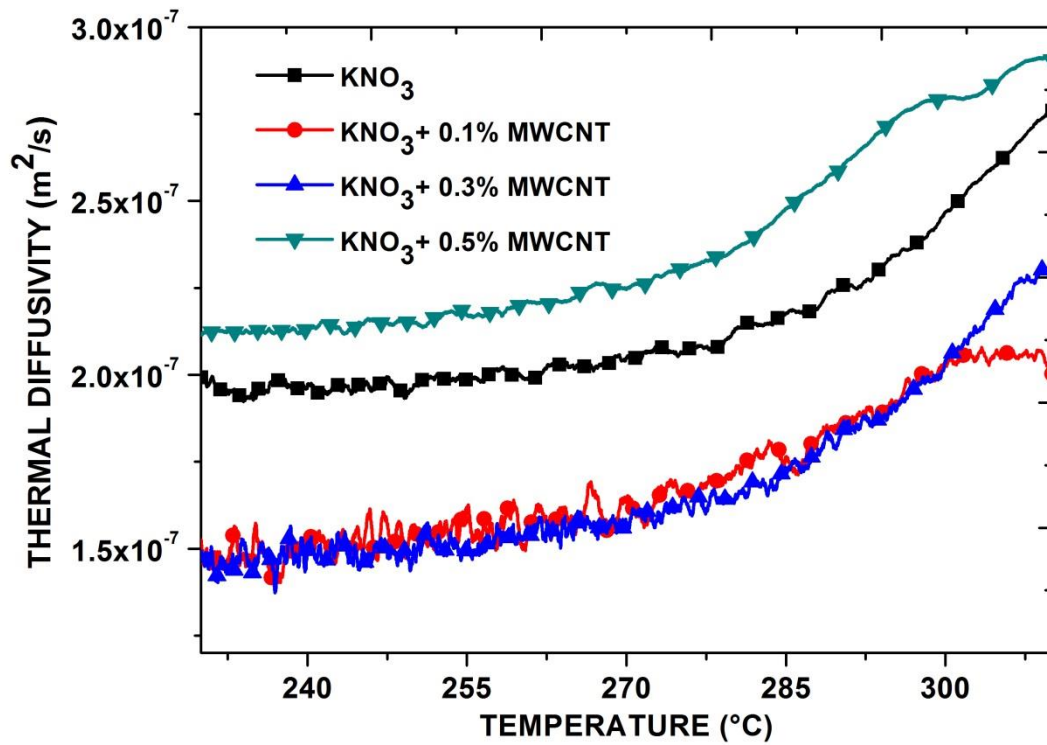


Fig 5.20: Thermal diffusivity curves of PCMs with varying concentration of MWCNT.

Table 5.3: Effect of nanoparticle addition on TES parameters of KNO₃ salt-PCM.

Particle Addition In PCM	Thermal Cycle Number	Solidification Temperature (°C)	Solidification Time (s)	Temperature At CR _p (°C)	Cooling Rate at CR _p (°C/s)	Temperature Drop in 1000s Post CR _p (°C)	ΔH (%)
KNO ₃ + MWCNT	0.1%	335	670	309	0.18	100	26.8
			740	309	0.20	97	14.8
	0.3%	335	654	312	0.18	95	30
			700	312	0.21	93	21.4
	0.5%	335	610	311	0.23	95	39.3
			720	312	0.21	98	18.0
KNO ₃ + Graphite	0.1%	335	600	300	0.16	95	41.6
			755	315	0.22	99	12.6
	0.3%	335	620	300	0.18	95	37.0
			743	305	0.20	101	14.4
	0.5%	335	590	304	0.17	98	44.0
			730	315	0.21	103	16.3
KNO ₃ +Graphene	0.1%	335	743	312	0.2	100	14.4
			777	320	0.27	102	9.4
	0.3%	335	700	312	0.26	111	21.4
			750	310	0.20	98	13.3
	0.5%	335	677	310	0.18	104	25.5
			683	311	0.23	107	24.0

The additives had considerable effect on the thermal diffusivity of the PCM. The addition of Graphite and MWCNT particles decreased the thermal diffusivity of KNO_3 -PCM while the addition of Graphene particles lead to an increase in the property values as shown in Figure 5.19. The decrease in the thermal diffusivity is the manifestation of an increase in the SHC. The decrease in thermal conductivity property cannot be a probable cause as the nanoparticle additions have been reported to have no influence on thermal conductivity of molten salts. An increased SHC enhances the energy density of the PCM. Various mechanisms of SHC enhancement such as the Nano layers, Meso layers influencing a larger volume, higher SHC of nano particles on virtue of its surface atoms with an excess volume for expansion, increase in the interfacial thermal contact resistance etc have been discussed earlier. On the other hand, the atoms in graphene sheets are less stressed compared to the atoms in MWCNT and have less excess volume for thermal expansion compared to the surface atom of nano grained graphite particles. The low energy graphene sheets would have a relatively poor influence in ordering the neighbouring ions, which causes weaker nano/meso layers. In addition to this, the graphene sheets show exceptionally higher thermal conductivity. These reasons account for the increase in the thermal diffusivity of the graphene+ KNO_3 PCM. The addition of graphene particles had considerably increased the cooling rates along with the increase in thermal diffusivity property.

The concentration of nanoparticles had an influence in the case of MWCNT+ KNO_3 PCMs additions alone. The thermal diffusivity values decreased on addition of 0.1% and 0.3% of MWCNT and the trend reversed in PCM with 0.5% MWCNT with a considerable increase as shown in Figure 5.20. In other cases the concentration level did not have any effect on the thermal diffusivity values.

5.5 EFFECT OF DISPERSANTS ON THE SOLIDIFICATION OF NANOSALT-PCM

The agglomeration of nanoparticles has a deleterious effect on the TES functions of nanosalt-PCMs. The benefits obtained on addition of nanoparticle to salt-PCMs would deplete significantly in successive thermal cycles as discussed earlier. Ultrasonication of the nanosalt bath in every thermal cycle can be performed to maintain the enhancements in TES parameters. This method possesses practical difficulties and will lower the cost-effectiveness of TES units. Another method to prevent agglomeration is the use of dispersants. TiO_2 and Carbon Black (CB) are commercially available dispersants used to prevent entanglement of CNT structures. The mixtures of MWCNT with Carbon Black and with TiO_2 were procured and dispersed separately in KNO_3 samples.

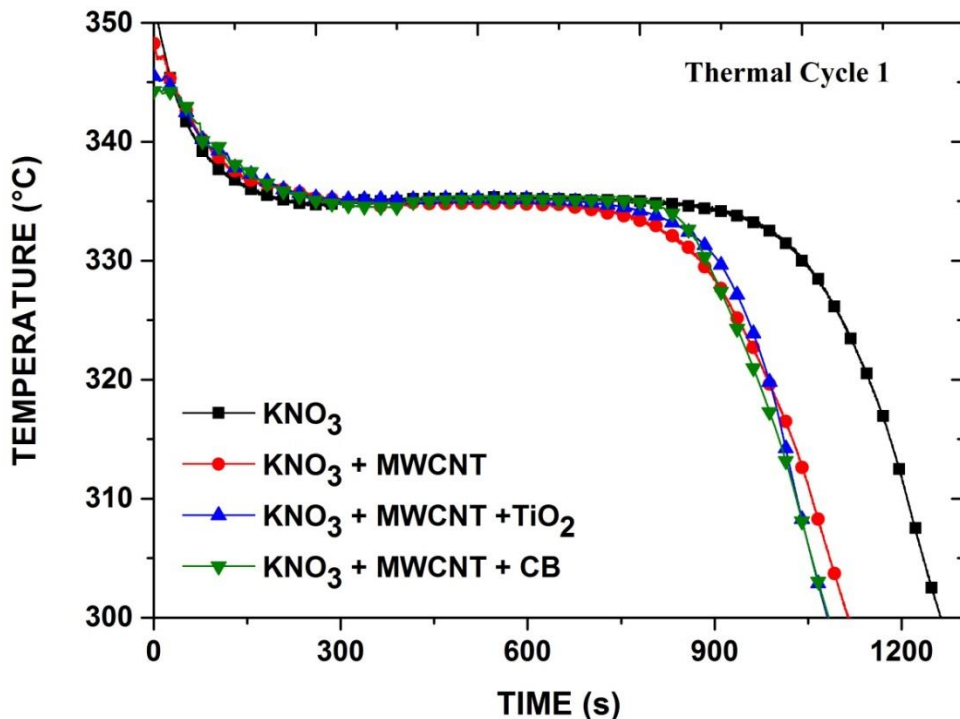


Fig 5.21: Cooling curves of nanosalt-PCM with dispersants.

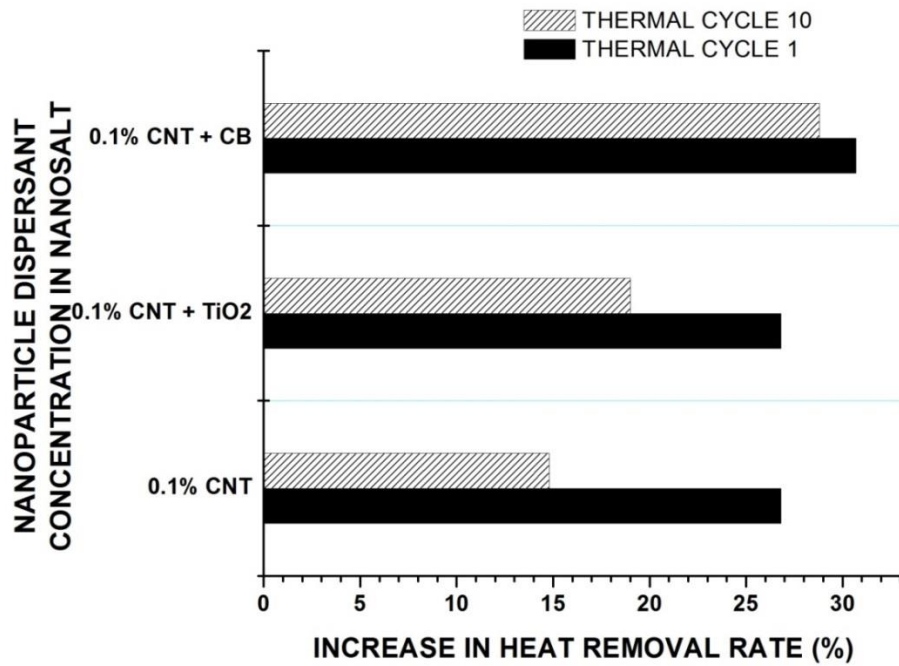


Fig 5.22: Effect of thermal cycling on heat removal rates of nanosalt-PCM with dispersant.

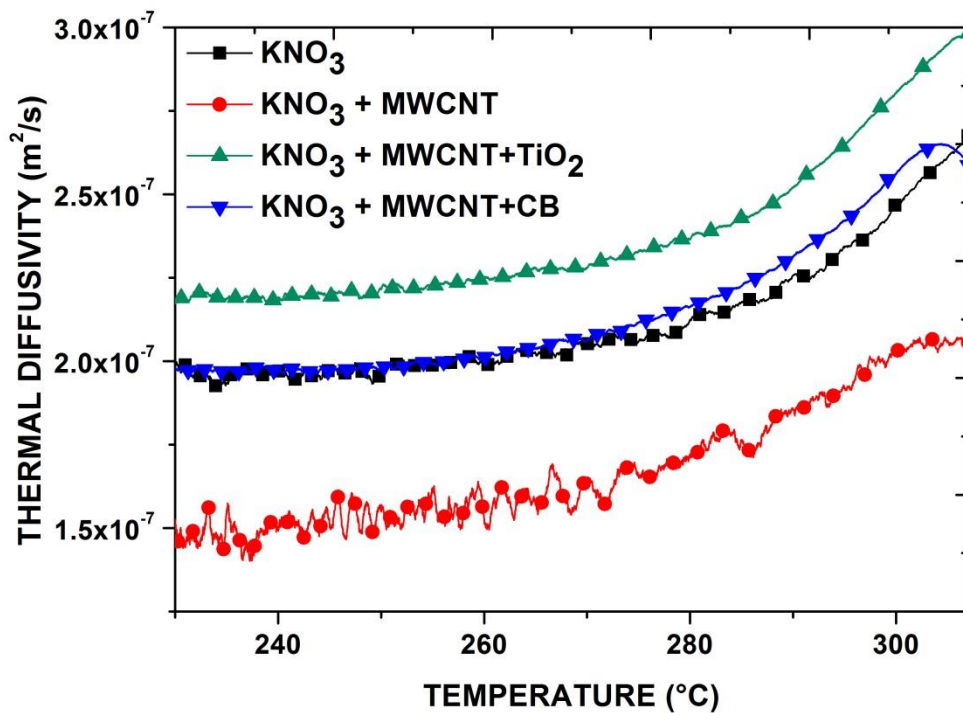


Fig 5.23: Effect of dispersants on thermal diffusivity curve of nanosalt-PCM.

5.5.1 MWCNT+TiO₂ (1:9) dispersed in KNO₃

The solidification time of MWCNT+KNO₃ PCM was negligibly influenced by the addition of TiO₂ as a dispersant. However, the deterioration of the PCM (decrease in ΔH) over the next 10 successive thermal cycles decreased. In 0.1%MWCNT+KNO₃ PCM the % ΔH decreased from 26% to 15% in 10 cycles. However, on addition of TiO₂ dispersant the % ΔH decreased from 26% to 19% in 10 cycles as shown in Figure 5.22 and Table 5.3. The dispersant mixture considerably influenced the cooling rates of the nanosalt. The cooling rates at the CR_P increased from 0.18 to 0.24°C on inclusion of TiO₂. This increase was maintained in the next 10 cycles. This had resulted as an increase in the temperature drop in 1000s after the CR_P, from 97-100°C to 108-114°C. The temperature of the sample at the CR_P too shifted to around 315°C from 309°C.

In addition to this, the use of MWCNT+TiO₂ as the dispersant had significantly increased the thermal diffusivity property of the nanosalt as shown in the Figure 5.23. The increase in thermal diffusivity along with the simultaneous increase in cooling rates as discussed earlier indicate an increase in the thermal conductivity property of the PCM. It is evident from the results that the dispersants moderately improved the thermal stability of the nanosalt-PCM without affecting its solidification time.

As the solidification time of the nanosalt was not affected by the dispersant addition the improvement obtained in latent heat removal rates remained unaffected in the initial thermal cycles. On thermal cycling, the deterioration of the PCM was limited by the dispersant which can be observed in Figure 5.22 and Table 5.4.

Table 5.4: Effect of dispersants on TES parameters of KNO₃ salt-PCM.

PCM	Thermal Cycle Number	Solidification Temperature (°C)	Solidification Time (s)	Temperature At CR _P (°C)	Cooling Rate at CR _P (°C/s)	Temperature Drop in 1000s Post CR _P (°C)	ΔH (%)
A	1	335	670	315	0.24	109	26.8
	10		709	315	0.26	108	19.8
B	1	335	650	311	0.20	98	30.7
	10		660	316	0.21	104	28.7

A = KNO₃ + MWCNT + TiO₂, B = KNO₃ + MWCNT + CB

5.5.2 MWCNT+Carbon Black (4:6) dispersed in KNO₃.

The addition of MWCNT+Carbon black dispersant mixture to KNO₃ had a beneficial effect on the solidification of the PCM. The solidification time of the PCM decreased to 650s indicating an increase in the heat removal rate during solidification by 31% (% Δ H). The change in the solidification time was maintained in the next 10 successive thermal cycles indicating an effective prevention of agglomeration of the MWCNT nanoparticle. The prevention of agglomeration of MWCNT in salt medium using dispersants is a critical outcome in the development of superior TES materials.

Other solidification parameters such as the cooling rate at CR_P, and the drop in temperature over 1000s after CR_P were not influenced at all by the use of carbon black. It is evident that carbon black particles did not influence the sensible heat release of the nanosalt. Instead it had a significant impact on the latent heat release rates. In addition to this, the thermal diffusivity values have moderately increased. This improvement did not diminish later on thermal cycling.

It is observed that the addition of MWCNT particles to PCM (KNO₃) lowered the thermal diffusivity, indicating an increase in the specific heat capacity of the PCM. Further, on addition of the dispersant (CB), the thermal diffusivity values increased to that of the base salt (KNO₃). The dispersants have higher thermal conductivity compared to that of the base salt, and nullified the decrease in thermal diffusivity caused by the MWCNT structures by influencing the hypothesized nano layers or meso layers.

5.6 ASSESSMENT OF PCM- CONTAINER HEAT TRANSFER USING A HOT-COLD PROBE TECHNIQUE

The performance of nano-PCMs during charging and discharging of thermal energy was assessed by analyzing the temperature gradients within a cylindrical metallic probe which is brought in contact with the PCM. The probe-PCM control experiment is a stand-in for a container-PCM unit in a TES system. This perspective is different from the conventional PCM characterization studies. It offers a better insight of

ability of PCMs to receive heat compared to that attained from the CACCA technique where only the release of thermal energy is analysed. In other words, this method assesses both the charging and discharging of thermal energy in a TES system.

The influence of thermophysical properties of the container material over the effectiveness of TES systems, along with modified PCMs was analyzed here. Cylindrical probes of Cu and SS304 were machined with a L/D ratio of 5 (Length = 60mm , Diameter =12mm). Copper and SS were chosen as they are industrially used in storing salt-PCMs.

Nano-PCMs of KNO_3 with MWCNT, Graphite and Graphene nano structures were prepared separately. The nanoparticle composition was maintained at 0.1% by weight of KNO_3 in all PCM composites. Two series of experiments were performed. Firstly, a probe at room temperature (cold probe) is immersed into a pool of molten PCM held at 360°C . 1Kg of PCM was used in every experiment. Secondly, a hot probe (at 570°C) was immersed into finely pulverized PCM (at room temperature). The probes were instrumented with 2 thermocouples of 1mm diameter each. The temperature history of probes was recorded, and processed to compute the heat flux transients at the probe-PCM interface.

Both the sets of experiments were performed and the respective thermal history, heating and cooling curves, were plotted as shown in Figures 5.24-5.27. The derivatives of heating and cooling curves of the probes were computed and are as shown in Figures 5.28-5.31. Heat flux at the probe surface (probe-PCM interface) was estimated. The integral heat flow curves of both hot and cold probes are shown in Figures 5.32-5.35.

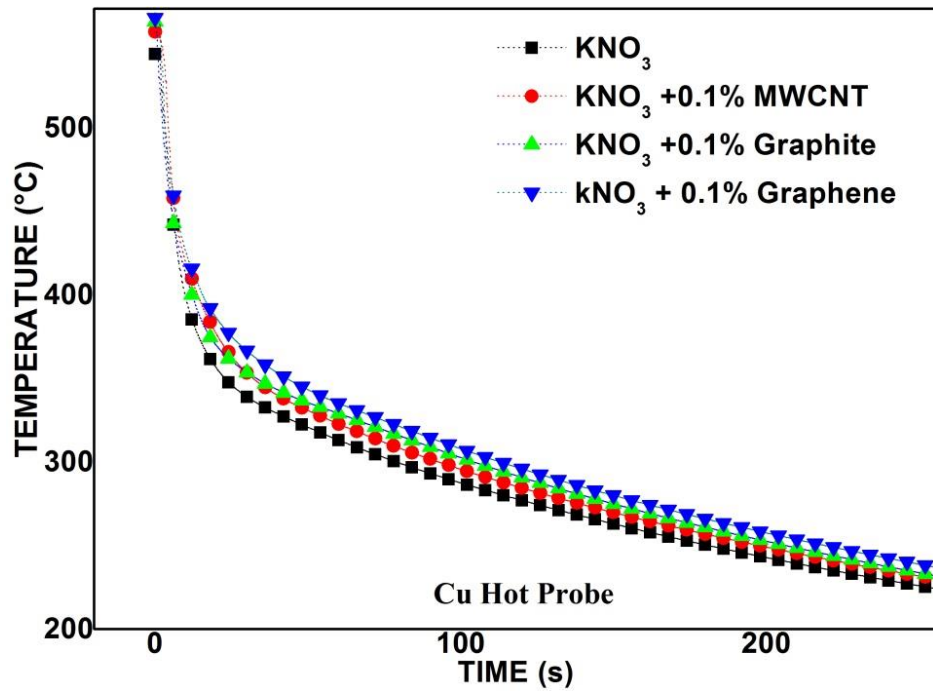


Fig 5.24: Cooling Curve of Cu Hot Probe when immersed in various PCM composites.

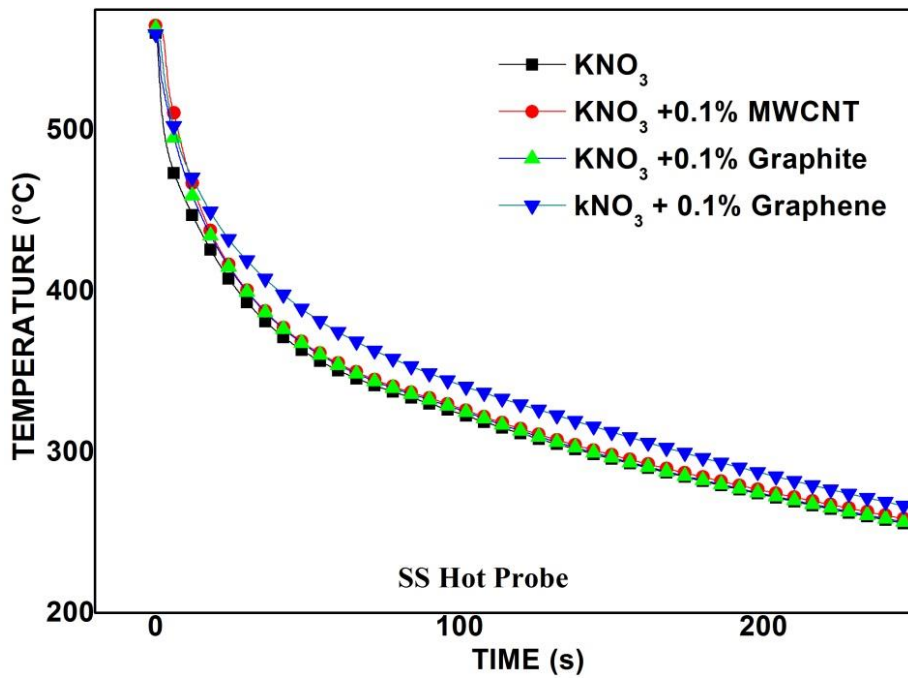


Fig 5.25: Cooling Curve of SS Hot Probe when immersed in various PCM composites.

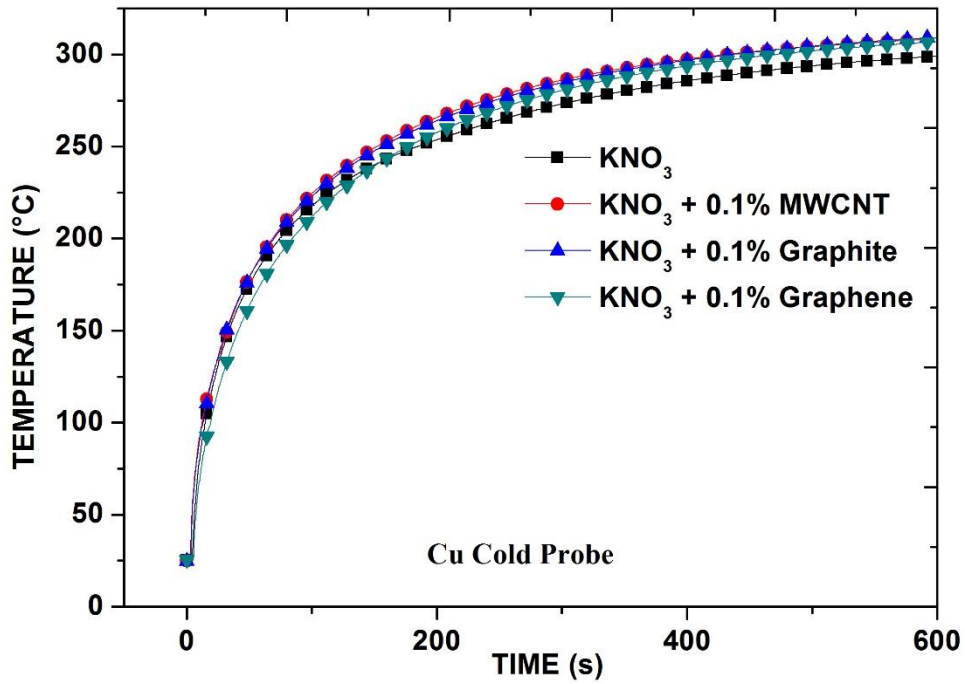


Fig 5.26: Heating Curve of Cu Cold Probe when immersed in various PCM composites.

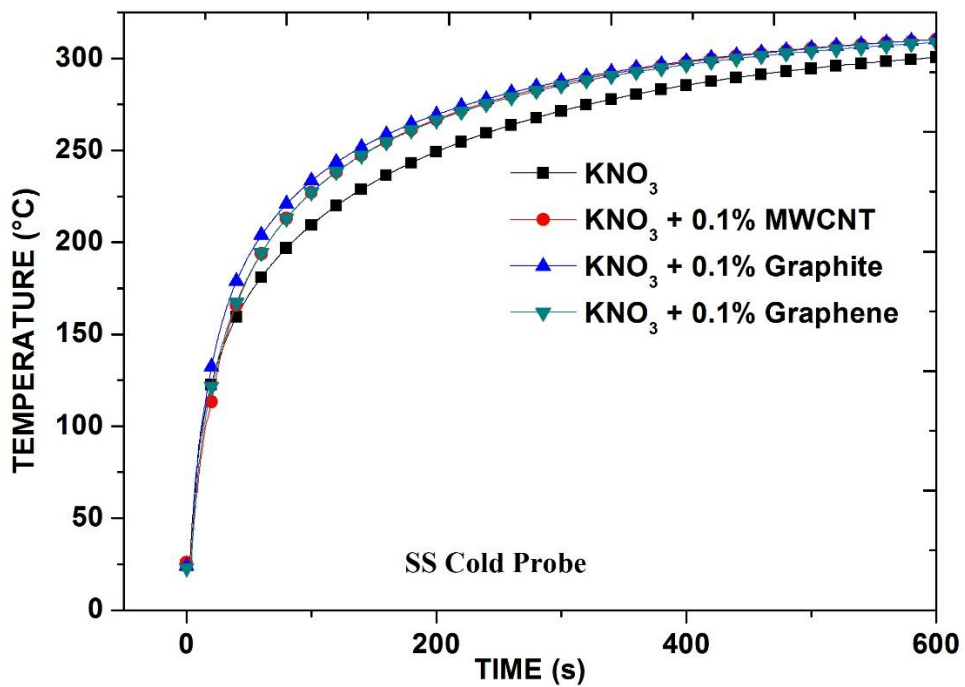


Fig 5.27: Heating Curve of SS Cold Probe when immersed in various PCM composites.

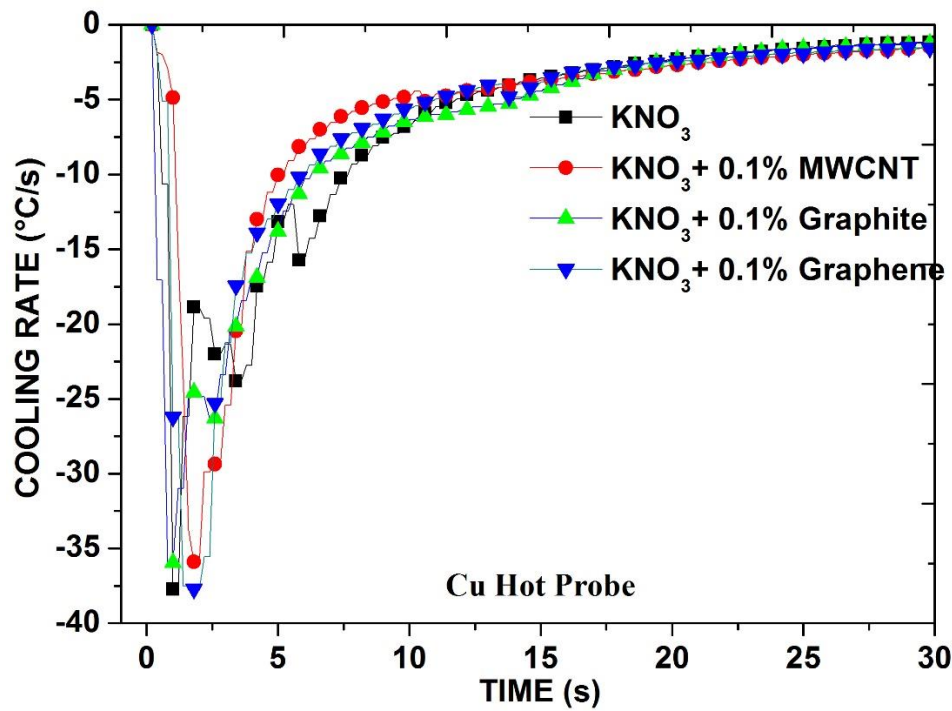


Fig 5.28: Cooling Rate Curve of Cu Hot Probe when immersed in various PCM composites.

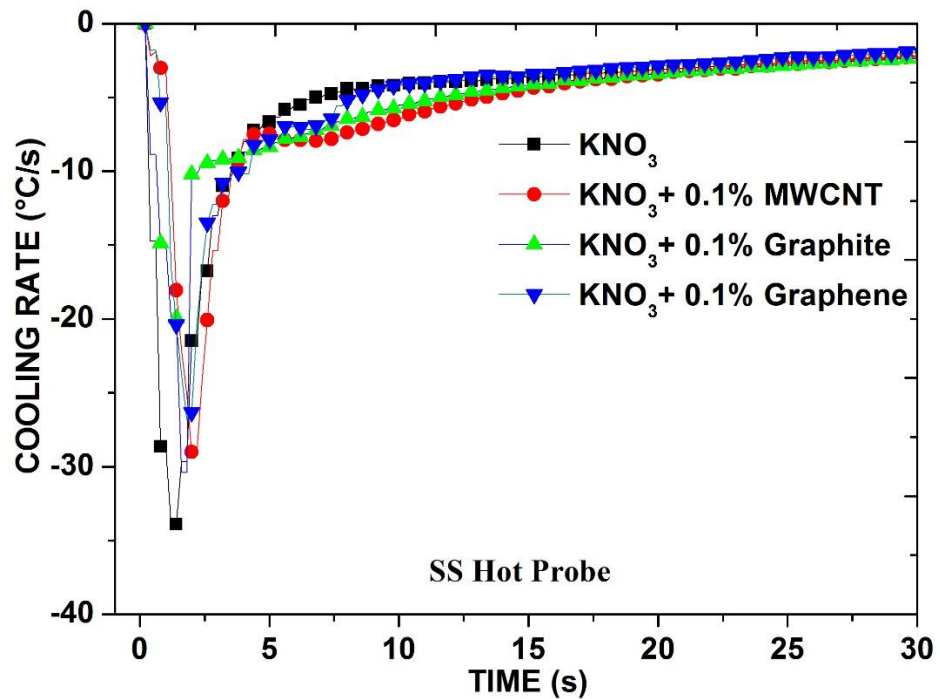


Fig 5.29: Cooling Rate Curve of SS Hot Probe when immersed in various PCM composites.

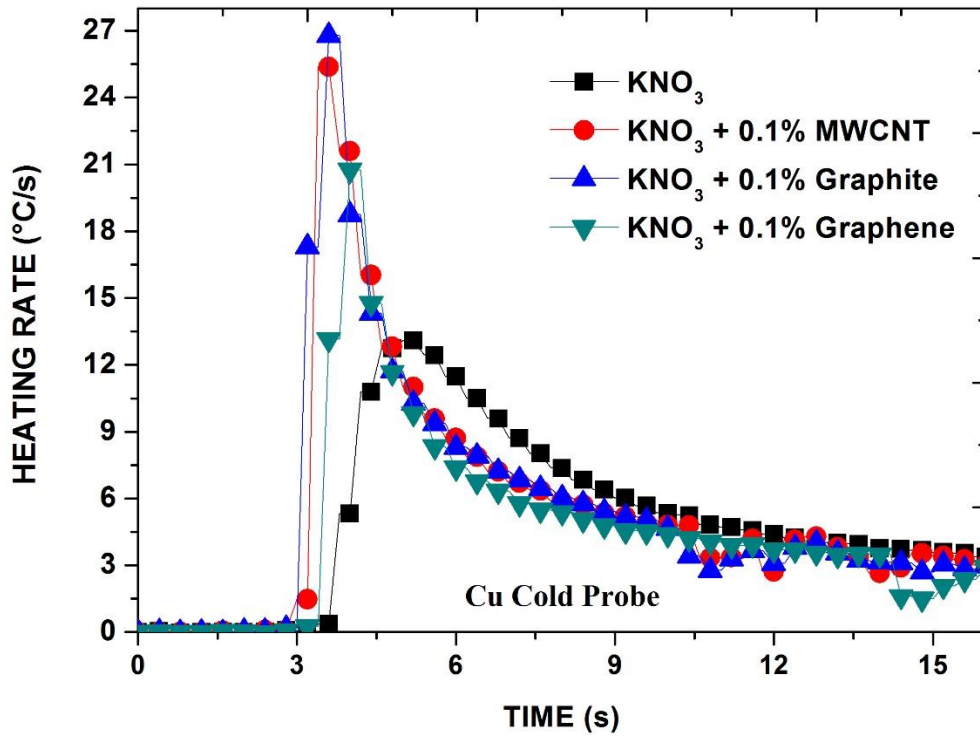


Fig 5.30: Heating Rate Curve of Cu Cold Probe when immersed in various PCM composites.

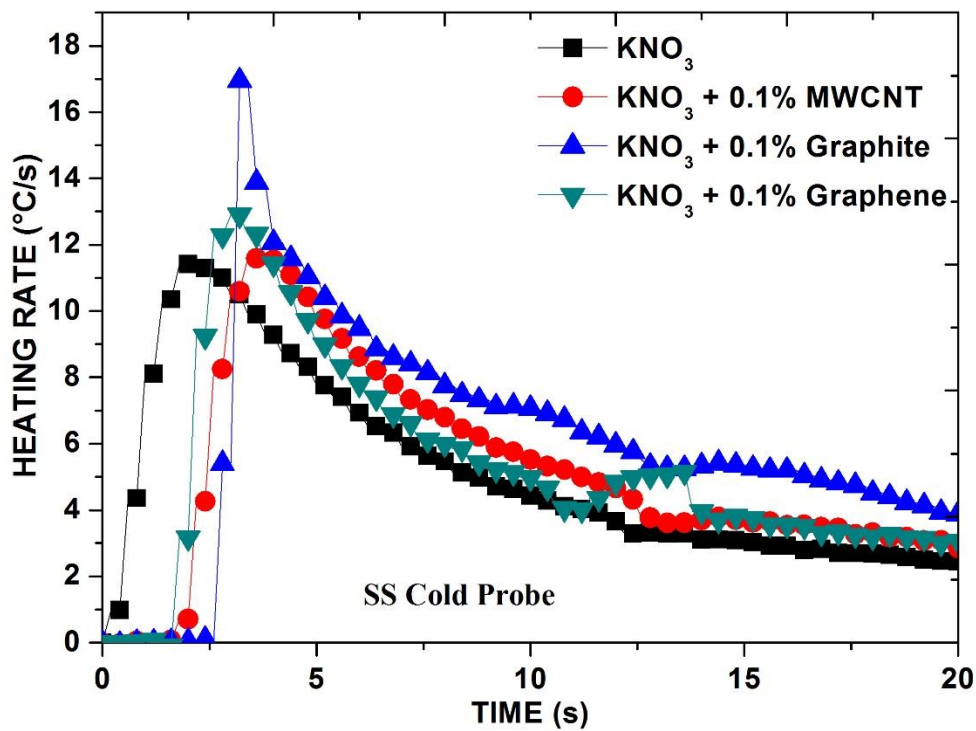


Fig 5.31: Heating Rate Curve of SS Cold Probe when immersed in various PCM composites.

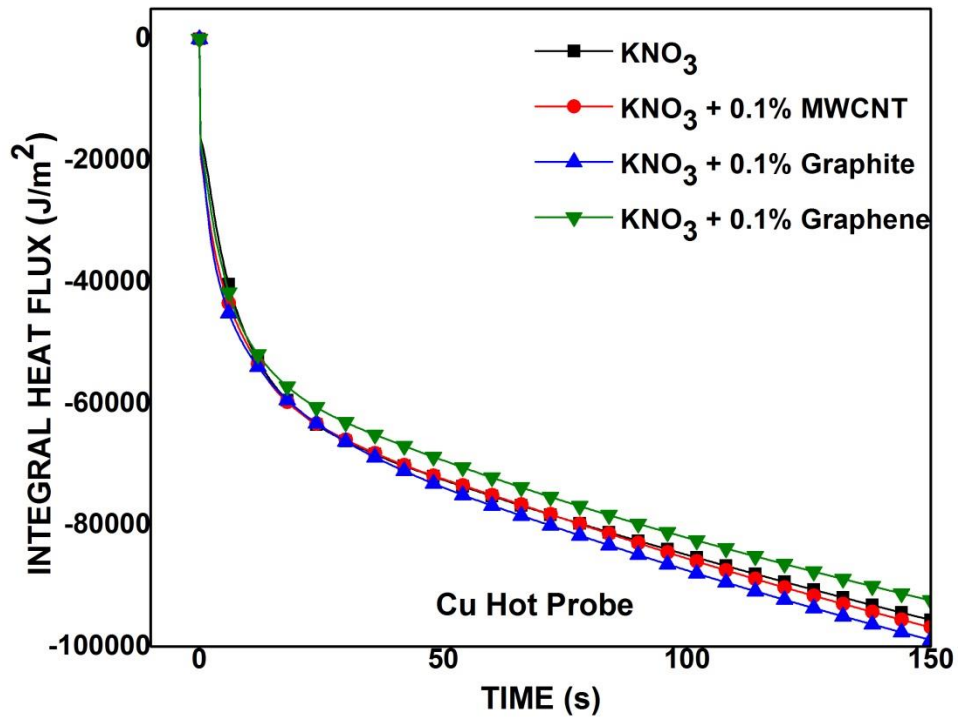


Fig 5.32: Integral heat flux curve of Cu Hot Probe when immersed in various PCM composites.

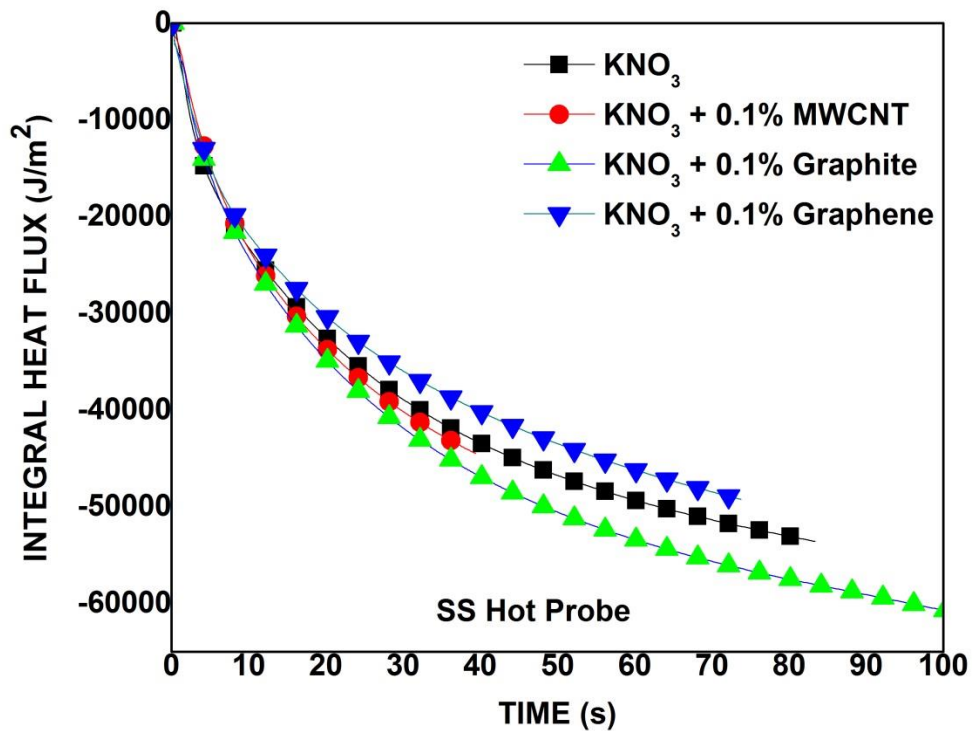


Fig 5.33: Integral heat flux curve of SS Hot Probe when immersed in various PCM composites.

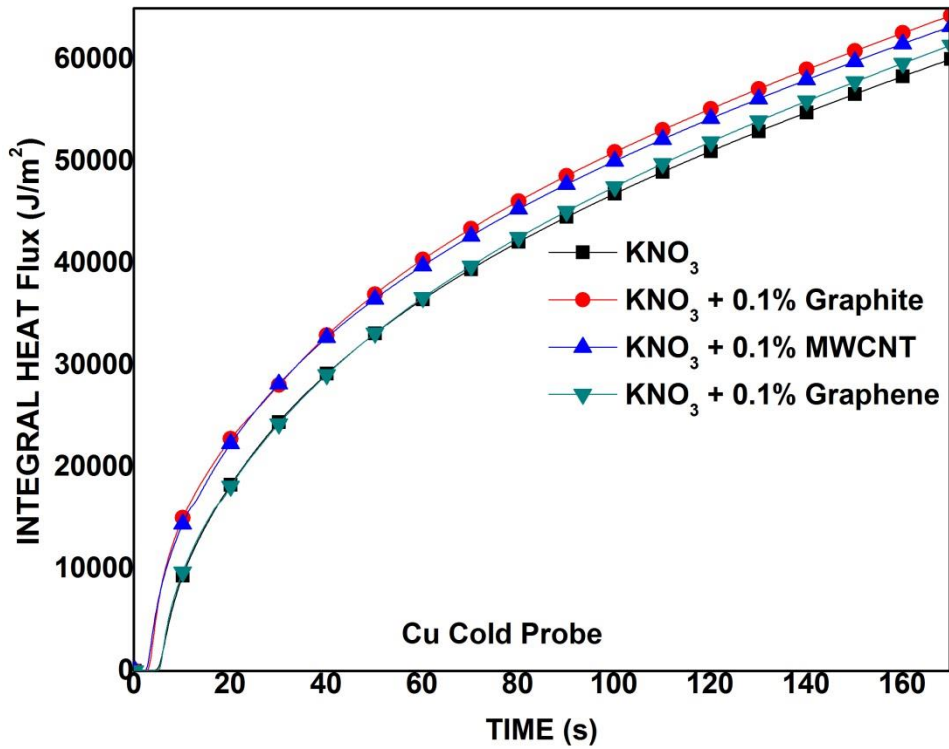


Fig 5.34: Integral heat flux curve of Cu Cold Probe when immersed in various PCM composites.

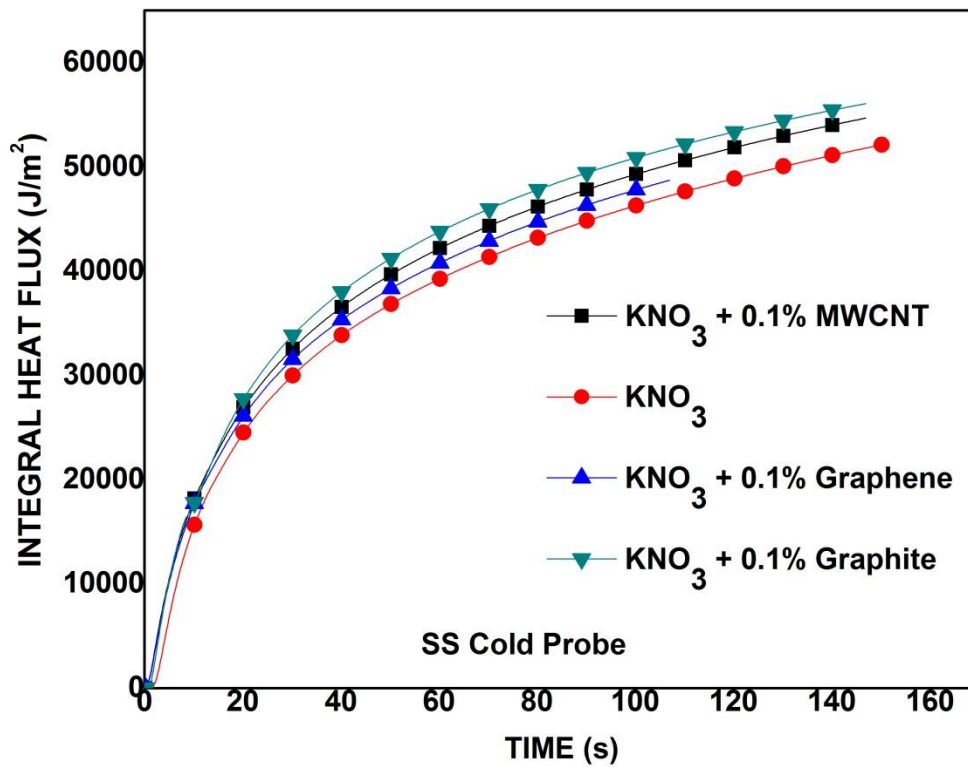


Fig 5.35: Integral heat flux curve of SS Cold Probe when immersed in various PCM composites.

In a cold Cu probe, higher peak heating rates were observed when immersed in molten Nano-PCMs compared to that in molten KNO_3 (pure PCM). As shown in Figure 5.30 and in Figure 5.31, the highest heating rates were observed when the probe was immersed into nano-PCM with graphite nanoparticle additives. Pure PCM offered the least heating rates. The substantial increase in heating rates is attributed to the significant decrease in the solidification time of the PCM samples on addition of graphite nanoparticles as observed in the previous studies. PCM with graphite additives offered an increase in heating rates by 116%, while MWCNT and Graphene added PCM offered an increase of 100% and 65% respectively.

Although an increase in peak heating rates was observed on nano additions to PCM, the magnitude of its increase observed in a SS probe is less compared to that observed in a Cu probe. It indicates that a container material with superior thermophysical properties offer an easy path for heat transfer offering higher heat transfer rates.

On the contrary, in hot probe experiments the cooling rates were not affected by addition of nanoparticles. Both Cu and SS probes showed negligible increase in the cooling rates when immersed in nanosalt-PCM. On contact with the hot probe surface, a thin layer of PCM would melt instantly. As salt PCMs have a negative coefficient of thermal expansion, an air gap is developed at the Probe-PCM interface. These air gaps can considerably reduce the charging rates of PCM. Another cause for this is the formation of oxide layers at the probe surface. As the probes were raised to temperatures above 500°C oxide layers form on the surface. The formation of oxide layer on the probes surface would increase thermal contact resistance retarding the heat transfer rates at the probe-PCM interface.

Integral heat flow curves were plotted. In cold probe experiments, the PCM with graphite additives offered the highest heat flow values over a period of time into both the Cu and SS probes. As the graphite added PCM had the lowest solidification time they offered thermal energy absorption at higher rates. In a span of 100 s, Cu probe absorbed 9% more heat energy from graphite added PCM compared to that from the pure PCM.

The differences in the heat flux between the probe and various nanosalt-PCMs were more prominent in cold probe experiments with SS probes. SS probes have higher thermal energy storage capacity compared to that of a Cu probe of the same volume. Although the rates of heat absorption is less as mentioned above, the total heat flow into an SS probe is more compared that in a Cu probe.

Similar trend was observed in hot probe experiments where the differences in the integral heat flow curves were more prominent in SS probes compared to that in a Cu probe, with graphite added PCM offering highest integral heat flux values followed by MWCNT and Graphene added PCM, and the pure PCM offering the least.

Heat flux curves indicate that the initial rates of heat transfer into the probes (Cold probe) is very much influenced by the thermo-physical properties of the probe material. The probe material (a stand-in for the container to storage PCMs) does have a crucial influence on the energy exchange between the HT fluids and the PCM. Cu with higher thermal conductivity and thermal diffusivity offered higher rates of heat transfer initially, which diminishes with time. In contrast SS with higher heat capacity and lower thermal diffusivity and conductivity, offered more heat transfer over large period of time. Both heat capacity and thermal diffusivity have a pivotal role in selection of container material for PCM storage.

Thermal cycling had a deleterious effect on the integral heat flow curves. Cycling affected the performance of Graphite added PCM the most, and the graphene added PCM was affected the least. This is in accordance with the observations from previous investigations where the agglomeration of nano particles lead to a decrease in the benefits attained. Graphite nanoparticles agglomerated the most and the benefits of decreased solidification time declined on thermal cycling. Graphene added PCM was least affected by thermal cycling.

The decrease in solidification time of KNO_3 on addition of nanoparticles was distinctly observed in these experiments. Graphite added PCM had the lowest solidification time as observed in previous investigations. This offered higher rates of latent heat release which resulted in higher heating/cooling rates of the probes in these experiments. In addition to this, the heat flux curves too justify the benefits of

decreased solidification time as the nanoparticle added PCMs ensured higher heat flux into the probes.

5.7 COMPARATIVE STUDY OF METAL (ZA8) AND SALT (KNO₃) PCMS

CACCA method was employed to analyse the solidification of both the PCMs. Figure 5.36 and Figure 5.37 show the cooling curves during solidification of ZA8 and KNO₃ respectively. The liquidus point in the cooling curve of ZA8 was observed at 405°C where, the Zn rich β -dendrites nucleate and grow till the sample cools down to 375°C. The formation of eutectic η -phase occurs iso-thermally at this temperature. This temperature represents the solidus point. At 254°C the eutectoid transformation of β -dendrites into η -phase and Al rich α -phase is observed. These events are observed both in cooling curve as well as in the cooling rate curve. The reversal of cooling rates is detected at every transition temperature in the cooling rate curve of ZA8 sample. Unlike ZA8, KNO₃ solidifies at a constant temperature of 335°C. Interestingly, the reversal in cooling rates is observed at temperature 306°C. In this case the point of reversal in cooling rate curve cannot be considered as solidus point as the thermal diffusivity of salts are much lower compared to that of metals. This point stands for the instant when the entire latent heat released during solidification is extracted, and the sample cools along with the container thereafter. In the case of metals, the lag between the solidus point and the concerned point of reversal in the cooling rate curve is negligibly small due to its superior thermal diffusivity property. Figure 5.42 too gives similar information on cooling rates during solidification at any concerned temperature range.

The thermal diffusivity values of PCMs were determined over various temperatures using the Fourier method. Figure 5.38 and Figure 5.39 shows the thermal diffusivity curves of ZA8 and KNO₃ respectively. Eq. (10) was used to obtain the thermal diffusivity values within the solidification range. Here, the end points between which the thermal diffusivity values were interpolated are not the solidus and liquidus points. They are chosen from pre-solidification and post-solidification regions where

the fluctuation in readings obtained are minimum. The liquidus and solidus points are marked as L and S respectively.

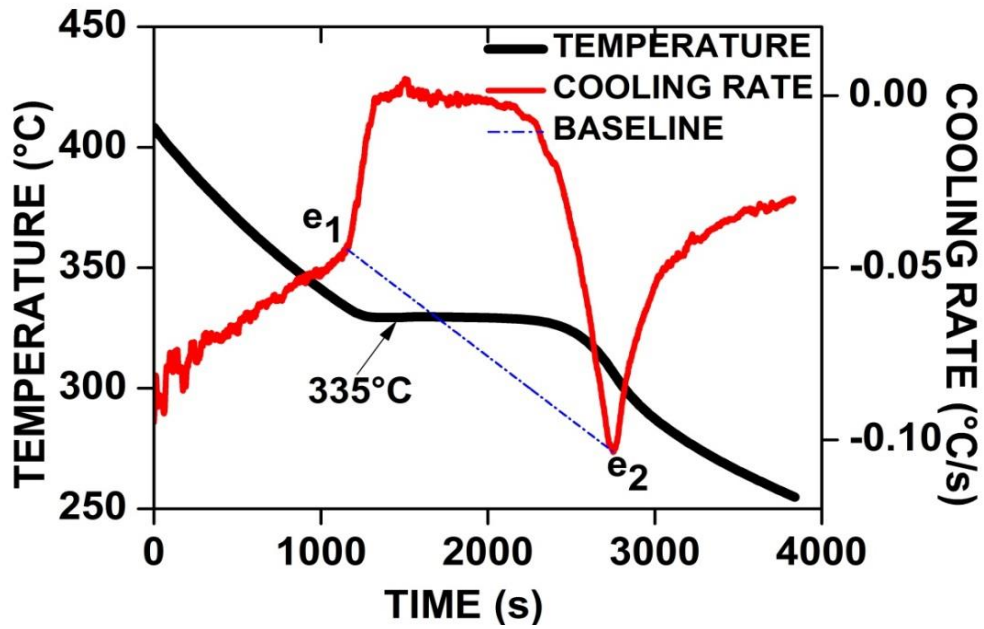


Fig 5.36: Cooling curve and Cooling rate curve of KNO_3 , Newtonian method.

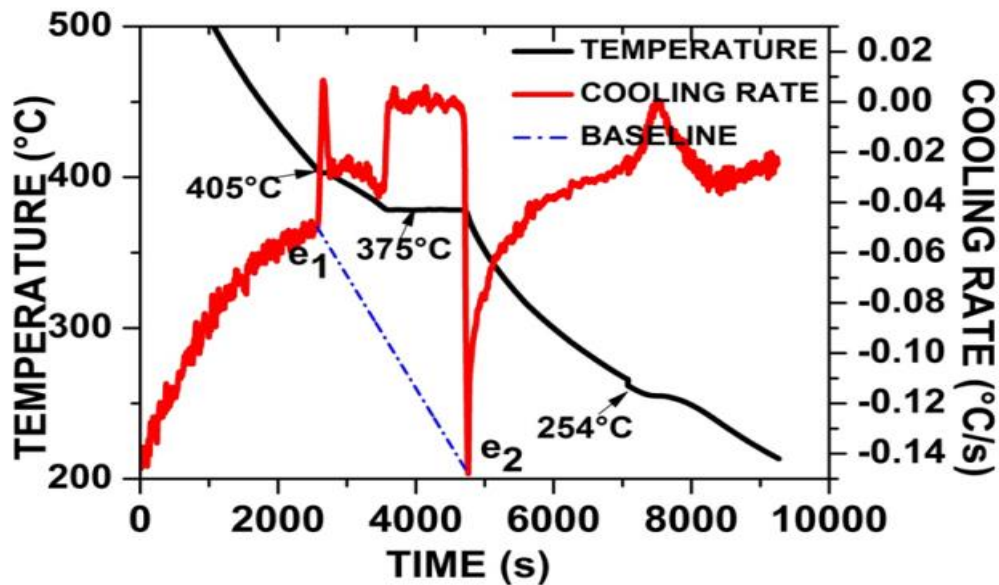


Fig 5.37: Cooling curve and Cooling rate curve of ZA8, Newtonian method.

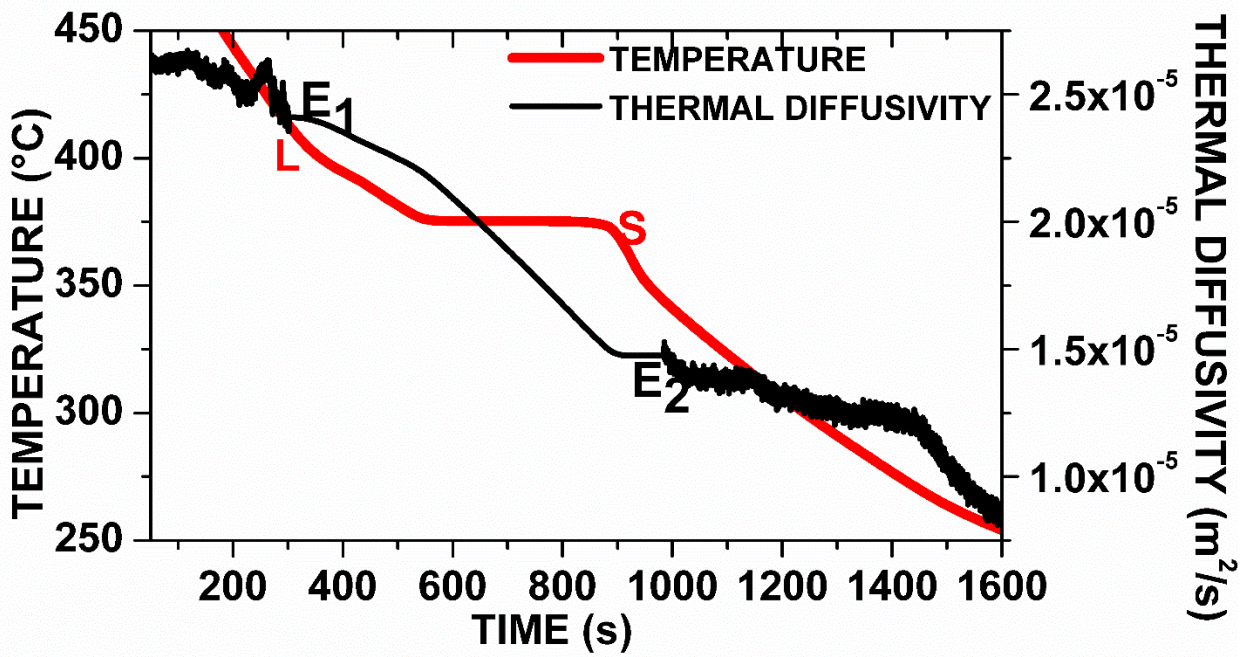


Fig 5.38: Thermal diffusivity curve of ZA8, Fourier method.

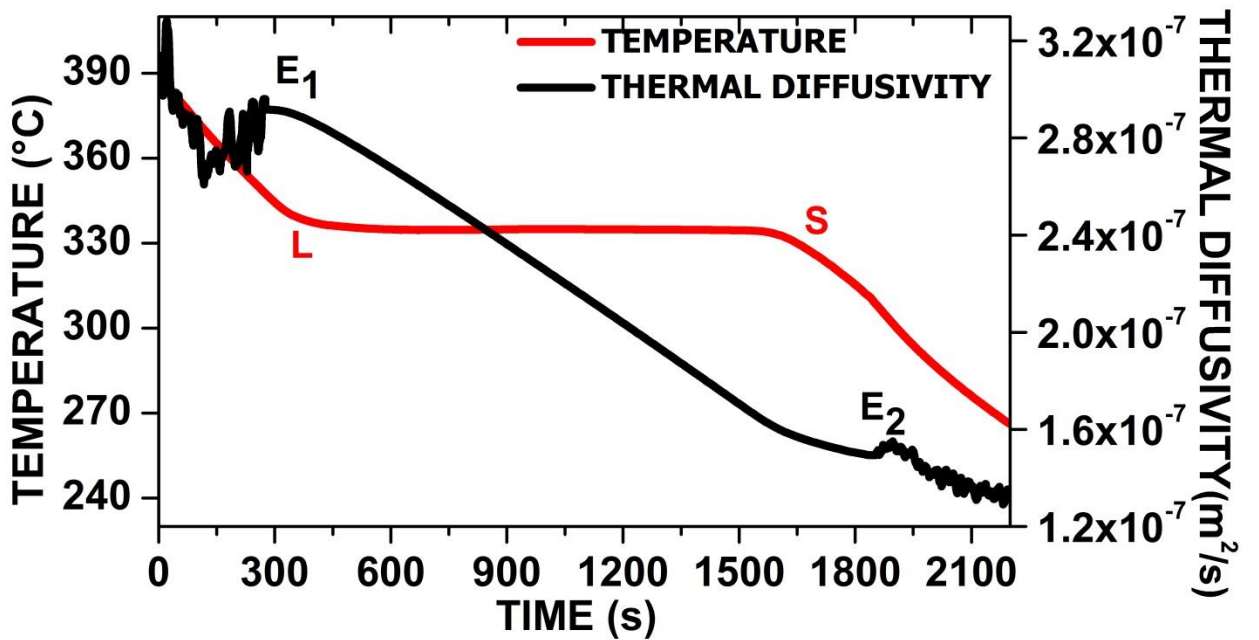


Fig 5.39: Thermal diffusivity curve of KNO₃, Fourier method.

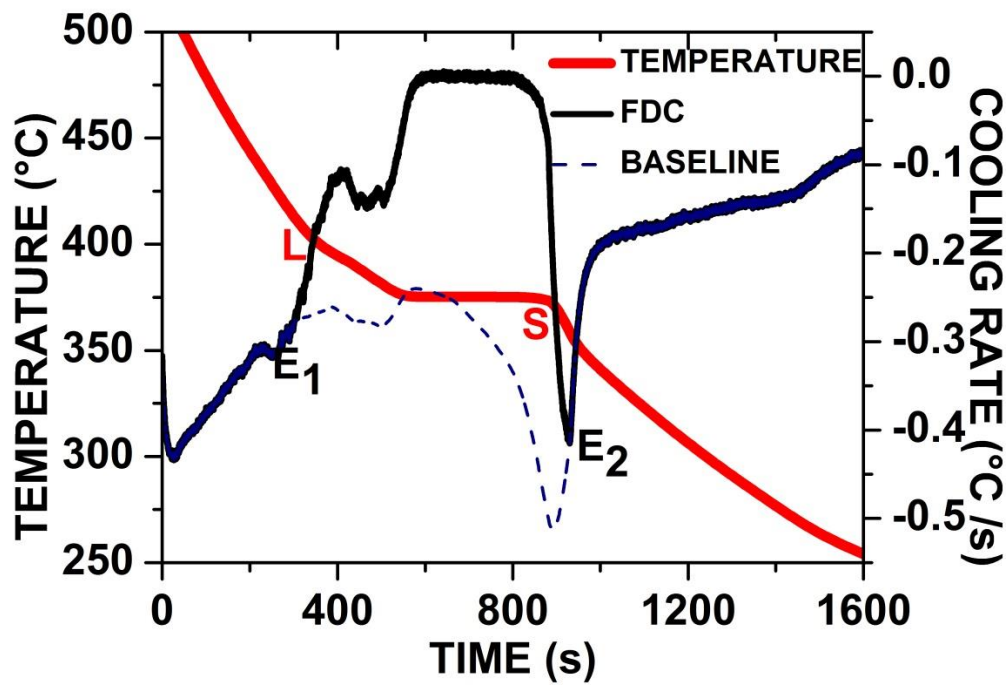


Fig 5.40: FDC and Baseline of ZA8, Fourier method

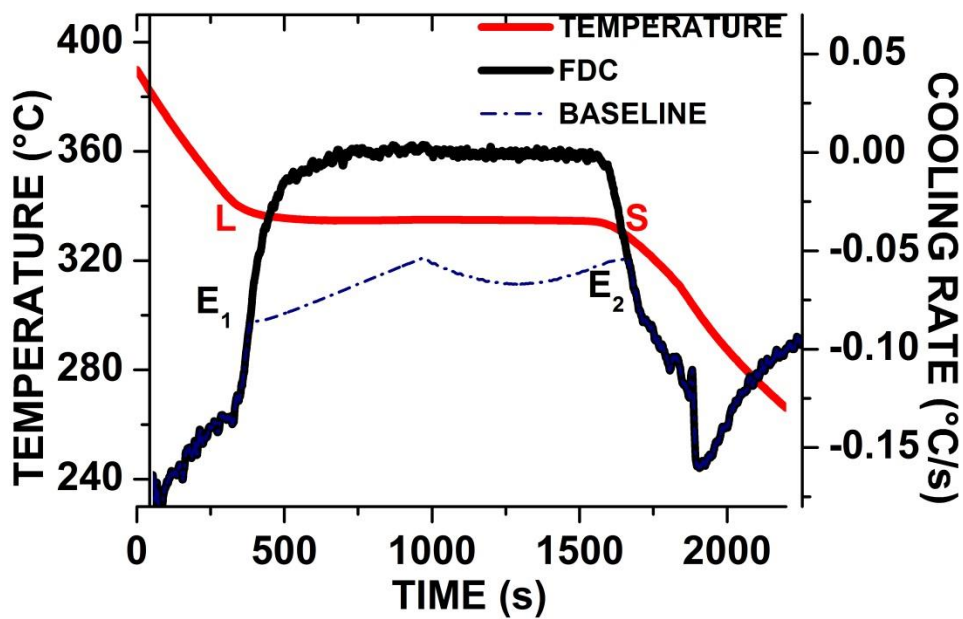


Fig 5.41: FDC and Baseline of KNO₃, Fourier method

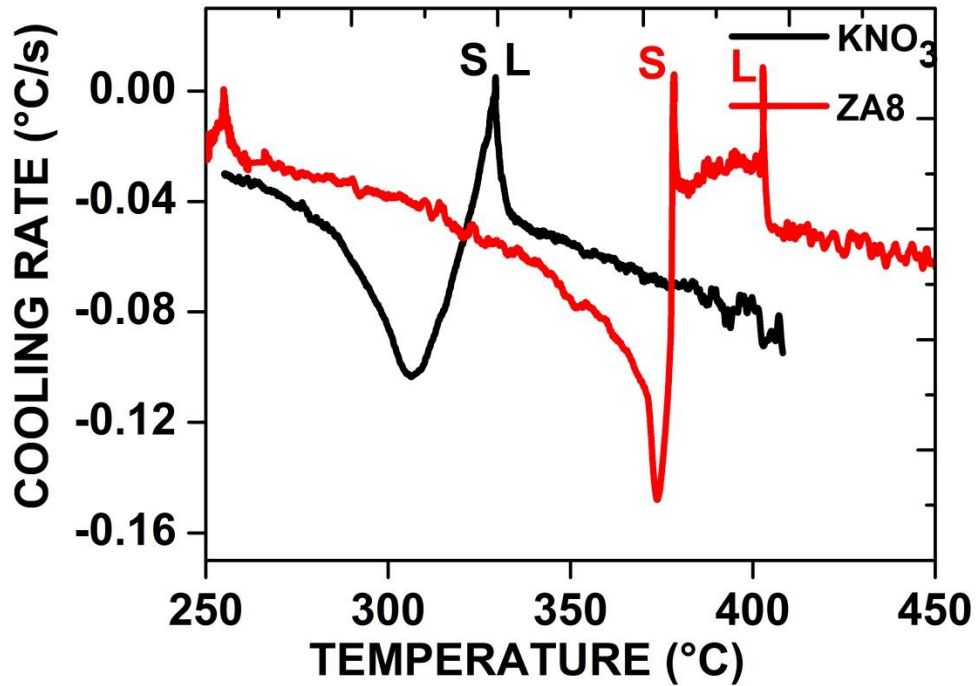


Fig 5.42: Cooling rate versus temperature curves, Newtonian method.

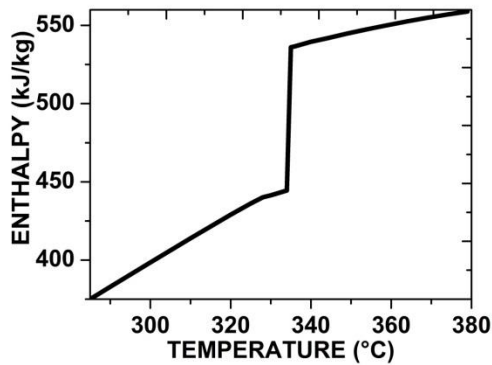


Fig 5.43: Enthalpy curve of KNO_3
Enthalpy value of 240kJ was assumed for KNO_3 at 200°C with a C_p of 1.2kJ/kg.K.

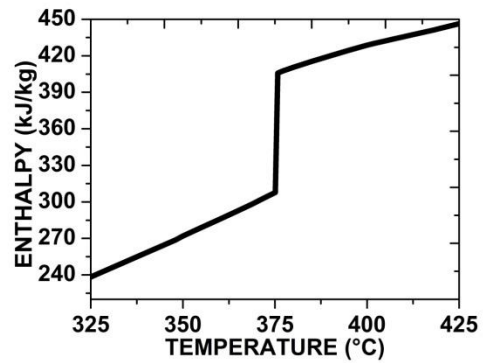


Fig 5.44: Enthalpy curve of ZA8
Enthalpy value of 150kJ was assumed for ZA8 at 254°C with a C_p of 0.6kJ/kg.K

The C_p value was predicted using Eq. (15) by taking values of density and thermal conductivity over concerned temperature range from the literature [Powell R. W. et al. (1966), and Kenisarin M. M. (2010)]. The thermophysical properties of ZA8 alloy was estimated using Eq. (16) and Eq. (17).

$$C_p = \frac{k}{\alpha \cdot \rho} \dots \dots (15)$$

$$\rho_{ZA8} = (0.92) \rho_{Zn} + (0.08) \rho_{Al} \dots \dots (16)$$

$$k_{ZA8} = (0.92) k_{Zn} + (0.08) k_{Al} \dots \dots (17)$$

Both the Newtonian and the Fourier techniques were employed to estimate the latent heat of solidification. The assumptions in both the methods had an influence on their results as the latent heat values obtained varied considerably. In Newtonian method, the Zero curve or Baseline was fitted linearly. The baseline was fitted between the end points, e1 and e2 on the cooling rate curve as shown in Figure 5.36 and Figure 5.37 for KNO₃ and ZA8 respectively. In Fourier method, the Baseline was fitted between E1 and E2 which represent the liquidus and the solidus points respectively in the cooling rate curve as shown in Figure 5.40 and Figure 5.41. The selection of the end points again needs to be meticulously performed. The end points are located in the region where the heat transfer is strictly considered to be via conduction without heat generation.

The mean Cp values obtained in the solidification range were 1.2 and 0.8 kJ/kg.K for KNO₃ and ZA8 respectively. The estimated latent heat of solidification are given in Table 5.5. The latent heat of fusion values obtained from Fourier method are closer to the values reported, 88kJ/kg for KNO₃ by Janz G.J. et al.(1979) and 110kJ/kg for ZA8 in Alloy Data (2006).

Table 5.5: TES parameters of PCMs predicted by CACCA method.

PCM	Phase Transition Temperature (°C)			Latent heat of Fusion (kJ/kg)		
	CACCA		Other Techniques	CACCA		Other Techniques
	N.T	F.T		N.T	F.T	
KNO₃	335	335	335[Janz G.J. et al.1979]	110	91	88[Janz G.J.et al.1979]
ZA8	405-375	405-375	404-375 (Alloy data 2006)	129	109	110[Alloy data 2006]

The cooling rates at the end points in Newtonian method depend on the crucible or container material too. Container material with higher heat diffusivity would cause a higher cooling rate at the end points, reducing the accuracy in latent heat estimation.

This aspect makes Fourier method more accurate over the Newtonian method. Another source of error here is the use of fraction solid values between the selected end points for the prediction of thermal diffusivity and C_p values. In the case of KNO_3 where the sample is homogenous with solidification at a fixed temperature ($335^\circ C$), the error is least. In contrast, this approach fails in the case of inhomogeneous materials like ZA8 alloy. Here the primary phase is rich in zinc while the presence of aluminium is observed in the eutectic phase during later part of solidification. Initially, during solidification the C_p value is approximately equal to that of pure zinc which is unaccounted in this method of predicting C_p using solid fraction, shown in Eq. (15). These inaccuracies have insignificant effect on the enthalpy curves estimated as the latent heat of fusion evolved is large enough to overcome these inaccuracies over C_p values. The enthalpy curves of ZA8 and KNO_3 are shown in Figure 5.43 and Figure 5.44 respectively. Table 4: Melting point and Latent heat of fusion of PCMs predicted by CACCA method.

Computer Aided-Cooling Curve Analysis offers a simple and inexpensive approach in thermal energy storage material studies using phase change materials. The effectiveness of this method grossly depends on the calibration and high sensitivity of the thermocouples used. The precise values of thermal conductivity and material density of PCMs studied are necessary in predicting C_p values. In developing new PCMs, devices to measure thermal conductivity and density can enhance the effectiveness of this technique significantly. Further, the selection of end points on cooling rate curves is another aspect that influences the accuracy of the obtained result. Both the PCMs, ZA8 and KNO_3 are suitable for TES applications. ZA8 is a suitable alternative for Nitrate salts as a TES material in the temperature range of $300-400^\circ C$. With superior thermal diffusivity, ZA8 offers better heat transfer characteristics compared to that of nitrate salts.

6. CONCLUSION

Based on the present investigation, the following conclusions were drawn.

1. A significant decrease in the solidification time of salt-PCM was observed on addition of nanoparticles, without affecting the solidification temperature (335°C) of KNO_3 . Nanoparticles offered an easy path for thermal transport. The maximum decrease in solidification time was observed on the addition of graphite particles while the decrease was minimum on graphene particle addition. The decrease in solidification time is beneficial as the same amount of stored energy can now be withdrawn at a higher rate. The addition of nanoparticles therefore, increased the discharging rates of TES systems based on salt-PCMs.
2. Solidification time of nanosalt-PCMs vary with the concentration of nanoparticles in the PCM. The solidification time decreased significantly with an increase in the concentration of MWCNT.
3. The addition of nanoparticles did have an influence on the thermal diffusivity property of the salt-PCM. The addition of MWCNT and graphite decreased the thermal diffusivity property while the addition of graphene particles lead to an enhancement of this property in the salt-PCM. The decrease in thermal diffusivity property was attributed to the formation of nanolayers on addition of MWCNT and graphite nanoparticles in the salt-PCM. The low energy graphene sheets have relatively poor influence in ordering the neighboring ions causing weaker nanolayers. In addition to this, the graphene sheets show exceptionally higher thermal conductivity accounting for an increase in thermal diffusivity property in the salt-PCM.
4. Thermal cycling had a deleterious effect on TES functionalities of nanosalt-PCM. Agglomeration of nanoparticles was observed on thermal cycling which lead to an increase in solidification time which in turn decreased the discharge

rate of thermal energy. In other words, the benefits of nanoparticle addition decreased on thermal cycling. Highest change in solidification time was observed in graphite added PCM while the graphene embedded PCM showed minimum changes. Graphene particle embedded PCMs were found to be more stable during thermal cycling.

5. The use of dispersants in nanosalt-PCMs improved their response to thermal cycling. The use of dispersants such as Carbon Black and TiO₂ was beneficial in decreasing the deterioration of MWCNT added PCM over thermal cycling by limiting the change in solidification time. This is a critical outcome in the development of superior TES materials. As a dispersant, carbon black was more effective than TiO₂ in minimizing the deleterious effect of thermal cycling on TES parameters of nanosalt-PCMs.
6. The dispersion of graphite microparticles into the salt-PCM too offered a considerable enhancement in the energy discharge rates of the PCM. Although the enhancement in heat removal rates on the addition of micro particles were considerably less compared to that from the addition of nano particles, the enhancement in heat removal rates observed on addition of micro particles to the salt-PCM were consistent throughout the period of 10 thermal cycles. Thus, the microparticle dispersed salt-PCMs are more stable compared to nanosalt-PCMs in their respective response to thermal cycling.
7. A novel Hot-Cold Probe technique was proposed to assess the heat transfer characteristics at the PCM - Container interface. Heat flux curves indicate that both heat capacity and thermal diffusivity property have a pivotal role in selection of container materials for PCM storage. The heating/cooling rate curves and the heat flow curves justify the results obtained from the CACCA studies of the concerned PCMs.
8. Both metal (ZA8) and salt (KNO₃) PCMs are suitable candidates for TES applications in the concerned temperature range. The metallic PCM offered

higher cooling rates with much superior thermal diffusivity. ZA8 is a suitable alternative for nitrate salts as a TES material in the temperature range of 300-400°C.

SUMMARY

Additives have significantly influenced the TES parameters of the salt-PCM. The decrease in solidification time on addition of both the nano and micro sized particles have significantly increased the heat transfer rates during discharge of thermal energy in a TES system. The benefits obtained on nanoparticle addition were observed to diminish on thermal cycling due to their agglomeration. Use of dispersants prevent the agglomeration of nanoparticles in salt-PCMs which can improve the stability of nanosalt-PCMs during thermal cycling.

The proposed Hot/Cold probe technique can effectively be used to assess heat transfer at the PCM – Container interface. The results obtained from this technique are in agreement with that obtained from CACCA.

By virtue of their superior thermal conductivity and thermal diffusivity, metallic PCMs can be suitable alternative for salt-PCMs for TES applications.

FUTURE SCOPE OF INVESTIGATION

The response of nanosalt-PCMs to thermal cycling shall be investigated to over 5000 thermal cycles to assess their suitability for an industrial uptake in large scale. Further, the influence of nanoparticles on melting of PCMs (during charging of PCMs) shall be investigated in future. Direct measurement of various properties of nanosalt-PCMs shall be performed to comprehensively analyse the effect of nanoparticle addition on various TES function of salt-PCMs. The anomalous increase in specific heat capacity of salt-PCMs on addition of nanoparticles shall be investigated.

REFERENCES

- Adinberg R., Zvegilsky D. and Epstein M. (2010). "Heat transfer efficient thermal energy storage for steam generation." *Energy Conversion and Management*, 51, 9–15.
- Akgun M., Aydin O. and Kaygusuz K. (2007). "Experimental study on melting/solidification characteristics of a paraffin as PCM." *Energy Conversion and Management*, 48, 669–678.
- Alkan C. (2006). "Enthalpy of melting and solidification of sulfonated paraffins as phase change materials for thermal energy storage." *Thermochimica Acta*, 451, 126–130.
- Alloy data (2006), NADCA product specification standards for Die casting A-3-14-06.
- Aran Solé A., Miró L., Barreneche C., Martorell I. and Cabeza L. F. (2013). "Review of the T history method to determine thermo physical properties of phase change materials (PCM)." *Renewable and Sustainable Energy Reviews*, 26, 425–436.
- Atif R. and Inam F. (2016). "Reasons and remedies for the agglomeration of multi-layered graphene and carbon nanotubes in polymers", *Beilstein journal of nanotechnology*, 7, 1174-1196.
- Babaei H., Keblinski P. and Khodadadi J. M. (2013). "Thermal conductivity enhancement of paraffins by increasing the alignment of molecules through adding CNT/grapheme." *International Journal of Heat and Mass Transfer*, 58, 209–216.
- Barreneche C., Solé A., Miro L., Martorell I., A. Inés Fernández A. I. and Cabeza L. F. (2013). "Study on differential scanning calorimetry analysis with two

operation modes and organic and inorganic phase change material (PCM).” *Thermochimica Acta*, 553, 23– 26.

Bauer T. and Tamme R. (2006). “PCM-graphite composites for high temperature thermal energy storage” in: *Proceedings of the 10th International Conference on Thermal Energy Storage—Ecostock2006 Conference*, Pomona, NJ (USA).

Bey S., Fois M., Krupa I., Ibos L., Benyoucef B. and Candau Y. (2014). “Thermal characterization of polymer matrix composites containing microencapsulated paraffin in solid or liquid state.” *Energy Conversion and Management*, 78, 796–804.

Birchenall C. E. and Reichmann A. F. (1980). “Heat storage in eutectic alloys.” *Metallurgical Transactions A*, 11A, 1415-1420.

Bo H., Gustafsson E. M. and Setterwall F. (1999). “Tetradecane and hexadecane binary mixtures as phase change materials (PCMs) for cool storage in district cooling systems.” *Energy*, 24, 1015–1028.

Brown E. N., Kessler M. R., Sottos N. R. and White S. R. (2003). “In situ poly(urea-formaldehyde) microencapsulation of dicyclopentadiene” *Journal of Microencapsulation*, 20(6), 719-730.

Cabedo P. A., Mondragon R., Hernandez L., Cuenca R. M., Cabedo L. and Julia J. E. (2014), “Increment of specific heat capacity of solar salt with SiO₂ nanoparticles”, *Nanoscale Research Letters*, 9, 582.

Cabeza L. F., Svensson G., Hiebler S. and Mehling H. (2003). “Thermal performance of sodium acetate trihydrate thickened with different materials as phase change energy storage material.” *Applied Thermal Engineering*, 23, 1697–1704.

Chieruzzi M., Cerritelli G. F., Miliozzi A. and Kenny J. M. (2013), “Effect of nanoparticles on heat capacity of nanofluids based on molten salts as PCM for thermal energy storage”, *Nanoscale Research Letters*, 8, 448.

- Cui Y., Liu C., Hu S. and Yu X. (2011). “The experimental exploration of carbon nanofiber and carbon nanotube additives on thermal behavior of phase change materials.” *Solar Energy Materials & Solar Cells*, 95, 1208–1212.
- Das S. K., Choi S. U. S., Yu W. and Pradeep T. (2008) “*Nanofluids: Science and Technology*”, John Wiley & Sons, 1-33
- Djurdjevic M. B., Odanovic Z. and Talijan N. (2011) “Characterization of the Solidification Path of AlSi5Cu(1–4 wt.%) Alloys Using Cooling Curve Analysis.” *JOM*, 30(11), 51-57.
- Fang G., Li H., Yang F., Liu X. and Wu S. (2009). “Preparation and characterization of nano-encapsulated *n*-tetradecane as phase change material for thermal energy storage.” *Chemical Engineering Journal*, 153, 217–221.
- Farkas D. and Birchenall C.E. (1985). “New eutectic alloys and their heats of transformation.” *Metallurgical Transactions A*, 16A, 323-328.
- Fras E., Kapturkiewicz W., Burbielko A. and Lopez H. F. (1993) “ A New concept in thermal analysis of castings” *AFS Transactions*, 101, 505-511.
- Garus S. and Purohith I. (2007). “Making solar thermal power generation in India a reality – Overview of technologies, opportunities and challenges.” *The Energy and Resources Institute (TERI)*, India.
- Ge Z., Ye F., Cao H., Leng G., Qin Y and Ding Y. (2014), “Carbonate-salt-based composite materials for medium- and high-temperature thermal energy storage”, *Particuology*, 15, 77–81.
- Glatzmaier G. C., Gomez J., Ortega J., Starace A. and Turchi C. (2011). “High temperature phase change materials for thermal energy storage applications.” *NREL/CP-5500-52390, SolarPACES2011 Conference*, Granada, Spain.
- Gök O., Yilmaz M. O. and Paksoy H. O. (2006). “Stabilization of glauber’s salt for latent heat storage” in: *Proceedings of the 10th International Conference on Thermal Energy Storage—Ecostock2006 Conference*, Pomona, NJ(USA).

Gschwander S., Schossig P. and Henning H. M. (2005). "Micro-encapsulated paraffin in phase-change slurries." *Solar Energy Materials & Solar Cells*, 89, 307–315.

Haq I., Shin J. and Lee Z. H. (2004). "Computer-Aided Cooling Curve Analysis of A356 Aluminium Alloy." *Metals and Materials international*, 10(1), 89-96.

Harikrishnan S. and Kalaiselvam S. (2012). "Preparation and thermal characteristics of CuO-oleic acid nanofluids as a phase change material." *Thermochimica Acta*, 533, 46– 55.

Hentschke R. (2016), "On the specific heat capacity enhancement in nanofluids", *Nanoscale Research Letters*, 11, 88.

Herrmann U., Kelly B. and Price H. (2004) "Two-tank molten salt storage for parabolic trough solar power plants." *Energy*, 29, 883–893.

Ho C. J. and Gao J. Y. (2009). "Preparation and thermophysical properties of nanoparticle-in-paraffin emulsion as phase change material." *International Communications in Heat and Mass Transfer*, 36, 467–470.

Hoshi A., Mills D.R., Bittar A. and Saitoh T.S. (2005). "Screening of high melting point phase change materials (PCM) in solar thermal concentrating technology based on CLFR" *Solar Energy*, 79, 332–339.

Inaba H. and Tu P. (1997). "Evaluation of thermophysical characteristics on shape-stabilized paraffin as a solid-liquid phase change material." *Heat and Mass Transfer*, 32, 307–312.

IRENA working paper. (2012) "Concentrating Solar Power", *Renewable energy technologies : cost analysis series*, IRENA, 1(2/5).

Janz G.J., Allen C.B., Bansal N.P., Murphy R.M. and Tomkins R. P. T. (1979). "Physical properties data compilations relevant to energy storage. II. Molten salts: Data on single and multicomponent salt systems." *NSRDS-NBS 61, Part II.*, US Department of Commerce.

JNN Solar Mission, Scheme/Document,

<http://www.mnre.gov.in/solarmission/jnnsnm/introduction-2/>, (aug.20 2014).

Jo B. and Banerjee D. (2015), “Enhanced Specific heat capacity of molten salt-based carbon nanotubes nanomaterials”, *Journal of Heat Transfer ASME*, 137, 091013-1.

Kenisarin M.M. (2010). “High-temperature phase change materials for thermal energy storage.” *Renewable and Sustainable Energy Reviews*, 14, 955–970.

Khodadadi J. M. and Hosseinizadeh S. F. (2007). “Nanoparticle-enhanced phase change materials (NEPCM) with great potential for improved thermal energy storage.” *International Communications in Heat and Mass Transfer*, 34, 534–543.

Kim S. and Drzal L. T. (2009). “High latent heat storage and high thermal conductive phase change materials using exfoliated graphite nanoplatelets.” *Solar Energy Materials & Solar Cells*, 93, 136–142.

Kotze J. P., von Backstrom T. W. and Erens P. J. (2013). “High temperature thermal energy storage utilizing metallic phase change materials and metallic heat transfer fluids.” *Journal of Solar Energy Engineering*, 135, 0350011-6.

Kumar T. S. (2004). “A serial solution for the 2-d inverse heat conduction problem for estimating multiple heat flux components”, *Numerical Heat Transfer, Part B: Fundamentals*, 45:6, 541-563.

Kuravi S., Trahan J., Goswami D. Y., Rahman M. M. and Stefanakos E. K. (2013). “Thermal energy storage technologies and systems for concentrating solar power plants.” *Progress in Energy and Combustion Science*, 39, 285-319.

Laing D., Bahl C. B, Bauer T., Lehmann D. and Steinmann W. D. (2011) “Thermal energy storage for direct steam generation.” *Solar Energy*, 85, 627–633.

Lasfargues M., Geng Q., Cao H. and Ding Y. (2015), “Mechanical dispersion of nanoparticles and its effects on the specific heat capacity of impure binary nitrate salt mixtures”, *Nanomaterials*, 5, 1136-1146.

Li B., Zeng D., Yin X. and Chen Q. (2010). “Theoretical prediction and experimental determination of room-temperature phase change materials using hydrated salts as agents.” *J Therm Anal Calorim*, 100, 685–693.

Li J., Xue P., Ding W., Han J. and Sun G. (2009). “Micro-encapsulated paraffin/high-density polyethylene/wood flour composite as form-stable phase change material for thermal energy storage” *Solar Energy Materials & Solar Cells*, 93, 1761-1766

Liao Z., Li X., Wang Z., Chang C. and Xu C. (2014) “Phase change of molten salt during the cold filling of a receiver tube.” *Solar Energy*, 101, 254–264.

Liu M., Belusko M., Tay N. H. S. and Bruno F. (2014) “Impact of the heat transfer fluid in a flat plate phase change thermal storage unit for concentrated solar tower plants.” *Solar Energy*, 101, 220–231.

Malekan M. and Shabestari S. G. (2011). ”Computer aided cooling curve thermal analysis used to predict the quality of aluminium alloys.” *J Therm Anal Calorim*, 103, 453-458.

Marín J. M., Zalba B., Cabeza L. F. and Mehling H. (2003) “Determination of enthalpy- temperature curves of phase change materials with the temperature-history method: improvement to temperature dependent properties.” *Measurement Science and Technology*, 14, 184–189.

Medrano M., Yilmaz M.O., Nogués M., Martorell I., Roca, J. and Cabeza L. F. (2009). “Experimental evaluation of commercial heat exchangers for use as PCM thermal storage systems.” *Applied Energy*, 86, 2047-2055.

Mehling H. and Cabeza L. F., (2008) “Heat and cold storage with PCM: An up to date introduction into basics and applications” *Heat and Mass Transfer series*, Springer 2008 edition, 57-102.

MENA new energy, <http://analysis.newenergyupdate.com/csp-today/global-csp-capacity-reaches-495-gw-south-africas-redstone-csp-project-signs-ppa-after-two>, 24 April, 2018

Michels H. and Pitz-Paal R. (2007). “Cascaded latent heat storage for parabolic trough solar power plants.” *Solar Energy*, 81, 829–837.

Morisson V., Rady M., Palomo E. and Arquis E. (2008). “Thermal energy storage systems for electricity production using solar energy direct steam generation technology.” *Chemical Engineering and Processing*, 47, 499–507.

Oh S. H., Kauffmann Y., Scheu C., Kaplan W. D. and Ruhle M. (2005), “Ordered Liquid Aluminum at the Interface with Sapphire”, *Science*, 310, 661-663.

Prabhu K. N. and Ashish A. A. (2002). “Inverse modeling of heat transfer with application to solidification and quenching”, *Materials And Manufacturing Processes*, 17, No. 4, 469–481.

Qingwen S., Yi L., Jianwei X., Hu J. Y. and Yuen M. (2008). “Thermal stability of composite phase change material microcapsules incorporated with silver nanoparticles.” *Polymer*, 48, 3317-3323.

Rady M. (2009). “Granular phase change materials for thermal energy storage: Experiments and numerical simulations.” *Applied Thermal Engineering*, 29, 3149–3159.

Salaun F., Devaux E., Bourbigot S., Rumeau P., Chapuis P. O., Saha S. K. and Volz S. (2008). “Polymer nanoparticles to decrease thermal conductivity of phase change materials.” *Thermochimica Acta*, 477, 25–31.

Salunkhe P.B. and Shembekar P.S. (2012). “A review on effect of phase change material encapsulation on the thermal performance of a system.” *Renewable and Sustainable energy Reviews*, 16, 5603-5616.

Sari A. and Kaygusuz K. (2002). “Thermal performance of palmitic acid as a phase change energy storage material.” *Energy Conversion and Management*, 43, 863–876.

Sarı A. and Kaygusuz K. (2003). "Some fatty acids used for latent heat storage: thermal stability and corrosion of metals with respect to thermal cycling" *Renewable Energy*, 28, 939–948.

Sarı A., Sarı H. and Onal A. (2004). "Thermal properties and thermal reliability of eutectic mixtures of some fatty acids as latent heat storage materials." *Energy Conversion and Management*, 45, 365–376.

SECI, www.mnre.gov.in/file-manager/advertisement/adv_seci_april2013.pdf, (aug.20 2014).

Sharma A., Tyagi V. V., Chen C. R. and Buddhi D. (2009). "Review on thermal energy storage with phase change materials and applications." *Renewable and Sustainable Reviews*, 13, 318-345.

Shin D. and Banerjee D. (2014), "Specific heat of nanofluids synthesised by dispersing Al₂O₃ nanoparticles in alkali salt eutectic", *International Journal of Heat & Mass transfer*, 74, 210-214.

Sudheer R. and Prabhu K. N. (2016), "A Computer Aided Cooling Curve Analysis method to study phase change materials for thermal energy storage applications." *Materials and Design*, 95, 198–203

Sun J. Q., Zhang R. Y., Liu Z. P. and Lu G. H. (2007). "Thermal reliability test of Al–34%Mg–6%Zn alloy as latent heat storage material and corrosion of metal with respect to thermal cycling." *Energy Conversion and Management*, 48, 619–624.

Tan Z., Wang L. and Shi Q. (2009), "Study of heat capacity enhanced in some nanostructured materials", *Pure Applied Chemistry*, 81, 1871-1880.

Wang B. X., Zhou L. P. and Peng X. F. (2006), "Surface and Size Effects on the Specific Heat Capacity of Nanoparticles", *International Journal of Thermophysics*, 27, 139-151.

Wang L., Tan Z., Meng S., Liang D. and Li G. (2001), “Enhancement of molar heat capacity of nanostructured Al_2O_3 ”, *Journal of Nanoparticle Research*, 3, 483-487.

Wang X., Liu J., Zhang Y., Di H. and Jiang Y. (2006). “Experimental research on a kind of novel high temperature phase change storage heater.” *Energy Conversion and Management*, 47, 2211–22.

Work Programme and Budget for 2014-2015: Report of the Director-General, International Renewable Energy Agency (IRENA), Fourth session of the Assembly, Abu Dhabi, 18 – 19 January 2014.

Wu S., Wang H., Xiao S. and Zhu D. (2012). “Numerical Simulation on Thermal Energy Storage Behavior of Cu/paraffin nanofluids PCMs.” *Procedia Engineering*, 31, 240 – 244.

Wu S., Zhu D., Li X., Li H. and Lei J. (2009). “Thermal energy storage behavior of $\text{Al}_2\text{O}_3\text{-H}_2\text{O}$ nanofluids.” *Thermochimica Acta*, 483, 73–77.

Xiao X., Zhang P. and Li M. (2013). “Thermal characterization of nitrates and nitrates/expanded graphite mixture phase change materials for solar energy storage.” *Energy Conversion and Management*, 73, 86–94.

Xie Q. (2016), “Thermal storage properties of molten nitrate salt-based nanofluids with graphene nanoplatelets”, *Nanoscale Research Letters*, 11, 306.

Xuan Y., Huang Y. and Li Q. (2009). “Experimental investigation on thermal conductivity and specific heat capacity of magnetic microencapsulated phase change material suspension.” *Chemical Physics Letters*, 479, 264–269.

Yang R., Xub H. and Zhang Y. (2003). “Preparation, physical property and thermal physical property of phase change microcapsule slurry and phase change emulsion.” *Solar Energy Materials & Solar Cells*, 80, 405–416.

Ye F., Ge Z., Ding Y. and Yang J. (2014), “Multi-walled carbon nanotubes added to $\text{Na}_2\text{CO}_3/\text{MgO}$ composites for thermal energy storage”, *Particuology*, 15, 56–60.

Yinping Z., Yi J. and Yi J. (1998). "A simple method, the T –history method, of determining the heat of fusion, specific heat and thermal conductivity of phase-change materials." *Measurement Science and Technology*, 10, 201–205.

Zalba B., Marin J. M., Cabeza L. F. and Mehling, H. (2003). "Review on thermal energy storage with phase change: materials, heat transfer analysis and applications." *Applied Thermal Engineering*, 23, 251-283.

Zhang H., Xu Q., Zhao Z., Zhang J., Sun Y. C, Sun L., Xu F. and Sawada Y. (2012). "Preparation and thermal performance of gypsum boards incorporated with microencapsulated phase change materials for thermal regulation" *Solar Energy Materials & Solar Cells*, 102, 93-102.

Zhang P., Xia L and Wang R. Z. (2011). "The thermal response of heat storage system with paraffin and paraffin/expanded graphite composite for hot water supply" *World Renewable Energy Congress-Sweden*.

PUBLICATIONS

List of Journal Publications

Sudheer R. and Prabhu K. N. (2015), “Characterization of Metal-PCMs for Thermal energy Storage Applications”, Materials Science Forum, 830-831, 505-508.

Sudheer R. and Prabhu K. N. (2016), “A Computer Aided Cooling Curve Analysis method to study phase change materials for thermal energy storage applications”, Materials and Design, 95, 198–203.

Sudheer R. and Prabhu K. N. (2017), “Cooling curve analysis of micro and nano graphite particle embedded salt-PCMs for thermal energy storage applications”, Journal of Materials & Engineering Performance, ASM International, 26, 4040-4045.

Sudheer R. and Prabhu K. N., “Assessment of pcm- container heat transmission using a hot/cold probe technique”, Accepted for publication in Heat Transfer – Asian Research.

Sudheer R. and Prabhu K. N., “Determination of thermal energy storage parameters of nano-salt PCMs by computer aided cooling curve analysis”, Under Review

List of Papers in Conference Proceedings

Sudheer R. and Prabhu K. N., (2018) “Heat Transfer Characteristics of Nanoparticles Dispersed Nitrate salt-PCM For Thermal Energy Storage Applications”, Proceedings of the International Conference on Sustainable Energy and Environmental Challenges, SEEC-2018-148, 609-611

List of Papers Presented at Conferences

27th International Conference on Diamond and Carbon Materials (DIAM) 2016, Montpellier, France. “Effect of micro and nano graphite particle addition to salt-PCMs for thermal energy storage materials.”

International Conference on Advance Materials and Processes (ADMAT) 2017, Thiruvananthapuram, India. “Salt based phase change materials for thermal energy storage applications.”

Bio-Data

Name: SUDHEER R.

Date of Birth: 26-July 1987

Permanent Address: Meena Mahal, TC 9/2412, SEKT 73, Kurups Lane
Sasthamangalam P.O., Thiruvananthapuram-695010
Kerala, India

Email: sudheerrajagopalan@gmail.com

Contact Number: +91-9480855808, 0471-2310294

Educational Qualification:

Master of Technology	Process Metallurgy	National Institute. of Technology Karnataka, India	2013
Bachelor of Technology	Mechanical Engineering	GEC Barton hill University of Kerala, India	2009
P.G. Diploma	Automobile Technologies	Annamalai University, India	2010

- SUDHEER R.